REACTIVE OXYGEN SPECIES-INDUCED NECROTIC CELL DEATH

by

Ruiyu Xie

A Dissertation Submitted to the Faculty of the

DEPARTMENT OF PHARMACOLOGY AND TOXICOLOGY

In Partial Fulfillment of the Requirements
For the Degree of

DOCTOR OF PHILOSOPHY

In the Graduate College

THE UNIVERSITY OF ARIZONA

2009

THE UNIVERSITY OF ARIZONA
GRADUATE COLLEGE

As members of the Dissertation Committee, we certify that we have read the dissertation prepared by Ruiyu Xie

entitled Reactive Oxygen Species-Induced Necrotic Cell Death

and recommend that it be accepted as fulfilling the dissertation requirement for the Degree of Doctor of Philosophy

_____ Date: 04/27/09
Terrence J. Monks

_____ Date: 04/27/09
Myron K. Jacobson

_____ Date: 04/27/09
Serrine S. Lau

_____ Date: 04/27/09
Qin M. Chen

_____ Date: 04/27/09
Bernard W Futscher

Final approval and acceptance of this dissertation is contingent upon the candidate's submission of the final copies of the dissertation to the Graduate College.

I hereby certify that I have read this dissertation prepared under my direction and recommend that it be accepted as fulfilling the dissertation requirement.

_____ Date: 04/27/09
Dissertation Director: Terrence J. Monks

STATEMENT BY AUTHOR

This dissertation has been submitted in partial fulfillment of requirements for an advanced degree at the University of Arizona and is deposited in the University Library to be made available to borrowers under rules of the Library.

Brief quotations from this dissertation are allowable without special permission, provided that accurate acknowledgment of source is made. Requests for permission for extended quotation from or reproduction of this manuscript in whole or in part may be granted by the head of the major department or the Dean of the Graduate College when in his or her judgment the proposed use of the material is in the interests of scholarship. In all other instances, however, permission must be obtained from the author.

SIGNED: Ruiyu Xie

ACKNOWLEDGEMENTS

My thanks and appreciation goes to Dr. Terrence Monks for his persevering guidance as my advisor through out the time for me to complete the research and to write the dissertation. I also would like to thank the members of my dissertation committee, Dr. Serrine Lau, Dr. Myron Jacobson, Dr. Bernard Futscher, and Dr. Qin Chen, who have generously given their time and expertise to improve my work. I thank them for their contribution and support.

Live cell imaging and measurement of intracellular Ca^{2+} concentration was done under the guidance of Dr. Scott Boitano. Colleagues from Southwest Environmental Health Sciences Center: Dr. George Tsaprailis, Andrea Hunt, and Yelena Feinstein (Proteomics Core) helped in mass spectrometry of the analysis of histones and peroxiredoxin III; Douglas Cromey (Cellular Imaging Core) helped in confocol microscopy for the live cell imaging and measurement of intracellular reactive oxygen species generation; and Barb Carolus (Flow Cytometry Facility) helped in flow cytometry.

I would like to thank all members in Dr. Monks and Lau's laboratory. I also need to thank people and laboratories (esp. Jacobson lab and Boitano lab) to share their facilities.

My thanks must also go to staffs in Department of Pharmacology and Toxicology for their administrative assistance, especially Jeanice Smith and Nancy Colbert for their assistance and patience.

Funding: National Institutes of Health grants RO1 DK59491 to Terrence J. Monks and NIEHS Center grant P30 ES06694.

My family, both in US and in China, is always the place for me to rest and to look for motivations. They consistently help me to keep perspective on what is important in life.

DEDICATION

To my grandparents **Zongshang Xie**, Fendian Zhou, my parents Pindi Xie and Meili Kuang, my husband Xiaohui Hu, my loving son Zhaoting Tse Hu, and all of my family and friends for their endless love and support.

TABLE OF CONTENTS

LIST OF FIGURES

LIST OF ABBREVIATIONS

ADP-ribose	adenosine 5'-diphosphate ribose
AIF	apoptosis inducing factor
ANT	adenine nucleotide translocase
BSA	bovine serum albumin
CsA	cyclosporine A
CYP	cytochrome P450
DAPI	4'6-Diamidino-2-phenylindole dihydrochloride
DMEM	dulbecco's modified eagle medium
DNA	deoxyribonucleic acid
DTT	dithothreitol
EGFR	epidermal growth factor receptor
ER	endoplasmic reticulum
ERK	extracellular signal receptor activated kinase
FBS	fetal bovine serum
gadd	growth arrest and DNA damage
GPx	glutathione peroxidase
GR	glutathione reductase
Grx	glutaredoxin
GSH	glutathione
GST	glutathione-S-transferase

γ-GT	Gamma-glutamyl transpeptidase
HQ	hydroquinone
H_2O_2	hydrogen peroxide
HPLC	high performance liquid chromatography
JNK	jun N-terminal kinase
MAPK	mitogen activated protein kinase
MPT	mitochondrial permeability transition
PAR	polymers of ADP-ribose
PARG	polyadenosine diphosphoribose glycohydrolase
PARP	polyadenosine diphosphoribose polymerase
PBS	phosphate buffered saline
PI	propidium iodide
Prx	peroxiredoxin
ROS	reactive oxygen species
SOD	superoxide dismutase
TBS	tris-buffered saline
TGHQ	2,3,5-Tris(Glutathion-S-yl)-hydroquinone
TR	thioredoxin reductase
Trx	thioredoxin

ABSTRACT

Mechanisms of cell death extend beyond the simple apoptosis/necrosis relationship to include regulated modes of cell death that do not readily fit either of the classic descriptors. One such mechanism of cell death involves poly(ADP-ribose)polymerase-1 (PARP-1)-mediated cell death. 2,3,5-Tris(Glutathion-S-yl)-hydroquinone (TGHQ), a reactive oxygen species (ROS) generating nephrotoxic and nephrocarcinogenic metabolite of hydroquinone, causes necrotic renal cell death, the basis for which is unclear. We therefore investigated TGHQ-mediated cell death in human renal proximal tubule epithelial HK-2 cells. TGHQ induced ROS generation, DNA strand breaks, hyperactivation of PARP-1, rapid depletion of nicotinamide adenine dinucleotide (NAD), elevations in intracellular Ca^{2+} concentrations, loss of mitochondrial membrane potential, and subsequent necrotic cell death. Interestingly, PARP-1 hyperactivation was not accompanied by the translocation of apoptosis-inducing factor (AIF) from mitochondria to the nucleus, a process usually associated with PARP-dependent cell death. Inhibition of PARP-1 with PJ34 blocked TGHQ-mediated accumulation of poly(ADP-ribose) polymers, NAD consumption, and the consequent necrotic cell death. However, HK-2 cell death was only delayed by PJ34, and cell death remained necrotic in nature. In contrast, chelation of intracellular Ca^{2+} with BAPTA-AM completely abrogated TGHQ-induced necrotic cell death. Ca^{2+} chelation not only prevented the collapse in the mitochondrial potential but also attenuated PARP-1 hyperactivation. Conversely, inhibition of PARP-1 modulated TGHQ-mediated changes in Ca^{2+} homeostasis. Moreover, TGHQ caused a sequential oxidation of peroxiredoxin III (PrxIII), a protein considered the primary antioxidant defense within mitochondria. Thus, TGHQ induced two

acidic shifts in PrxIII, with both pI shifted spots representing oxidized forms of PrxIII. Transient expression of a dominant negative version of PrxIII resulted in a significant increase in TGHQ-induced cytotoxicity, whereas overexpression of wild-type PrxIII significantly attenuated cytotoxicity. Our studies provide new insights into PARP-1-mediated necrotic cell death. Changes in intracellular Ca^{2+} concentrations appear to couple PARP-1-hyperactivation to subsequent cell death, but in the absence of AIF release from mitochondria. NAD depletion, mitochondrial membrane depolarization, Ca^{2+}-mediated calpain activation, and PrxIII oxidation, all contribute to TGHQ-driven ROS-mediated necrotic cell death.

CHAPTER 1: INTRODUCTION

1.1. GENERAL COMMENTS

Everyday humans are exposed to a wide range of chemicals from a variety of sources, including food packaging, pesticides, toys, cosmetics and the pharmaceutical industry. Chemical exposure can lead to adverse health effects. Thus, understanding mechanisms of chemical toxicity and their potential risks to humans is essential for limiting chemical-induced toxicities. The complex mechanisms of chemical toxicity make them extremely difficult to determine. However advances in molecular and cellular technologies are permitting a more precise understanding of mechanisms of toxicity.

The kidneys are particularly susceptible to chemical-induced injury because: (i) they receive 20-25% of cardiac output, although they comprise less than 1% of total body weight; (ii) they can actively concentrate toxic substrates by removing water from the glomerular filtrate; and (iii) they are metabolically active. Thus in certain cases the kidney can metabolize chemical substrates with the subsequent generation of more biologically reactive intermediates.

Certain chemicals induce kidney disease via the generation of highly reactive oxygen species (ROS). Therefore, understanding ROS-induced signaling pathways in acute and chronic renal diseases not only assists in the discovery of potential novel therapeutics, but may also assist in preventing chemical-mediated ROS-driven kidney disease. The goals of the studies reported in this thesis are to determine the mechanism of ROS-induced nephrotoxicity at the molecular and cellular level.

1.2. HYDROQUINONE

Hydroquinone (HQ, chemical abstract service chemical name: 1,4-benzenediol; registration number: 121-31-9), an aromatic organic compound, is an odorless, white granular solid highly soluble in water. It is a type of phenol, having the chemical formula $C_6H_4(OH)_2$, incorporates two hydroxyl groups bonded to the benzene ring in the 1,4 (para) position (IPCS, 1996).

1.2.1. Exposure

HQ is ubiquitously present in the environment, either in synthetic products, or in a variety of natural products present in plants (DeCaprio, 1999; IPCS, 1996). For example, HQ is present in wheat germ, in coffee bean extracts, and in tea prepared from the leaves of blueberry, cranberry, and bearberry (Varagant, 1981). In addition, humans are exposed to HQ indirectly via the biotransformation of benzene, a well known human hematotoxicant and carcinogen (Glatt et al., 1989; Niculescu et al., 1996; Smith et al., 1990; Witz et al., 1996).

More than 40,000 tons of HQ was produced in 1979 and approximately 35,000 tons in 1992 (IPCS, 1996). HQ has a variety of uses associated with its capacity to behave as a reducing agent (DeCaprio, 1999). For example, it is a major component in most photographic developers. In medical preparations, HQ is used as a topical application in skin lightening (Engasser and Maibach, 1981; Goldman, 2000). It has also been found in mainstream smoke from non-filtered cigarettes, and in sidestream smoke (Pryor, 1997). Furthermore, HQ is used as an antioxidant to prevent redox-sensitive ingredients in food from oxidation (DeCaprio, 1999). HQ is also widely used in hair dyes

and color preparations. Therefore, humans are exposed to HQ via smoking, cosmetics, medicine, via the consumption of foods, and via inhalation of polluted air (Devillers et al., 1990). Furthermore, people may be exposed to HQ occupationally, such as workers involved in the chemical synthesis industry and in the synthesis of antioxidants, drugs, food stabilizers, and in photo development (Key, 1977; NIOSH, 1978). Occupational exposure to HQ during manufacturing is limited to 0.13 to 0.79 mg/m^3 (IPCS, 1996).

1.2.2. Absorption, Distribution, Metabolism, and Excretion

HQ is rapidly absorbed via either ingestion or inhalation. In contrast, dermal absorption is slower, with a dermal absorption rate of 3 $\mu g/cm^2$ and a permeability constant of 2.25 $\times 10^{-6}$ cm/hour (Bucks et al., 1988). However, other factors including concentration, vehicle of exposure, and duration of exposure also affect the final amount of HQ absorbed.

Following absorption HQ is widely distributed in animal tissue. Studies with radio-labeled HQ in rats revealed that HQ is heterogeneously distributed into most tissues after oral administration, with the highest levels of radioactivity found in the kidney and liver (Divincenzo et al., 1984). In contrast, after intravenous injection, HQ is concentrated in the thymus, bone borrow, and spleen white pulp (Greenlee et al., 1981). Thus, HQ distribution is dependent on the routes of administration/exposure.

After absorption, HQ is metabolized in the liver, mainly by phase II metabolic enzymes to form hydrophilic conjugates, and excreted rapidly via the urine. HQ can be detoxified by glucuronidation and sulfation. However, HQ can also be metabolized via oxidation and subsequent conjugation to glutathione (GSH) forming quinone-thioethers

(Lau et al., 1988b). The proposed metabolic pathway of HQ is illustrated in Figure 1.1. HQ is initially oxidized to 1,4-benzoquinone by cytochrome P450, or other enzymes such as prostaglandin H synthase or myeloperoxidases (Lau and Monks, 1987; Subrahmanyam et al., 1990). 1,4-Benzoquinone can undergo nucleophilic addition of GSH to form 2-(glutathion-S-yl)HQ. Sequential oxidation and GSH addition leads to the eventual formation of 2,3,5-tris-(glutathion-S-yl)hydroquinone (TGHQ), which is far more toxic than HQ (Monks, 1995). GSH conjugation to HQ increases its ability to redox cycle, and its nucleophilicity. Furthermore, GSH conjugation can target HQ to specific organs, such as the kidney (Monks and Lau, 1994).

The susceptibility of the kidney to quinone-thioethers is due to the relatively high levels of two metabolic enzymes, γ-glutamyl transpeptidase (γ-GT) and cysteinylglycine dipeptidase, each of which are present in the brush border membrane of proximal tubule epithelia cells in the S3 region of the kidney. After GSH conjugation, HQ-GSH can undergo further metabolism via the mercapturic acid pathway (Figure 1.2). γ-GT catalyzes the cleavage of the γ-glutamyl moiety of GSH to form cysteinylglycine conjugates. Dipepidases then cleave glycine from the cysteinylglycine conjugates to generate the corresponding cysteinyl conjugates, which are readily taken up by renal epithelial cells via the L-amino acid transporter (Monks and Lau, 1997; Monks and Lau, 1998). Finally, the cystein-S-yl HQ conjugates are converted into mercapturic acids (N-acetylcysteine conjugates) via the activity of an acetyltransferase. All of the HQ-thioether conjugates in the mercapturic acid pathway retain the ability to redox cycle and create an oxidative stress. Moreover, the HQ-thioethers also retain the ability to form covalent

adducts with a variety of cellular macromolecules. The combination of nucleophilic adduction to cellular macromolecules and the generation of oxidative stress likely contribute to HQ-thioether-mediated nephrotoxicity (Whysner et al., 1995). Urinary metabolites of HQ in Fischer 344 rats include a large fraction as glucuronide and sulfate conjugates, and smaller amounts of mercapturic acid conjugates, indicating that the GSH conjugates of HQ are generated as *in vivo* metabolites (Deisinger et al., 1996; Divincenzo et al., 1984).

Almost 90% of hydrophilic HQ metabolites are excreted via the urine. Moreover, the pattern of urinary metabolites varies dependent upon the dose, suggesting that the ability to eliminate HQ is saturated at higher doses (English, 1988). In addition, plasma concentrations of HQ reach two separate peaks, indicating the possibility of enterohepatic recycling of HQ (English, 1988).

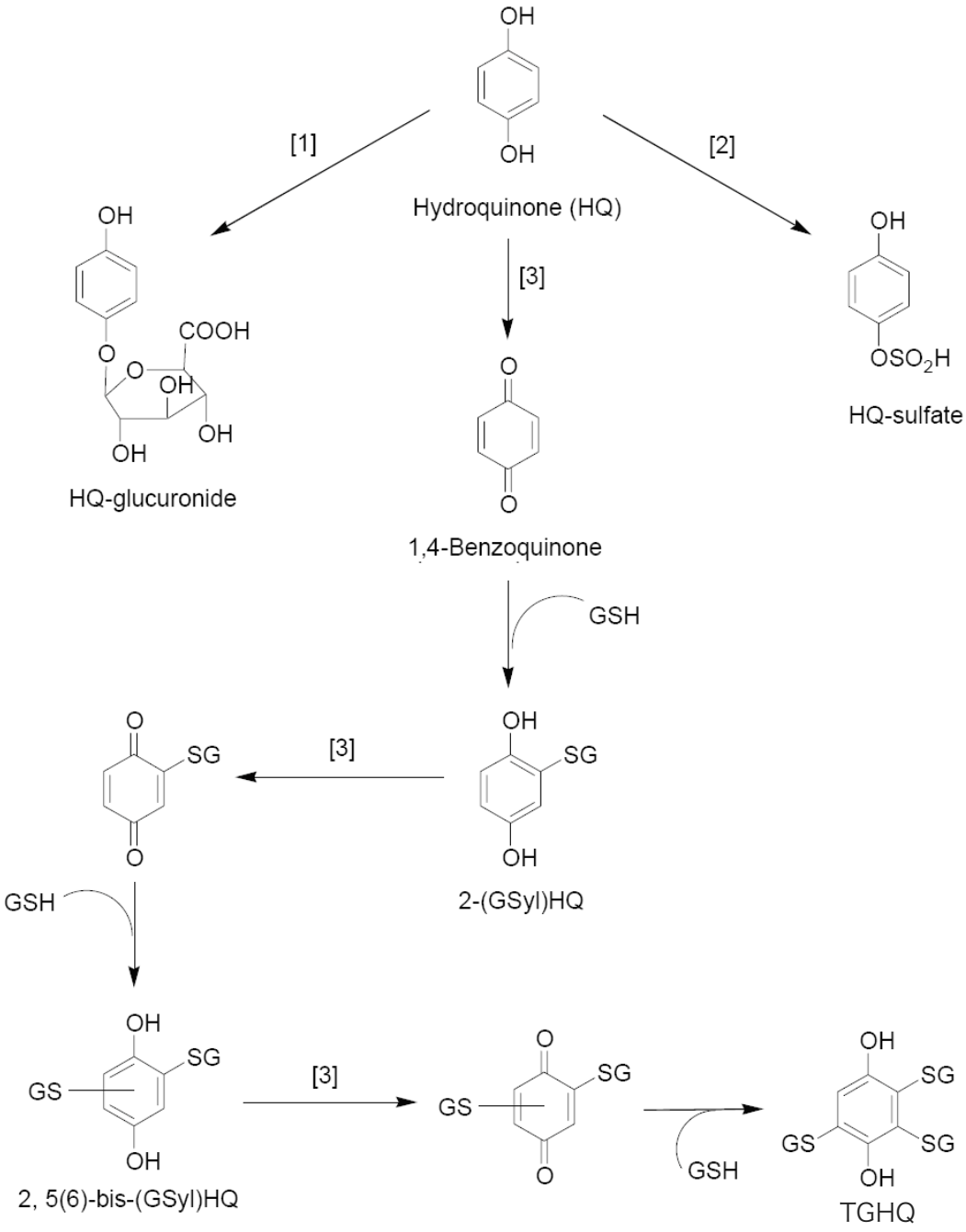

Figure 1. 1. Metabolism of hydroquinone.

Formation of quinone-thioethers. Multi-GSH HQ conjugates are of toxicological significance, contributing to HQ mediated nephrotoxicity. (1). Glucuronyl transferase with UDP-glucuronic acid (UDPGA); (2), Sulfotransferase with 3-phosphoadenosine-5′-phosphosulfate (PAPS); (3), CYP450.

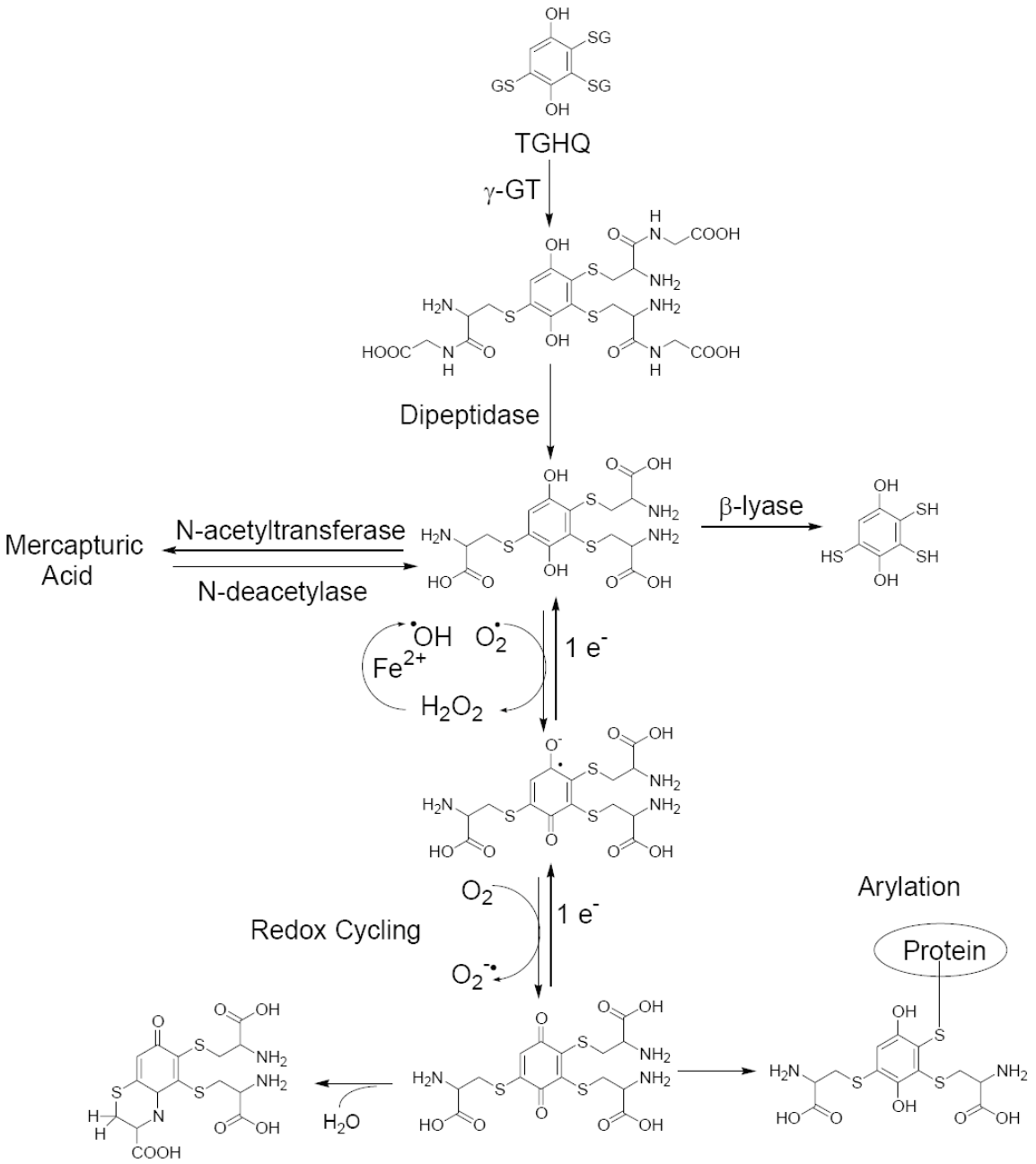

Figure 1.2. Bioactivation of TGHQ and the mechanisms of ROS generation.

The HQ-cysteine conjugates can generate ROS via redox cycling between the quinone and semiquinone. In addiction, the 1,4-benzoquinone cysteine conjugate can bind to protein causing macromolecular damage.

1.3. TOXICITY OF HYDROQUINONE AND QUINONE-THIOETHERS

The chemical basis of HQ toxicity has been extensively studied, and two primary mechanisms have been proposed to explain its toxic effect. HQ can undergo enzymatic or non-enzymatic redox cycling to generate ROS, including superoxide anion ($O_2^{\bullet -}$), hydrogen peroxide (H_2O_2), and hydroxyl radical (•OH) (Monks et al., 1992; O'Brien, 1991). ROS generated during the redox cycling of HQ can induce oxidative stress and damage the cell. For example, oxidation of catalytic cysteine residues on essential proteins results in enzymatic inactivation, and oxidation of nucleic acids leads to the formation of 8-oxo-2'-dexoyguanosine and subsequent DNA damage (Camhi et al., 1995; Martinez et al., 2003). Moreover, lipid oxidation leads to the generation of additional toxic products, resulting in damage to the cell membrane and DNA, the latter via the formation of malondialdehyde a product of lipid peroxidation (Marnett, 1999).

GSH conjugated HQ is also readily oxidized to the one-electron reduced semiquinone intermediate, before being oxidized to GSH conjugated 1,4-benzoquinone. Since the reverse reduction reaction occurs simultaneously, this reversible oxidation-reduction cycle is termed redox cycling. During this process, an oxygen molecule is reduced to $O_2^{\bullet -}$ via an electron from HQ. $O_2^{\bullet -}$ subsequently undergoes either enzymatic or spontaneous dismutation to generate H_2O_2 which can generate the highly toxic oxidant •OH, which is probably the reactive species responsible for quinone-mediated oxidative damage (Monks and Lau, 1997).

Alternatively, 1,4-benzoquinone can act as an electrophile, mediating the covalent adduction of biological molecules at various nucleophilic sites, such as protein thiols. The

formation of covalent adducts with numerous cellular macromolecules, particularly on their functional groups, can lead to the loss of essential biological function. For example, covalent adduction on lysine rich regions of cytochrome c by 1,4-benzoquinone and its corresponding thioether conjugates, causes alterations in protein structure, and consequently inhibition of its ability to promote the processing of caspase-3 (Fisher et al., 2007). In addition, HQ and its thioether metabolites which covalently bind to macromolecules are still capable of redox cycling. In this manner, the redox reaction is "fixed" to a molecule resulting in a localized oxidative stress (Monks et al., 1992). The biological and pharmacological properties of quinone-thioethers determine their toxicities in mammal, as discussed in the following sections. In particular, the work presented in this thesis primarily focuses on the mechanism of HQ-mediated nephrotoxicity. Other toxicities associated with exposure to HQ, such as hematotoxicity, will also be discussed in order to provide a more complete understanding of HQ-mediated toxicities.

1.3.1. HQ-mediated Nephrotoxicity

HQ and its metabolites are nephrotoxic (Monks and Lau, 1997; Monks et al., 1985) and nephrocarcinogenic (IARC, 1999; Lau et al., 2001; Levitt, 2007). Among the various GSH conjugated HQ metabolites, TGHQ is the most potent nephrotoxicant. A single dose (7.5 μmol/kg) of TGHQ in Fischer 344 rats results in significant increases in the urinary excretion of renal enzymes, including γ-GT, alkaline phosphatase, and glutathione S-transferase (GST), concomitant with tubular necrosis in the S3 segment (Peters et al., 1997). Typical nephrotoxicity is characterized by loss of brush border membrane

integrity, loss of cellular contents, margination of heterochromatin, DNA fragmentation, and renal necrotic cell death (Monks and Lau, 1998).

The nephrotoxicity of quinone-thioethers is due to the relatively high levels of γ-GT and dipeptidase in the brush border membrane of kidney proximal tubule epithelium. These two enzymes metabolize polyphenolic GSH conjugates to form cysteinyl conjugates which can enter renal cells via the L-amino acid transporter system. Inhibition of γ-GT with acivicin (AT-125) completely protects rats from quinone-thioether mediated nephrotoxicity (Monks et al., 1988). The essential role of γ-GT has also been demonstrated in an in vitro system, which revealed rat renal epithelial (NRK) cells are less sensitive to TGHQ relative to porcine renal proximal tubule epithelial (LLC-PK1) cells due to the lower levels of γ-GT present in NRK cells (Jia, 2004). Thus, metabolism by γ-GT is required for quinone-thioether induced nephrotoxicity. However, γ-GT is not the only factor contributing to the susceptibility to quinone-thioethers. Although renal γ-GT levels are similar in both mice and guinea pigs, only guinea pigs are susceptible to TGHQ mediated nephrotoxicity, most likely because of differences in the ratio of N-deacetylation:N-acetylation between mice and guinea pigs (Lau et al., 1995). N-acetylation of cysteinyl conjugates is generally considered to be a detoxication step for quinol-thioethers because the redox activty of N-acetylcysteine conjugates is much less than that of the corresponding cysteine conjugates. Therefore, the low N-deacetylation:N-acetylation ratio in mice results in less susceptibility to TGHQ compared to guinea pigs, which have a high N-deacetylation:N-acetylation ratio.

Studies of quinone-thioether-induced cytotoxicity have primarily been conducted in. LLC-PK1 cells, which are derived from porcine renal proximal tubule epithelium, and express relatively high levels of γ-GT. TGHQ induces necrotic cell death in LLC-PK1 cells (Dong et al., 2004b; Ramachandiran et al., 2002; Tikoo et al., 2001), which is associated with its ability to generate ROS and cause DNA single strand breaks (Jeong et al., 1996; Mertens et al., 1995). Early studies on 2-bromo-*bis*-(glutathion-S-yl)hydroquinone [2-Br-*bis*-(GSyl)HQ] and 2-bromo-6-(glutathion-S-yl)hydroquinone [2-Br-6-(GSyl)HQ] demonstrated that quinone-thioethers induce a rapid cell cycle arrest, as indicated by (i) an increase in *gadd153* expression, a gene responsive to growth arrest and DNA damage, (ii) a rapid inhibition of DNA synthesis, (iii) a decrease in histone mRNA, and (iv) a low mitotic index (Jeong et al., 1997a; Jeong et al., 1997b; Jeong et al., 1996). In addition, chelation of intracellular Ca^{2+} with EGTA-AM, prior to exposure to 2-Br-*bis*-(GSyl)HQ or 2-Br-6-(GSyl)HQ decreased *gadd153* induction (Jeong et al., 1996), indicating that intracellular Ca^{2+} is involved in the quinone-thioether-mediated stress response.

TGHQ also induces activation of epidermal growth factor receptor (EGFR), and its downstream effectors mitogen activated protein kinases (MAPKs), including extracellular signal-regulated protein kinase (ERK), c-Jun N-terminal kinases (JNK), and p38 MAPK (Dong et al., 2004b; Ramachandiran et al., 2002). Moreover, inhibition of ERK and p38 MAPK with pharmacological inhibitors PD98059 and SB202190, respectively, attenuated TGHQ-induced necrotic cell death (Dong et al., 2004b; Ramachandiran et al., 2002). IN contrast, inhibition of either JNK or EGFR had no effect

on TGHQ-induced cell death. TGHQ also increases the DNA binding activity of MAPKs' downstream effectors, the transcription factor AP-1 (activator protein 1) and NF-κB (nuclear factor kappa B) (Ramachandiran et al., 2002). NF-κB may be involved in the cytoprotective effects observed during ERK inhibition by PD98059 (Ramachandiran et al., 2002). In addition to the transcription factors, another downstream effectors of MAPKs, histone H3, is activated by a novel phosphorylation in response to TGHQ both, *in vitro* and *in vivo* (Dong et al., 2004a; Palmer, 2004; Tikoo et al., 2001). Histone H3 phosphorylation is modulated by ADP-ribosylation and is accompanied by an increase in chromatin condensation (Tikoo et al., 2001). Addition of a poly(ADP-ribose) polymerase (PARP) inhibitor, 3-aminobenzamide, results in a decrease in histone H3 phosphorylation and an increase in cell survival (Jeong et al., 1997a; Tikoo et al., 2001), suggesting that activation of PARP may exacerbate quinone-thioether-mediated cytotoxicity. Abnormal histone H3 phosphorylation might also lead to necrotic cell death by stimulating premature chromatin condensation. Together, in LLC-PK1 cells TGHQ induces ROS generation, DNA strand breaks, growth arrest, EGFR and MAPKs activation, histone H3 phosphorylation, chromatin condensation and subsequently necrotic cell death. Although LLC-PK1 represents a good *in vitro* model to study HQ-induced nephrotoxicity, the fact that they are derived from the New Hampshire Mini-pig means that they do not exhibit the same genetic background as humans. Thus, a human-derived renal epithelial cell line, HK-2, provides a more relevant model with which extend studies on HQ- and ROS-mediated kidney diseases.

HK-2, human kidney-2, is a well-differentiated proximal tubule epithelial cell line derived from normal adult human kidney. HK-2 cells have been immortalized by transfection with human papilloma virus (HPV 16) E6/E7 genes (Ryan et al., 1994). HK-2 cells retain the phenotype of proximal tubule cells, including the expression of γ-GT, alkaline phosphatase, leucine aminopeptidase, acid phosphatase, cytokeratin, integrin, and fibronectin (Racusen et al., 1997; Ryan et al., 1994). In addiction, HK-2 cells retain the functional characteristics of proximal tubular epitheliu, as revealed by the presence of Na^+-dependent/phlorizin-sensitive sugar transporter and parathyroid-responsive but antidiuretic hormone-insensitive adenylate cyclase (Ryan et al., 1994). HK-2 cells have been utilized in a number of studies on transporters, growth arrest, hypoxia, oxidative stress-mediated cell death, and ischemia/reperfusion-induced renal injury (Esposito et al., 2009; Lee et al., 2008; Sautin et al., 2005; Sun et al., 2009; Sung et al., 2008; Xie and Guo, 2007; Yan et al., 2009). Additionally, experimental results obtained from primary cultured renal proximal tubule cells can also be reproduced in HK-2 cells (Mitsuoka et al., 2009; Morais et al., 2005; Peraldi et al., 2009; Ryan et al., 1994; Verzola et al., 2004). We therefore initiated the use of HK-2 cells as an *in vitro* model with which to further explore stress signaling in response to ROS-mediated nephrotoxicity.

1.3.2. HQ-mediated Hematotoxicity

HQ and its metabolites not only induce nephrotoxicity, but also target bone marrow, leading to hematotoxicity. HQ is endogenously generated after benzene exposure. Benzene is hematotoxic and causes aplastic anemia, myelodysplastic syndrome, and acute myelogenous leukemia in humans (Snyder et al., 1993b). After

absorption, benzene is metabolized in the liver, mainly by cytochrome P450 2E1 to form phenol (Snyder et al., 1993a). Phenol is subsequently oxidized to HQ which undergoes sequential GSH conjugation to form various quinone-thioethers. A number of HQ metabolites have been identified in the bone morrow of DBS/2 mice and Sprague-Dawley rats exposed to a benzene (Bratton et al., 1997). In addition, HQ reproduce benzene-mediated erythrotoxicity *in vivo* (Bratton et al., 1997). Studies on benzene-mediated acute myelogenous leukemia have suggested that benzene-induced hematotoxicity is due to the inappropriate induction of apoptotic signaling in bone marrow (Vaughan et al., 2005). However, little is known about the roles of apoptosis in benzene or HQ-mediated hematotoxicity.

Studies from our laboratory have revealed that TGHQ induces apoptosis in human promyelocytic leukemia (HL-60) cells via the generation of ROS (Yang et al., 2005). TGHQ depletes cellular GSH levels, leading to the activation of the ceramide signaling pathway during which caspase-3 and phosphatases are activated (Bolton et al., 2000). TGHQ also stimulates sphingomyelin turnover, and induces cytochrome *c* release from mitochondria, leading to caspase activation and subsequently to apoptotic cell death (Bratton et al., 2000; Yang et al., 2005).

Although HQ induced-nephrotoxicity and hematotoxicity share some common mechanisms of actions, including metabolism to form reactive GSH-conjugates and consequent generation of ROS, the molecular mechanisms by which quinone-thioethers mediate cytotoxicity are clearly different between the kidney and bone marrow. TGHQ induces classic apoptotic cell death in bone marrow cells (Bolton et al., 2000; Yang et al.,

2005), whereas TGHQ induces necrosis in renal epithelial cells (Dong et al., 2004b; Ramachandiran et al., 2002), suggesting that TGHQ-mediated cell death is context dependent. In Chapter 3, we adress the role of poly(ADP-ribose)polyermerase-1 in TGHQ-mediated necrotic cell death, and its effect on the cell fate determination.

1.4. OXIDATIVE STRESS

1.4.1. Reactive Oxygen Species

ROS are essential for HQ-mediated cytotoxicity, since scarvenging H_2O_2 with catalase blocks MAPK activation, histone H3 phosphorylation and subsequent necrotic cell death in LLC-PK1 cells (Dong, 2004). Therefore, a complete understating of the ROS-mediated stress response is to understand HQ and quinone-thioether mediated nephrotoxicity. ROS are highly reactive chemical forms of oxygen, and include $O_2^{\bullet -}$, H_2O_2, and •OH. ROS are produced endogenously during normal cellular metabolism, or from external sources, such as reactive chemicals or UVA/UVB exposure (Pryor et al., 2006; Thannickal and Fanburg, 2000). Several enzymes including NAD(P)H oxidase, cyclooxygenase, xanthine oxidase and lipoxygenase, are capable of forming $O_2^{\bullet -}$ from molecular oxygen. Cycoloxygenase also catalyzes an one-electron oxidation of NAD(P)H, resulting in the generation of a free radical intermediate form of NAD(P)H (Kukreja et al., 1986). This intermediate then reduces oxygen to form $O_2^{\bullet -}$. In addition, intracellular ROS are generated as the byproduct of cellular respiration, during which electrons leak from the electron transport chain and directly reduce oxygen to $O_2^{\bullet -}$ (Andreyev et al., 2005). $O_2^{\bullet -}$ subsequently undergoes enzymatic or spontaneous dismutation to generate H_2O_2, which gives rise, in the presence of transition metals such

as Fe^{2+}, to the highly reactive oxidant •OH via the Haber-Weiss reaction (Figure 1.3). Moreover, in phagocytic cells, such as neutrophils and macrophages, ROS are generated by NADPH oxidase or myeloperoxidase as a bactericide (Forman and Torres, 2002). Physiological levels of ROS may play a crucial role in signal transduction by acting as second messengers (Forman et al., 2002; Martindale and Holbrook, 2002; Torres and Forman, 2003). However, increased oxidative metabolism, inflammation and other disease conditions can lead to increased superoxide production. Excessive ROS cause severe damage to intracellular macromolecules and have been implicated in atherosclerosis, diabetes, Parkinson's disease, myocardial infarction, Alzheimer's disease, renal ischemia/reperfusion injury, and many other pathological conditions (Droge, 2002; Martindale and Holbrook, 2002; Mates et al., 1999).

(A)

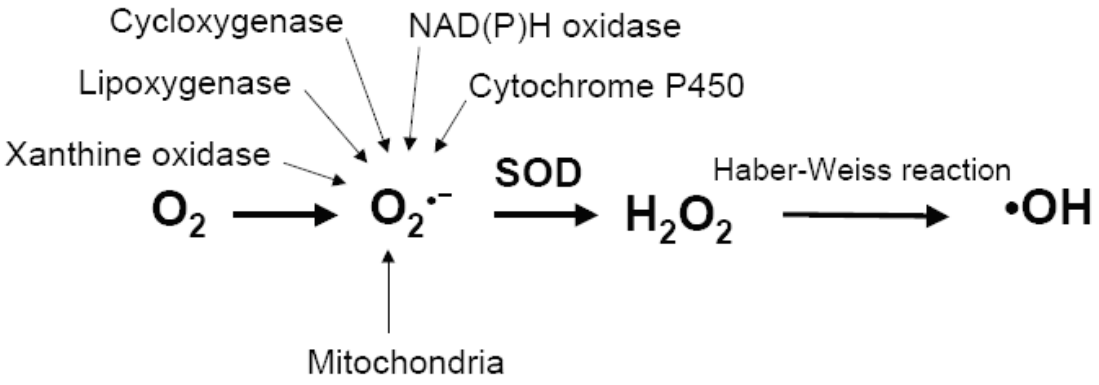

(B)

Haber-Weiss reaction

(1) $H_2O_2 + Fe^{2+} \longrightarrow {\bullet}OH + OH^- + Fe^{3+}$

(2) $Fe^{3+} + O_2^{\bullet-} \longrightarrow Fe^{2+} + O_2$

Figure 1.3. Intracellular ROS generation.

(A) ROS are generated in cells by several pathways. $O_2^{\bullet-}$ is generated by the leakage of electrons from mitochondria. $O_2^{\bullet-}$ is also generated by NAD(P)H oxidase, lipoxygenase, cyclooxygenase, xanthine oxidase, and NADPH cytochrome P450 reductase. Superoxide dismutase converts $O_2^{\bullet-}$ into H_2O_2. H_2O_2 produces a highly reactive radical •OH by the Haber-Weiss reaction. **(B)** The formation of •OH through the Haber-Weiss reaction. (1) This reaction is also known as Fenton reaction. (2) Fe^{3+} is recycled to Fe^{2+} by $O_2^{\bullet-}$. ($O_2^{\bullet-}$, superoxide anion radical; H_2O_2, hydrogen peroxide; •OH, hydroxyl radical; SOD, superoxide dismutase)

1.4.2. Antioxidant Defense Systems

In order to protect themselves from oxidative damage, cells have developed a number of antioxidant defense systems to counteract the potential adverse effects of ROS (Ueda et al., 2002). However, once these antioxidant defenses are overwhelmed, cells become subject to oxidative damage (Fridovich, 1978b; Mates and Sanchez-Jimenez, 1999). Enzymatic and non-enzymatic antioxidants protect cells by scavenging ROS (Halliwell, 1995). The primary defense systems include several antioxidant enzymes, such as superoxide dismutase (SOD), catalase, and glutathione peroxidase (GPx) (Fridovich, 1999). SOD is an important antioxidant in nearly all cells exposed to oxygen (Fridovich, 1978c). There are three major families of SOD, depending on the metal cofactor: Cu/Zn type, Fe and Mn types, and Ni type (Michiels et al., 1994). All SOD isozymes catalyze the conversion of $O_2^{\bullet -}$ to H_2O_2 (Fridovich, 1978a). Catalase is one of the most efficient antioxidant enzymes and is located in peroxisomes, where it catalyzes the decomposition of H_2O_2 to H_2O and O_2 (Lledias et al., 1998). GPx is also involved in the detoxication of H_2O_2 by catalyzing its reduction of H_2O_2 to water (Figure 1.4). However, this process is accompanied by the concomitant conversion of GSH to its oxidized form, glutathione disulfide (GSSG), which can be reduced back to GSH via glutathione reductase, and its cofactor NADPH.

Other ROS scavengers including glutaredoxin (Grx), thioredoxin (Trx, and peroxiredoxins (Prx), all of which participate in the ‘‘secondary’’ antioxidant defense system (Figure 1.4) (Jones, 2008; Nordberg and Arner, 2001). Grx reduces disulfide bonds in proteins, with the concomitant conversion of GSH to GSSG (Lillig et al., 2008).

GSSG is then recycled to GSH through glutathione reductase (GR) in the presence of NADPH. GSH is the major non-protein sulfhydryl group in the cellular reducing pool. GSH also binds to electrophiles preventing them from alkylating critical protein sulfhydryl groups (Shan et al., 1990). Moreover, GSH is involved in the detoxication of H_2O_2 and in protein disulfide reduction. Therefore, intracellular GSH levels are crucial in protecting cells from ROS. The Trx system is composed of Trx, thioredoxin reductase (TR), and NADPH, and plays an important role in maintaining the naturally reduced status of proteins (Arner and Holmgren, 2000). Prx protects cells against oxidative damage by the formation of a disulfide within two active cysteines present on different subunits of the homodimer (Fujii and Ikeda, 2002). The disulfide is then reduced back to the Prx active thiol form by the Trx-TR system (Winterbourn and Hampton, 2008).

Cellular responses to ROS consist of signaling pathways to either induce cell death or promote cell survival by repairing the cellular damage (Madeo et al., 1999). Cell fate is determined by the relative capacity of antioxidant defense systems and the ability of cells to repair cellular injury. Other factors, including cell type and differential activation of the stress signaling pathways also determine the outcome to ROS exposure. Many stress-signaling pathways are activated in response to ROS (Ryter et al., 2007). The precise mechanisms by which these pathways specifically contribute to ROS-induced renal cell death are the main focus of the current studies. The following subsection will provide a brief introduction on the concept of cell death, and the correlative signaling pathways associated with ROS-induced cell death.

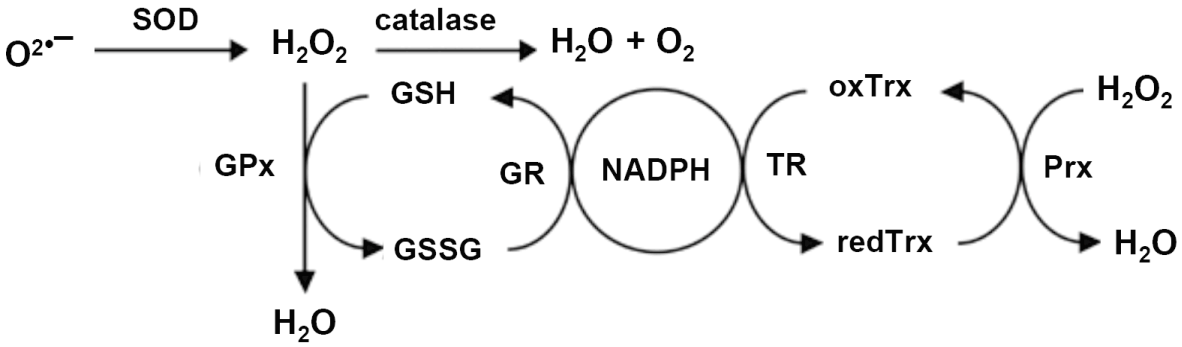

Figure 1.4. Cellular antioxidant defense systems.

The primary antioxidant defense system includes superoxide dismutase (SOD), catalase, and glutathione peroxidase (GPx). The secondary defense system consists of glutathione (GSH), glutathione reductase (GR), thioredoxin (Trx), thioredoxin reductase (TR), and peroxiredoxin (Prx). SOD converts O_2^- into H_2O_2 which is degraded to H_2O by catalase and GPx. Thioredoxin and peroxiredoxin has H_2O_2 reducing activity as well as a function in refolding oxidised proteins.

1.5. PROGRAMMED CELL DEATH

Mechanisms of cell death are usually classified into two pathways, apoptosis and necrosis (Kanduc et al., 2002; Majno and Joris, 1995; Trump et al., 1997) . Apoptosis is a genetically controlled process, requiring the coordinated suppression and expression of key genes, and is characterized by an orchestrated series of processes that can be separated into two general phases, the "commitment" phase and the "execution" phase. In addition, apoptosis requires energy, and usually involves the participation of individual, non-contiguous cells. The morphological features of apoptosis usually include; cell shrinkage, chromatin condensation and margination, DNA fragmentation into nucleosomal-sized remnants, membrane blebbing, and the formation of apoptotic bodies (Krysko et al., 2008; Taatjes et al., 2008). *In vitro*, apoptotic bodies cannot be engulfed and removed by phagocytes, with cells eventually losing plasma membrane integrity in a process termed either "late apoptosis" or "secondary necrosis" (Silva et al., 2008).

Cell death in the absence of classic apoptotic markers is often considered necrosis. It has generally been considered that necrosis is a passive process, with the cell responding to external stress, such as oxidative stress, in an uncoordinated, random fashion, dependent upon the nature of the specific stress (Majno and Joris, 1995). In contrast to apoptosis, necrosis is characterized by cell and organelle swelling that eventually leads to the loss of plasma membrane integrity (Krysko et al., 2008). However, it is now evident that mechanisms of cell death extend beyond the simple apoptosis/necrosis relationship to include regulated modes of cell death that do not readily fit either of the classic descriptors of cell death (Borst and Rottenberg, 2004; Golstein and Kroemer, 2007; Henriquez et al.,

2008; Proskuryakov et al., 2003). Recognition of these other modes of regulated, non-apoptotic cell death has important implications for human health and disease (Degterev and Yuan, 2008).

Besides apoptotic programmed cell death, other non-apoptotic programmed cell death pathways have now been discovered. Three modes of non-apoptotic, orchestrated cell death include; (i) autophagic cell death, (ii) necroptosis (necrosis-like programmed cell death), and (iii) poly(ADP-ribose)polymerase-1 (PARP-1)-mediated cell death (Degterev and Yuan, 2008), each with their own unique biochemical and morphological features. More importantly, each mode of non-apoptotic cell death plays important roles in pathophysiology. Autophagy has been observed in the maintenance of intracellular homeostasis and non-cell-autonomous virus infection (Pattingre et al., 2008; Yuan, 2008). Administration of the necroptosis inhibitor Nec-1, provides significant tissue protection and functional improvements in a variety of acute tissue injuries in mouse models of brain and heart ischemia/reperfusion injury, by mechanisms that are clearly distinct from the inhibition of apoptosis (Degterev et al., 2005; Smith et al., 2007). Finally, PARP-1 inhibitors provide clear protection in mouse models of ischemia/reperfusion injury (Martin et al., 2000; Thiemermann et al., 1997), inflammatory diseases (Miesel et al., 1995), neurodegeneration (Cosi and Marien, 1999) and diabetes (Pieper et al., 1999a). There does appear to be a degree of overlap between these different modes of cell death, and particularly between the necroptotic and PARP-1-mediated processes. Since PARP-1-mediated cell death is tightly associated with DNA damage, it is the focus of my studies and will be explained in the next section.

1.5.1. PARP-1-mediated Cell Death

Poly (ADP-ribose) polymerases (Pars) belong to a larger family of cell signaling enzymes that catalyze the transfer of polymers of ADP-ribose (PAR) from nicotinamide adenine dinucleotide (NAD) to acceptor proteins. Pars are involved in a number of cellular processes, such as DNA repair, programmed cell death, transcriptional regulation, telomere cohesion, mitotic spindle formation, intracellular trafficking, and energy metabolism (Schreiber et al., 2006). In humans, the Pars superfamily comprises 17 members. Among them, PARP-1, the DNA nick sensor enzyme, is rapidly activated in response to genotoxic stress (Ame et al., 2004). Upon DNA strand breaks, PARP-1 catalyzes the synthesis of PAR, using NAD as the sole substrate. PARP-1 cleaves NAD into nicotinamide and ADP-ribose, and covalently attaches PAR to itself and other suitable acceptors, such as histones (Dantzer et al., 2006). PARP-1 is required for DNA repair, functions as a structural component of chromatin, and contributes to the efficient maintenance of genome integrity and stability (Ding et al., 1992; Kim et al., 2004). PAR synthesized in response to DNA damage is rapidly degraded by an enzyme termed poly(ADP-ribose) glycohydrolase (PARG) (Juarez-Salinas et al., 1979). The PAR metabolic cycle is summarized in Figure 1.5.

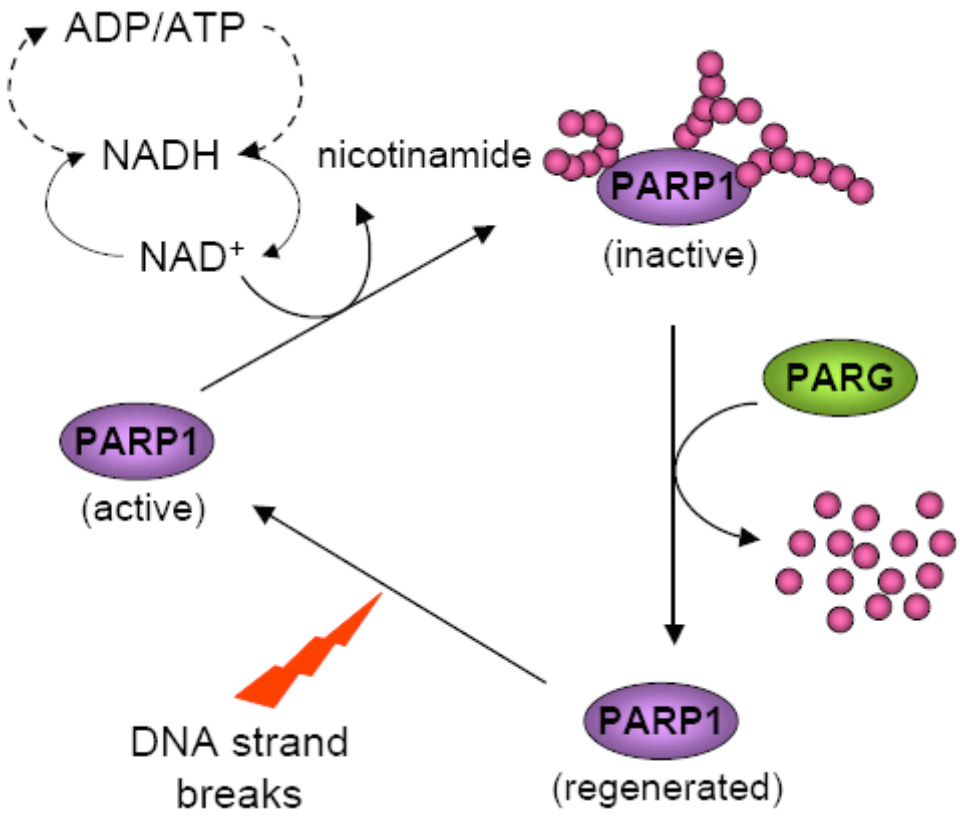

Figure 1.5. Metabolism cycle of PAR.

PARP1 catalyzes the synthesis of PAR using NAD as the sole substrate. PARP-1 cleave NAD into nicotinamide and ADP-ribose, and covalently attaches ADP-ribose polymers to itself and other target proteins. PARP-1 is inhibited when extensively modified by poly(ADP-ribosyl)ation. PAR are rapidly degraded by poly(ADP-ribose) glycohydrolase (PARG) to regenerate an active form of PARP-1. (●: ADP-ribose)

PARP-1 is involved in both DNA repair and programmed cell death, and therefore plays a crucial role in determining cell fate (Figure 1.6). For example, under mild to moderate genotoxic stress, PARP-1 facilitates DNA repair and cell survival by recruiting scaffolding proteins XRCC1, DNA ligase III, and polymerase beta, which together mediate base excision repair (Burkle et al., 2002; El-Khamisy et al., 2003). If DNA breaks are repaired, the damaged cells survive. Cells treated with PARP inhibitors are hypersensitive to DNA-damaging agents because of the inhibition of strand break rejoining. Early studies demonstrated that PARP inhibitors enhance the cytotoxic effect of DNA damage, leading to the development of numerous different PARP inhibitors as chemosensitizing or radiosensitizing drugs in cancer chemotherapy. However, excessive DNA damage triggers hyperactivation of PARP-1, resulting in the rapid depletion of cellular NAD and subsequent cell death (Pieper et al., 1999b). The mechanism of PARP-1-dependent cell death has been proposed to be due to energy depletion (Chatterjee and Thiemermann, 1998). More recent studies revealed that either pharmacological inhibition or genetic deletion of PARP-1 provides remarkable protection in experimental models of diseases, such as diabetes (Burkart et al., 1999; Pieper et al., 1999a), myocardial infarction (Bowes et al., 1999; Pieper et al., 2000), stroke (Szabo and Dawson, 1998), and neuronal ischemia (Eliasson et al., 1997; Endres et al., 1997). In addition, PARP inhibitors not only block necrotic cell death (Filipovic et al., 1999; Ha and Snyder, 1999), but appear to shift the mode of cell death form necrosis to apoptosis in oxidant-stressed endothelial cells (Walisser and Thies, 1999).

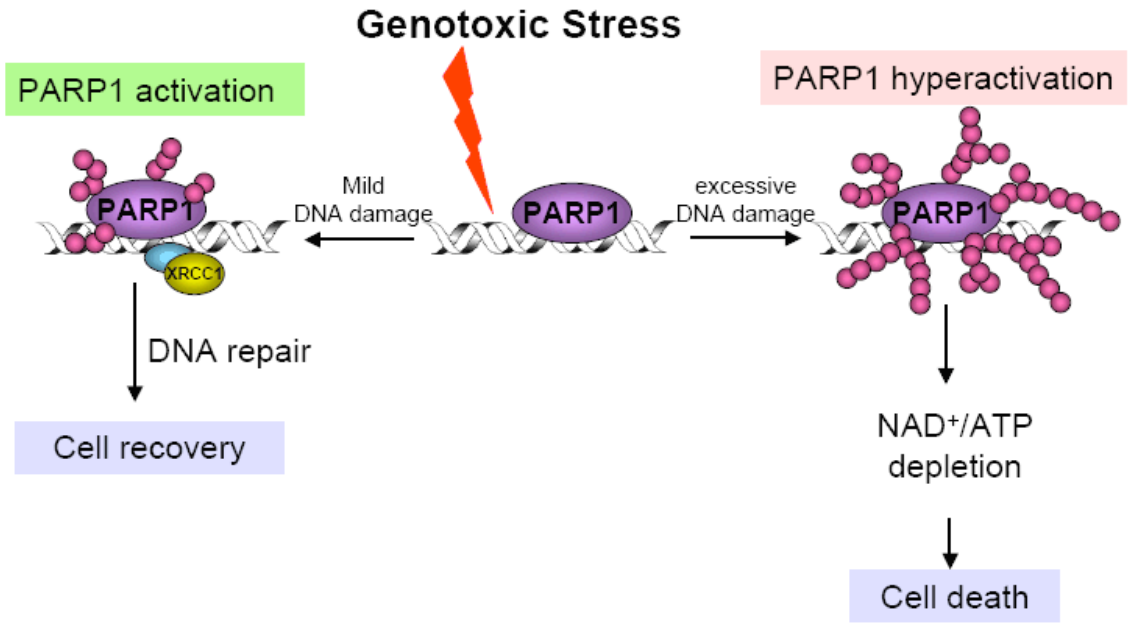

Figure 1.6. PARP-1 in cell fate determination.

PARP-1 plays a pivotal role in both DNA repair and cell death. DNA strand breaks activate PARP-1 which mediates the synthesis of PAR. Upon mild genotoxic stress, PARP-1 mediates the repair of DNA strand breaks via the activation and recruitment of DNA repair enzymes, including scaffolding proteins (XRCC1), DNA ligases (DNA ligase III), and polymerases (DNA pol beta). However, wherein DNA damage is excessive, PARP-1 is hyperactivated. Over-activation of PARP-1 leads to depletion of intracellular energy (NAD and ATP), and therefore cells commit to die. (●: ADP-ribose)

Initial studies have revealed that 2-Br-*bis*-(GSyl)HQ-induced renal cell death was attenuated via the inhibition of PARP (Jeong et al., 1997a), suggesting that activation of PARP-1 may be involved in HQ-mediated cytotoxicity. However, the mechanism by which PARP-1 mediates renal cell death is unknown. Therefore, my research is designed to examine the PARP-1 signaling cascade in response to TGHQ-mediated renal cell death. In addition, TGHQ induces necrosis in renal epithelial cells (Ramachandiran et al., 2002), but apoptosis in hematopeic cells (Bratton et al., 2000). Whether inhibition of PARP-1 also shifts the mode of cell death mediated by TGHQ in HK-2 cells will also be investigated in Chapter 3.

PARP-1 activation transduces DNA damage into intracellular signals that activate various cell death pathways. In caspase-dependent cell death, PARP-1 is cleaved by caspases into two fragments. The cleavage of PARP-1 prevents extensive NAD consumption, and therefore facilitates apoptotic cell death. Additionally, inactivation of PARP-1 may also promote apoptotic cell death by inhibiting DNA repair following severe DNA injury. In contrast, in a caspase-independent manner, inhibition of PARP-1 may prevent cell death by inhibiting the release of apoptosis-inducing factor (AIF) from mitochondira. Mitochondrial AIF release is mediated by PAR, the product of PARP-1 activation. Following release from mitochondria AIF translocates to the nucleus where it causes chromatin condensation, large-scale DNA fragmentation, and ultimately necrosis-like cell death (Yu et al., 2006; Yu et al., 2002). AIF plays a key role in PARP-1-dependent neuronal cell death, and blocking AIF nuclear translocation is protective (Wang et al., 2004a). Caspase-dependent apoptotic cell death and PARP-1-dependent necrotic-like cell

death highlight the diversity in cell death signaling, and it is important to define the molecular and cellular cell death cascade for each death stimulus.

1.5.2. Ca^{2+}-mediated Cell Death

Oxidative stress can disrupt intracellular Ca^{2+} homeostasis leading to cell injury or even cell death (Bellomo et al., 1982; Ermak and Davies, 2002; Richter and Kass, 1991). In normal cells, cytosolic Ca^{2+} concentration range between 10-100 nM, whereas extracellular and endoplasmic reticulum (ER) Ca^{2+} concentrations reach millimolar levels (Duchen, 2000). Thus, a nearly 10,000-fold Ca^{2+} gradient exists across the plasma and ER membranes. Transport of Ca^{2+} across the plasma membrane is mediated through specific Ca^{2+} channels, including leak channels, ligand-gated channels and voltage-gated channels (Berridge et al., 2003; Marks, 1997). The inositol trisphosphate (IP_3) receptor mediates the release of Ca^{2+} from ER upon IP_3 binding (Hanson et al., 2004; Patterson et al., 2004). Oxidative stress mediates an increase in cytosolic Ca^{2+} concentration by triggering Ca^{2+} influx from either the extracellular environment and/or from ER, which results in the disruption of intracellular Ca^{2+} homeostasis and subsequent cellular injury (Feissner et al., 2009). Since quinone-thioethers are redox-active, and catalyze the generation of ROS, it is likely that TGHQ-mediated renal injury occurs through the disruption of intracellular Ca^{2+} homeostasis. In addition, previous studies revealing that chelation of intracellular Ca^{2+} with EGTA-AM causes a decrease in 2-Br-*bis*-(GSyl)HQ and 2-Br-6-(GSyl)HQ-mediated induction of the grow arrest gene *gadd153* (Jeong et al., 1996), is consistent with this hypothesis. Therefore the role of intracellular Ca^{2+} in

TGHQ-induced renal cell death will be investigated in Chapter 4. The following section will focus on various downstream effectors which contribute to Ca^{2+}-mediated cell death.

1.5.2.1.Calpain

Rapidly rising cytosolic Ca^{2+} concentrations lead to Ca^{2+} sensitive protein calpain activation, loss of lysomosal membrane integrity, and subsequent necrotic cell death (Harriman et al., 2002; Verkhratsky, 2007). Thus, calpains, a family of Ca^{2+}-activated cysteine proteases, contribute to necrotic cell death (Schanne et al., 1979). Physiologically, calpains play critical roles in proliferation, differentiation, migration and embryogenesis (Liu et al., 2004). Upon elevation of intracellular Ca^{2+} concentrations, calpains become activated and mediate disruption of the lysosomal membrane. Lysosomes contain over 80 types of hydrolytic enzymes, release of which into the cytoplasm results in degradation of cellular structures and cell death (Liu et al., 2004). Thus in Chapter 4, the role of calpain in TGHQ-induced cell death will also be investigated.

1.5.2.2. Mitochondrial Ca^{2+} Overload

Mitochondria play an important role in maintaining cellular ion homeostasis, indeed it is the second largest reservoir of cellular Ca^{2+} (Kroemer et al., 1997). The rapid accumulation of vast amounts of Ca^{2+} into mitochondria contributes to cell injury (Bernardi and Rasola, 2007; Vanlangenakker et al., 2008). Functioning mitochondria protect cells from Ca^{2+} overload by buffering intracellular Ca^{2+} concentrations in a membrane potential ($\Delta\Psi$)-dependent manner. Continuing elevations in cytosolic Ca^{2+}

induce a progressive increase in mitochondrial Ca^{2+} uptake, during which Ca^{2+} crosses the outer mitochondrial membrane primarily through the voltage dependent anion channel (VDAC) (Bathori et al., 2006; Rapizzi et al., 2002), and enters the inner mitochondrial membrane through a mitochondrial Ca^{2+} uniporter, and down an electrochemical gradient (Kirichok et al., 2004). Activation of both VDAC and the Ca^{2+} uniporter is Ca^{2+} dependent and is important for the control of intracellular Ca^{2+} homeostasis (Deryabina et al., 2004; Nicholls, 2005). Ca^{2+} export from mitochondria is mediated by the Na^{2+}/Ca^{2+} and H^{+}/Ca^{2+} exchangers (Bernardi, 1999). If the mitochondrial Ca^{2+} exchangers are overwhelmed, mitochondrial Ca^{2+} increases to levels sufficient to trigger a process termed the mitochondrial permeability transition (MPT) (Bernardi, 1999). In addition, increased Ca^{2+} in the mitochondrial matrix stimulates the activation of Ca^{2+} sensitive proteases which can cause inactivation of Ca^{2+} sequestering transport systems. This would further increase mitochondrial Ca^{2+} and Ca^{2+}-dependent protease activity in a continuous cycle, which eventually leads to the loss in the balance between mitochondrial Ca^{2+} import and export, and subsequent activation of the MPT (Brookes et al., 2004). Mitochondrial Ca^{2+} overload is one of the most important inducers of the MPT, which requires the formation of pores in the inner mitochondrial membranes, with a size exclusion limit of $\leq$1.5 kDa (Dong et al., 2006). A sustained MPT leads to loss of mitochondrial homeostasis, collapse of mitochondrial membrane potential, and lethal damage (Crompton, 1999; Lemasters et al., 2002). Several proteins, including the adenine nucleotide translocase (ANT), voltage-dependent anion channel (VDAC) and cyclophilin D, have been implicated in the formation of MPT pores (Crompton et al., 1998), and

MPT development is retarded by an inhibitor of cyclophilin D, cyclosporin A (Crompton et al., 1999; Waldmeier et al., 2003).

The ability of TGHQ to generate ROS raises several questions. Does TGHQ stimulate elevations in intracellular Ca^{2+} concentrations? Can TGHQ induce a collapse in the mitochondrial membrane potential, and if so can cyclosporine A protect against TGHQ-induced MPT and subsequent cell death? Studies described in Chapter 4 are designed to address these questions.

1.6. MITOCHONDRIA AND CELL DEATH

Mitochondria play a central role in maintaining cell viability by conserving cellular bioenergetics and ion homeostasis (Kroemer et al., 1997). Changes in mitochondrial membrane integrity are known to precede cell death via apoptosis or necrosis (Lemasters et al., 1998). Indeed, mitochondria play a pivotal role in most, if not all, modes of cell death.

There are three fundamentally different cell-death signals originating from mitochondria. The caspase-dependent pathway is initiated by the release of cytochrome c from mitochondria. Cytochrome c subsequently activates a number of caspases by facilitating apoptosome formation, resulting in classical apoptosis (Hengartner, 2000; Strasser et al., 2000). The second cell death pathway originating from mitochondria includes the release of AIF, which is triggered by the translocation of PAR from the nuclei to the cytosol. This caspase-independent cell death is associated with chromatin condensation and margination of (Susin et al., 1999). The third distinct mitochondrial cell death pathway is mediated by mitochondrial ROS/Ca^{2+} accumulation, which leads to

programmed necrotic cell death (Mattson, 2000; Nicotera et al., 1999). However, caspases, AIF and ROS/Ca^{2+}, can also feed back on mitochondria, affecting mitochondrial function, and triggering the release of other cell death factors. It is very likely that more than one of these three pathways can be activated simultaneously. Cell fate is then determined by the relative speed of each process. Defects in any step of the above pathways will result in a switch from one type of cell death to the other (Daugas et al., 2000; Leist et al., 1997).

1.6.1. Mitochondrial ROS and Antioxidant Defenses

Mitochondria are of the core of cellular energy metabolism, consuming nearly 90% of cellular oxygen to synthesize ATP via oxidative phosphorylation. During this process, electrons leak to O_2 through a chain of respiratory pumps and generate $O_2^{\bullet -}$, which is converted to H_2O_2 either by spontaneous dismutation or via mitochondrial SOD (Starkov, 2008). The mitochondrial inner member contains many iron and copper complexes, and can catalyze reactions between H_2O_2 and •OH (Murphy, 2009). Furthermore, mitochondrial Ca^{2+} overload can enhance ROS generation, trigger the formation of the permeability transition pore, and lead to lethal damage. Mitochondria are thus a significant source of intracellular ROS, and are particularly vulnerable to oxidative stress (Orrenius, 2007). ROS induce damage to nucleic acids, protein, and lipids. Mitochondrial DNA is more susceptible to oxidative damage than nuclear DNA because of the lack of protective histone proteins. Mitochondrial proteins can be oxidized and modified by nitration, resulting in loss of function of many metabolic enzymes. ROS also mediate lipid peroxidation and contribute to the disruption of mitochondrial membrane integrity.

The rate of mitochondrial ROS production is influenced by cellular metabolic state and the capacity of the mitochondrial antioxidant defense system.

The first-line defense against ROS-mediated mitochondrial injury comprises several antioxidant molecules, including mitochondrial superoxide dismutase (MnSOD), thioredoxin-2 (Trx-2), and peroxiredoxin III (PrxIII) (Chae et al., 1999a; Majima et al., 1998; Tanaka et al., 2002). Among these antioxidants, PrxIII is thought to contribute to the primary antioxidant defense in the mitochondria and is essential for mitochondrial homeostasis (Wonsey et al., 2002). PrxIII, located exclusively in the mitochondrion, is a member of the antioxidant family of thioredoxin-dependent peroxidases (Watabe et al., 1997). In the presence of Trx, Prx behaves as an antioxidant by catalyzing the reduction of H_2O_2 and peroxides (Hofmann et al., 2002). Upon oxidative stress, the redox-sensitive cysteine of one subunit of Prx is oxidized to sulfenic forms (Cys-SOH), which then reacts with a neighboring Cys-SH on the second subunit to form an intermolecular disulfide. Prx can be "over-oxidized" to sulfinic (Cys-SO_2H) or sulfonic forms (Cys-SO_3H) which subsequently lose their peroxidase properties (Figure 1.7) (Seo et al., 2000; Wagner et al., 2002; Wood et al., 2003b).

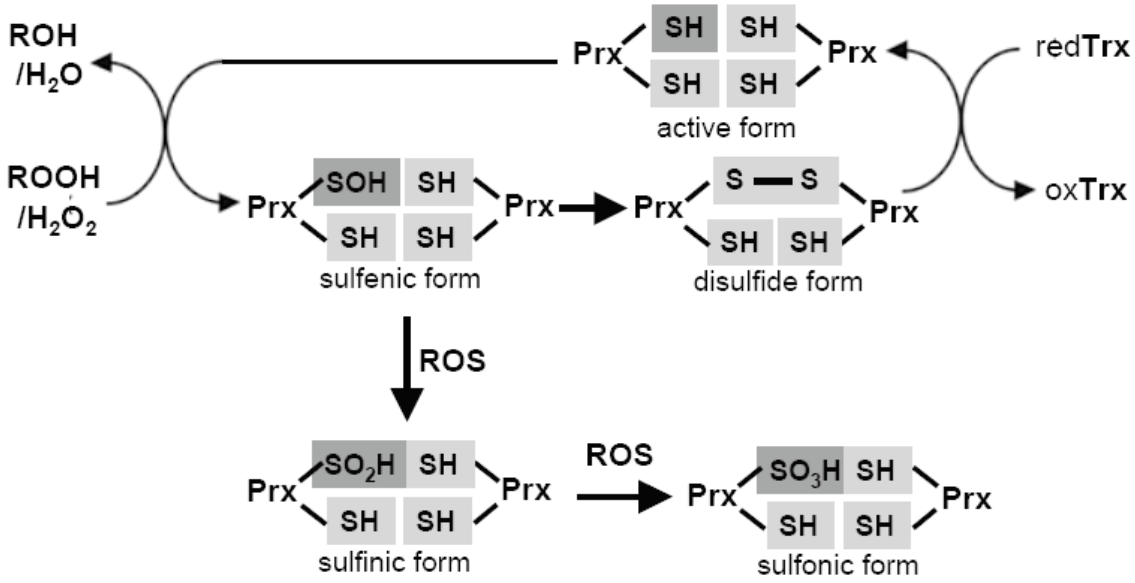

Figure 1.7. Catalytic cycles of Prx.

Prx catalyzes the reduction of peroxidase and H_2O_2, and is subsequently reduced by Trx-TR system. The active cysteine of Prx is oxidized to cysteinyl sulfenic acid (Cys-SOH), and then forms a disulfide with the other active cysteine which comes from the other subunit of the Prx homodimer. The disulfide is then reduced back to the Prx active thiol form by the Trx-TR system. However, under oxidative stress conditions, the sulfenic intermediate (Cys-SOH) can be easily over oxidized to sulfinic (Cys-SO_2H) or sulfonic (Cys-SO_3H) forms before it is able to form a disulfide. The reduction of the cysteinyl sulfinic or sulfonic acids is extremely slow.

Compared to MnSOD, PrxIII is more effective in protecting mitochondria against oxidative damage, because MnSOD catalyzes the dismutation of $O_2^{\bullet -}$ resulting in an increased production of H_2O_2. Moreover, PrxIII protects the cell not only by removing MnSOD-generated H_2O_2 but also by detoxifying peroxynitrite. PrxIII therefore regulates physiological levels of H_2O_2 and plays and important role in the mitochondrial antioxidant defense system. Loss of PrxIII function upon oxidation results in a further compromised antioxidant capacity, which is exacerbated the ongoing oxidative stress. Two-dimensional gel electrophoresis studies in our laborytory revealed that TGHQ induces significant changes in the expression pattern of PrxIII. Three spots with altered mobility were identified by mass spectrometry as PrxIII in cells exposed to TGHQ, suggesting that TGHQ induces modification of PrxIII probably via the oxidation of cysteine residues (Dong, 2004). A goal of the present studies is therefore to determine exactly how PrxIII is modified by TGHQ, and its role in TGHQ-induced renal cell death.

1.7. STATEMENT OF PURPOSE

HQ is ubiquitously present in the environment, and is metabolized to various GSH conjugates which contribute to HQ-mediated nephrotoxicity and nephrocarcinogenicity. Among all the HQ-derivatives, TGHQ is one of the most reactive metabolites. Although previous studies have focused on quinone-thioether-mediated renal toxicity in various cell and animal models, the precise mechanism of cytotoxicity remains unclear. Therefore studies described in this thesis were designed to determine the molecular and cellular mechanisms of TGHQ-mediated cytotoxicity in renal epithelial cells.

TGHQ induces toxicity either via the generation of ROS and/or via the covalent adduction of critical cellular macromolecules. Although prior studies from our laboratory revealed that TGHQ induces ROS-dependent necrotic cell death in LLC-PK1 cells, the effects of quinone-thioethers on human renal cells was not determined. The first aim of this study was therefore to characterize the cytotoxic effects of TGHQ in a human proximal tubule epithelial cell line, HK-2. HK-2 cell, derived from normal human adult kidney, is a more relevant *in vitro* model to study HQ and HQ-thioether-mediated nephrotoxicity. Moreover, if ROS generation is an essential element in TGHQ-induced cell death, TGHQ exposed HK-2 cells also provides a model for delineating the molecular mechanisms by which ROS mediate renal injury.

Quinone-thioethers induce rapid ROS-dependent DNA stand breaks in both LLC-PK1 cells (Jeong et al., 1996). Studies on the initial molecular response to DNA damage demonstrate a rapid activation of the DNA sensor protein PARP-1, the activation of which either facilitates DNA repair or induces programmed cell death, depending on the intensity of PAR formation. Because the inhibition of PARP attenuates quinone-thioether-mediated histone H3 phosphorylation and subsequent cell death in LLC-PK1 cells (Jeong et al., 1997a; Tikoo et al., 2001), we hypothesized that TGHQ induces substantial PARP-1 activation which exacerbates TGHQ-induced toxicity. In addition, PARP inhibitors not only block necrotic cell death (Filipovic et al., 1999; Ha and Snyder, 1999), but appear to shift the mode of cell death form necrosis to apoptosis in oxidant-stressed endothelial cells (Walisser and Thies, 1999). Previous findings from our laboratory demonstrated that TGHQ induces necrosis in LLC-PK1 cells (Ramachandiran

et al., 2002), but apoptosis in HL-60 cells (Bratton et al., 2000), suggesting that TGHQ-mediated cell death is context dependent. The next Specific Aim (Chapter 3) was therefore designed to determine whether inhibition of the death signaling molecule PARP-1 could modify the mode of cell death mediated by TGHQ in HK-2 cells.

A combination of stress-signaling pathways are activated during ROS-mediated cell injury (Martindale and Holbrook, 2002). One such pathway is indicated by changes in intracellular Ca^{2+}. Quinone-thioethers induced DNA damage in LLC-PK1 cells is accompanied by rapid cell cycle arrest (Jeong et al., 1996). Moreover, activation of the grow arrest and DNA damage inducible gene *gadd153* is significantly decreased in the presence of the intracellular Ca^{2+} chelator, EGTA-AM, suggesting that Ca^{2+} signaling influences the TGHQ-mediated stress response (Jeong et al., 1996). The role of intracellular Ca^{2+} in TGHQ-induced renal injury was therefore investigated in the HK-2 cell model (Chapter 4). A variety of Ca^{2+} effectors play important roles in Ca^{2+}-mediated cellular injury. For example, calpains, a family of Ca^{2+}-activated cysteine proteases, are activated upon intracellular Ca^{2+} elevation and contribute to cell death by triggering the release of a number of hydrolytic enzymes from lysosomes (Schanne et al., 1979). Rises in cytosolic Ca^{2+} levels also lead to mitochondrial $Ca2^{+}$ overload, resulting in mitochondrial membrane potential collapse and subsequent cell death. Although Ca^{2+} is recognized as playing a key role in cellular damage, the precise mechanisms by which Ca^{2+} contribute to cell death remain a subject of debate. Therefore, further investigations into the Ca^{2+} signaling pathways involved in TGHQ-mediated cell death are an important component of this dissertation (Chapter 4).

Because mitochondria are essential in maintaining cell viability by conserving cellular energy and ion homeostasis (Kroemer et al., 1997), damage to mitochondria may induce cell death via apoptosis or necrosis (Lemasters et al., 1998). In addition, mitochondria are particularly vulnerable to oxidative stress. Therefore, mitochondrial antioxidant defense systems are extremely important in protecting the cellular respiratory chain against ROS-mediated damage. The antioxidant PrxIII contributes to the primary antioxidant defense in mitochondria. Loss of PrxIII function upon oxidation results in a further exacerbation of mitochondrial oxidative stress. TGHQ stimulates significant mobility shifts of PrxIII revealed by two-dimensional gel electrophoresis, suggesting PrxIII is modified in response to TGHQ (Dong, 2004). TGHQ induces modification of PrxIII probably via the oxidation of its two conversed redox-active cysteine residues, C108 and C229, to sulfonic or sulfenic derivatives. To further examine the role of PrxIII in TGHQ-mediated cellular toxicity, we constructed a cysteine double mutant of PrxIII (C108S/C229S), and determined its effects in cells exposed to TGHQ (Chapter 5).

In summary, this dissertation focuses on dissecting the cellular signaling pathways involved in TGHQ-mediated toxicity in human renal epithelial cells. Because a variety of chemicals-induced renal injury and renal diseases are ROS dependent, an understanding of ROS-induced signaling pathways in human renal cells will assist in the discovery of potential novel therapeutics.

CHAPTER 2: MATERIALS AND METHODS

2.1. MATERIALS

2.1.1. Chemicals and Reagents

TGHQ was synthesized and purified in our laboratory as previously described (Lau et al., 1988a). TGHQ is nephrotoxic and nephrocarcinogenic in rats and therefore must be handled with protective clothing in a ventilated hood. U0126, SB202190, SB203580, PD15605, calpeptin, calpain inhibitor III, Cyclosporin A, PJ34, and BAPTA-AM were obtained from CalBiochem (La Jolla, CA). DAPI (4',6-diamidino-2-phenylindole, dihydrochloride), JC-1 (5,5'6,6'-tetrachloro- 1,1',3,3'-tetraethyl-benzimidazolylcarbocyanine iodide), H_2DCFDA (2´,7´-dichlorodihydrofluorescein diacetate), and Fura-2-AM [5-Oxazolecarboxylic acid,2-(6-(bis(carboxymethyl)amino)-5-(2-(2-(bis(carboxymethyl) amino)-5-methylphenoxy)ethoxy)-2-benzofuranyl)-, pentapotassium salt] were purchased from Invitrogen (Carlsbad, CA). All other chemicals were purchased from Sigma (St. Louis, MO).

2.1.2. Antibodies

Antibodies for phospho-histone H2AX (Ser139), H2AX, phospho-ERK1/2, ERK1/2, phosphor-p38 MAPK, p38 MAPK, phosphor-JNK1/2, JNK1/2, PARP-1, caspase-3 and cleaved caspase-3 were purchased from Cell Signaling Technology, Inc. (Danvers, MA). The antibody for poly(ADP-ribose) was from Biomol International (Plymouth Meeting, PA). Antibodies for peroxiredoxin III and peroxiredoxin-SO_3H were purchased from Abcam (Cambridge, MA). Goat anti-rabbit IgG Alexa 488 was

purchased from Invitrogen (Carlsbad, CA). All other secondary antibodies were obtained from Santa Cruz Biotechnology (Santa Cruz, CA).

2.1.3. Cell Lines and Culture Medium

HK-2 cells, an immortalized proximal tubule epithelial cell line from normal adult human kidney, and LLC-PK1 cells, a renal proximal tubule epithelial cell line derived from the New Hampshire Mini-Pig, were obtained from the American Type Culture Collection (Manassas, VA). HK-2 cells were cultured in Keratinocyte serum free medium (K-SFM) supplemented with 0.05 mg/ml bovine pituitary extract and 5 ng/ml epidermal growth factor (EGF), and LLC-PK1 cells were maintained in Dulbecco's modified Eagle's medium (DMEM) containing 10% fetal bovine serum (FBS).

2.2. METHODS

2.2.1. Synthesis and Purification of TGHQ

TGHQ was synthesized and purified according to established protocols (Lau et al., 1988a). Briefly, an equal volume of 167 mM GSH solution was added drop wise to a 167 mM 1,4-benzoquinone solution with stirring. The reaction mixture was incubated at room temperature with constant stirring for an additional 30 min, and then extracted twice with 3 volumes of ethyl acetate to remove the residual 1,4-benzoquinone and HQ formed by reduction during the reaction. The aqueous phase was collected, rotoevaporated, and lyophilized. The resulting light green powders containing multi-GSH-HQ conjugates were purified by HPLC. The crude compound was dissolved in 1% acetic acid in water, and injected onto a Beckman ODS reverse phase semi-preparative

column. The compound was eluted with methanol/acetic acid/water (10:89.1:0.9) at a flow rate of 3 ml/min. Fractions containing TGHQ were collected, rotoevaporated, and lyophilized. The purity of TGHQ (> 98%) was confirmed by HPLC analysis.

2.2.2. Cell Culture and Treatment Regimen

HK-2 and LLC-PK1 cells were maintained at 37°C in a humidified atmosphere of 5% CO_2, and subcultured every 3 days at 90% confluence. Cells were plated in 96-well, 24-well, 6-well, 4-well plates, or in100 mm dishes, and grown to ~80 % confluence before treatment. Cells were then washed twice, and treated with various agents in DMEM containing 25 mM HEPES [4-(2-hydroxyethyl)-1-piperazineethanesulfonic acid].

2.2.3. Plasmid Construction

The coding region of human PrxIII was subcloned in the vector pBudCE4.1 (Invitrogen, Carlsbad, CA) as a PCR fragment by using the *Hind*III/*Bam*HI sites. This recombinant plasmid was used as a template for site direct mutagenesis. The dominant negative mutant (C108S, C229S) was generated using QuikChange® II Site-Directed mutagenesis kit (Stratagene, La Jolla, CA). Clones containing the desired mutations were confirmed by DNA sequencing.

2.2.4. Transfection

LLC-PK1 cells were seeded in 24-well plates at a density of 1×10^4 cells/well and grown for 16 hr (50 % confluence). Cells were transiently transfected with wild-type PrxIII, dominant negative PrxIII (C108S, C229S), or empty vectors pBudCE4.1, using

Lipofectamine™ 2000 Transfection Reagent (Invitrogen, Carlsbad, CA) according to the manufacturer's instructions. Cells were initially incubated with a mixture of DNA, transfection reagent, and DMEM at 37°C for 4 hr, and then the medium changed to DMEM containing 10% FBS, and the cells incubated for a further 24 hr before treatment.

2.2.5. Neutral Red Cell Viability Assay

To determine the viability of LLC-PK1 cells after exposure to TGHQ, Neutral Red uptake was determined as previously described (Mertens et al., 1995). Briefly, cells were seeded in 24-well plates at a density of 1×10^4 cell/well and cultured to 80% confluence. Cells were washed twice and treated with various concentrations of TGHQ in DMEM containing 25 mM HEPES. After treatment, cells were washed twice and incubated with neutral red (0.25 mg/mL) dissolved in DMEM with 25 mM HEPES at 37°C for 1 hr. Cells were then washed with washing/fixation solution (1% formaldehyde and 1% calcium in water). Neutral red was extracted with extraction solution (1% acetic acid in 50% ethanol), and measured with a spectrophotometer at a wavelength of 540 nm. The absorbance of treated samples was compared to control samples, and expressed as % of control.

2.2.6. Mitochondrial Dehydrogenases Cell Viability Assay

To determine the viability of HK-2 cells after treatment with various agents, cells were seeded in 96-well plates at a density of 1×10^4 cells/well, and grown to 80% confluence. Cells were then washed twice with DMEM, without phenol red, containing

25 mM HEPES and treated with TGHQ with or without various inhibitors. Cell viability was assessed with the mitochondrial dehydrogenase activity assay according to the manufacture's instructions (Promega, Madison, WI), in which a tetrazolium compound, 3-(4,5-dimethylthiazol-2-yl)-5-(3-carboxymethoxyphenyl)-2-(4-sulfophenyl)-2H-tetrazolium (MTS), is reduced into a formazan product. After incubation with TGHQ, cells were washed twice with DMEM/HEPES, and then 20 μl MTS solution was added to 100 μl DMEM/HEPES and incubated for 2 hr at 37˚C. The absorbance of the formazan at 490 nm was measured directly from 96-well plates using a microplate reader.

2.2.7. Measurement of ROS Generation

Formation of ROS was measured *via* the reduction of non-fluorescent H_2DCFDA to fluorescent 2',7'-dichlorofluorescein (DCF) with live cell imaging via confocal microscopy. HK-2 cells were seeded on Delta T dishes (Bioptech, Butler, PA) at 1×10^5 cells/dish and cultured for 24 hr. Cells were incubated with 10 μM H_2DCFDA for 30 min before exposure to TGHQ, and then washed with DMEM/HEPES and treated with TGHQ (400, 800 μM) in the presence or in the absence of various inhibitors. Cells were imaged using a Zeiss LSM 510 confocal microscrope (Carl Zeiss Microimaging Inc., Thornwood, NY) with a 40 × dipping lens. During the experiment, culture dishes were maintained at 37˚C by attachment to a Delta TC3 temperature controller (BiopTechs, Butler, PA). Following exposure of cells to TGHQ, images were captured every 5 min for a total of 25 min. Changes in the fluorescence intensity of H_2DCFDA were analyzed by software available with the Zeiss confocal microscope.

2.2.8. Histones Extraction

HK-2 cells were washed and lysed in ice-cold low-salt buffer (10 mM Tris·HCl [pH 7.4], 10 mM NaCl, 2.5 mM EDTA) with 0.25 mM sucrose, 1% Triton X-100, 5 mM sodium pyrophosphate, 10 mM sodium glycerophosphate, 50 mM NaF, 1 mM Na_3VO_4, 1 mM PMSF and Complete™ protease inhibitor tablet. Histones were extracted with 0.25 M HCl overnight at 4˚C and then precipitated in 20% trichloroacetic acid on ice for 1 hr. The resulting pellet was washed with 0.25 M HCl in acetone and finally with acetone only. Pellets were dried in air and subjected to Western blot analysis.

2.2.9. Western Blot Analysis

Approximately 1×10^6 cells were lysed in buffer containing 20 mM Tris·HCl (pH7.4), 150 mM NaCl, 1 mM Na_2EDTA, 1 mM EGTA, 1% Triton X-100 as well as 5 mM sodium pyrophosphate, 10 mM sodium glycerophosphate, 50 mM NaF, 1 mM Na_3VO_4, 1 mM PMSF and complete™ protease inhibitor tablet (Roche, Indianapolis, IN). Following sonnication, cell lysates were centrifuged to remove cell debris. Protein concentrations were determined with detergent-compatible reagent (Bio-Rad Laboratories, Hercules, CA). Samples were incubated with sample buffer (125 mM Tris-HCl [pH 6.8], 86 mM 2-mercaptoethanol, 4% SDS, 10% glycerol [vol/vol], and 0.2 mg/ml bromophenol blue) for 5 min at 100˚C, and then resolved in 10% SDS-polyacrylamide gels. After electrophoresis, proteins were transferred to polyvinylidene fluoride (PVDF) Immobilon-P membranes (Millipore, Billerica, MA). Membranes were

stained with 0.2% Ponceau S to assure equal loading of samples. After blocking with 5% non-fat milk in Tris-buffered saline with 0.5% Tween 20 (TBS-T), membranes were incubated with primary antibody overnight at 4˚C and then incubated with secondary antibody coupled with the horseradish peroxidase for 1 hr at room temperature. Immunoblots were developed with enhanced chemoluminescence (ECL) reaction (Amersham, Piscataway, NJ) and exposed to X-ray film.

2.2.10. Two-Dimensional Gel Eletrophoresis

LLC-PK1 cells (1×10^6) were treated, washed in phosphate buffered saline (PBS), centrifuged, and resuspended in 100 μL of a modified RIPA buffer containing 50 mM Tris-HCl, pH 7.5, 150 mM NaCl, 1% NP-40, 0.5% sodium deoxycholate, 0.5% Triton X-100, and 10 mM EDTA. The cells were subjected to three cycles of freezing and thawing, followed by sonication (3 × 15s). Cell lysates were then centrifuged at 14,000×g for 15 min at 4°C. To remove DNA and RNA, samples were treated with DNase and RNase, followed by overnight acetone precipitation at –20°C. The protein pellet (100 μg) was resuspended in 185 μL of rehydration buffer, and incubated at room temperature for 1 h for complete protein solubilization. The protein mixture was subsequently centrifuged at 15,000×g for 30 min at ambient temperature, and the supernatant was loaded onto an 11 cm focusing tray. 2-D SDS-PAGE was performed using a Bio-Rad PROTEAN IEF Cell (Hercules, CA). A pre-cast IPG dry strip (pH 3-10) was layered onto the protein mixture (100 μg/sample) with the gel side down, and covered with mineral oil. After rehydration for 12 h at 50 V, the focusing was carried out automatically with the following program: 250 V for 15 min, from 250 V to 5,000 V for

2.5 h, and a final focusing step at 8000 V for 55000 VH. Focused IPG strips were equilibrated in 5 mL of equilibration solution (150 mM Tris-HCl, pH 8.8, 6 M urea, 30% v/v glycerol, 2% SDS with 2.5% DTT added for the first 10 min and 2% iodoacetamide added for the last 10 min). SDS-PAGE was carried out using a pre-cast Criterion 8-16% gradient gel in a Criterion Cell at 20 V for 10 min, and then at 200 V for 45 - 55 min. Gels were then fixed in 10% methanol-7% acetic acid for 40 min, stained with SYPRO Ruby protein stains (Bio-Rad) overnight, and finally destained in 10% methanol-7% acetic acid for 1 h. Images of stained 2-D gels were taken on a Vistra FluorImager SI (Amersham Phamacia Biotech, Piscataway, NJ), and analyzed using PDQUEST software package (Bio-Rad).

2.2.11. Immunofluorescent Staining

HK-2 cells were plated on cover slides in 6-well plates at a density of 2×10^5 cells/well and grown for 24 hr (~80 % confluence) before treatment. Cell monolayers were treated, rinsed twice with ice-cold phosphate buffered saline (PBS), and fixed with 4% para-formaldehyde for 15 min at room temperature. Cells were then washed three times with PBS and permeabilized with acetone for 10 min at -20˚C. Subsequently, monolayers were blocked with blocking solution containing 10% goat serum and 1% bovine serum albumin (BSA) in PBS at room temperature for 1 hr and washed with PBS three times. Cells were incubated with anti-phospho-H2AX in 1% BSA in PBS at 4˚C overnight, washed three times with PBS, and then incubated with goat anti-rabbit IgG Alexa 488 in 1% BSA in PBS at room temperature for 1 hr. Cells on the cover slides were washed three times in PBS and mounted for 20 min with Prolong gold antifade

reagent with 4'-6-diamidino-2-phenylindole (DAPI), at room temperature and viewed under a fluorescent microscope.

2.2.12. Annexin-V/PI Staining and Flow Cytometry

HK-2 cells were cultured on 100 mm^2 dishes at 1×10^6 cells/dish. Cells were treated with chemicals with or without inhibitors 24 hr after (~80% confluence) seeding. Cells were then trypsinized and washed with PBS. Subsequently, cells were incubated in 100 μl binding buffer (10 mM HEPES [pH 7.4], 140 mM NaCl and 2.5 mM $CaCl_2$) containing 20 μl Annexin V-FITC (Beckman Coulter, Inc., Fullerton, CA) and 10 μg/ml PI (Propidium Iodide) for 15 min in the dark. Cells were analyzed immediately after incubation by flow cytometry.

2.2.13. Determination of Total NAD Content

Cells were seeded on 35 mm^2 dishes at 2×10^5 cells/dish and cultured for 24 hr. Cells were pretreated with or without various inhibitors for 30 min before TGHQ treatment. Total intracellular NAD concentrations were extracted by addition of 1.0 M $HClO_4$ to dishes of cells on ice. Cell extracts were neutralized to pH 7.0 by addition of 2 M KOH/0.66 M KH_2PO_4. NAD concentrations were determined by enzymatic cycling assays as described (Jacobson and Jacobson, 1997).

2.2.14. DNA Fragmentation Analysis

Apoptotic DNA fragmentation in HK-2 cells was determined using the Quick Apoptotic DNA Ladder Detection Kit (Invitrogen, Carlsbad, CA). Briefly, cells were treated with 400 μM TGHQ with or without pretreatment of PJ34 (10 μM) for 30 min.

Medium containing TGHQ was replaced by normal culture medium after 4-hr TGHQ treatment. After 24 hr incubation, cells were trypsinized, harvested by centrifugation and then washed with PBS. DNA fragments were extracted according to the manufacturer's instructions. Finally, DNA fragments were visualized following electrophoresis on a 1% agarose gel.

2.2.15. Determination of Mitochondrial Membrane Potential

HK-2 cells were seeded at 2×10^5 cells per 6-well plate, and allowed to grow for 24 h. Log-phase cells were pretreated with or without inhibitors followed by TGHQ exposure. Cells were trypsinized, resuspended in 5 μg/ml JC-1 and incubated in a 37°C humidified incubator with 5% CO^2 for 15 min. After the staining, cells were washed with PBS and then analyzed via flow cytometry at the Arizona Cancer Center.

2.2.16. Live Cell Imaging of Intracellular Ca^{2+}

HK-2 cells were plated on collagen coated cover slides in 4-well plates at a density of 2×10^4 cells/well and grown for 48 hr (~80% confluence) before measurement. Cells were rinsed once with DMEM without phenol red containing 25 mM HEPES, and then loaded with the Ca^{2+}-sensitive fluorescent indicator, Fura-2-AM (5 μM), in DMEM/HEPES for 45 min at room temperature. Cells were rinsed once in DMEM/HEPES and incubated for an additional 20 min to allow for hydrolysis of the AM-ester. Cells were treated with various concentrations of TGHQ in the presence or in the absence of inhibitors. Cells were imaged with Olympus IX70 microscope after alternating excitation at 340 and 380 nm by a 75 W Xenon lamp linked to a Delta Ram V

illuminator (Photon Technologies Inc. (PTI), Monmouth Junction, NJ) and a gel optic line. Images of emitted fluorescence above 505 nm were recorded by an ICCD camera. The imaging system was under software control (ImageMaster, PTI). Images were collected after the indicated treatments and then fluorescence intensity of fold increase in Fura-2 were analyzed. Intracellular Ca^{2+} concentrations were calculated by ratiometric analysis of Fura-2 fluorescence (Grynkiewicz et al., 1985).

2.3. STATISTICAL ANALYSIS

All data are expressed as mean ± standard error. Mean values were compared using a post-hoc Student Newman Kuel's test. $p<0.05$ was considered to be statistically significant.

CHARPTER 3: PARP-1 HYPERACTIVATION CONTRIBUTES TO TGHQ-INDUCED NECROTIC CELL DEATH

3.1. INTRODUCTION AND RATIONALE

Mechanisms of cell death are usually classified into two pathways, apoptosis and necrosis. Necrosis typically occurs in response to toxic injury, including that induced by ROS. The generation of ROS has been implicated in the pathogenesis of renal ischemia/reperfusion injury, and many other pathological conditions. DNA strand breaks caused by ROS lead to the activation of PARP-1, the excessive activation of which results in the depletion of both NAD and ATP (Pieper et al., 1999b). It has been suggested that depletions in NAD and ATP in response to DNA damage contribute to cell death as a consequence of deficits in energy stores (Chatterjee and Thiemermann, 1998).

Although necrosis has generally been considered a passive process, it is now evident that necrosis is also tightly regulated. Recognition of regulated necrotic programmed cell death has important implications for human health and disease. One of the mediators of necrotic cell death has been revealed as poly (ADP-ribose) polymerase (PARP)-1. PARP-1 is a protein involved in a number of cellular processes, including transcriptional regulation, mitotic spindle formation, energy metabolism, DNA repair, and programmed cell death. PARP-1 is rapidly activated in response to DNA damage. Upon DNA strand breaks, PARP-1 catalyzes the synthesis of poly(ADP-ribose) using NAD as the sole substrate. PARP-1 cleaves NAD into nicotinamide and ADP-ribose, and covalently attaches ADP-ribose polymers to itself and other nuclear proteins such as

histones and various transcription factors. PARP-1 is inhibited when extensively modified by poly(ADP-ribose). PAR polymers are rapidly degraded by poly(ADP-ribose) glycohydrolase (PARG) to regenerate an active form of PARP-1.

Because inhibition of PARP-1 activity or PARP-1 gene deletion can prevent both ATP depletion and the induction of necrosis, it has been suggested that PARP-1-meidated necrosis is an "active" rather than a passive process (Ha and Snyder, 1999). PARP-1-mediated cell death represents a mechanism of cell death that extends beyond the classic apoptosis/necrosis descriptors of cell death. Inhibitors of PARP protect against hydrogen peroxide mediated cell death (Cristovao and Rueff, 1996). Deletion of PARP also protects against NMDA-receptor activated neurotoxicity (Eliasson et al., 1997; Endres et al., 1997), myocardial ischemia (Zingarelli et al., 1998), inflammation elicited by a variety of mediators (Oliver et al., 1999; Szabo et al., 1997; Zingarelli et al., 1999), and streptozocin-induced diabetes (Burkart et al., 1999; Masutani et al., 1999; Pieper et al., 1999a). In all these models of cell death, the experimental evidence indicates that cell death occurs by necrosis (Ankarcrona et al., 1995; Kerr et al., 1972; Nicotera et al., 1997; Wyllie et al., 1980). Moreover, PARP inhibitors not only block necrotic cell death (Filipovic et al., 1999; Ha and Snyder, 1999), but appear to shift the mode of cell death form necrosis to apoptosis in oxidant-stressed endothelial cells (Walisser and Thies, 1999). This interpretation raises the question of whether the machinery exists with which the cell can switch the mode of cell death. The answer to this question has profound clinical implications. For example, in many clinical situations, such as inflammation, vascular stroke, and myocardial infarction, the predominant

mechanism of cell death appears to be necrotic. By extension, it has been predicted the PARP inhibitors may have therapeutic benefit (Ha and Snyder, 1999). Consistent with this hypothesis, PARP-1 inhibition or gene deletion attenuates tissue injury associated with stroke, myocardial infarct, and diabetic pancreatic damage (Eliasson et al., 1997; Endres et al., 1997; Zingarelli et al., 1998).

In the majority cases of PARP-mediated cell death, hyperactivation of PARP-1 promotes the translocation of AIF from the mitochondria to the nucleus (Hong et al., 2004; Kang et al., 2004; Yu et al., 2006; Yu et al., 2002). Mitochondrial AIF release is mediated by PAR and /or by the activation of JNK and p38 MAPK which lie downstream of PARP-1 hyperactivation (Kwon et al., 2008; Song et al., 2007; Takada et al., 2008; Xu et al., 2006; Yu et al., 2006). Following release from mitochondria AIF translocates to the nucleus where it causes chromatin condensation, large-scale DNA fragmentation, and ultimately cell death. A proposed mechanism of PARP-1-mediated cell death is illustrated in Figure 3.1. Pharmacological inhibition and genetic deletion of AIF produce markedly protective effects, suggesting that AIF appears to be a key regulator during PARP-1-mediated cell death (Slemmer et al., 2008; Wang et al., 2004a). However, the signal transduction pathways activated during the "commitment" phase of necrotic cell death are insufficiently characterized. We therefore investigated the mechanism of ROS mediated necrotic cell death in human renal proximal tubule epithelial HK-2 cells.

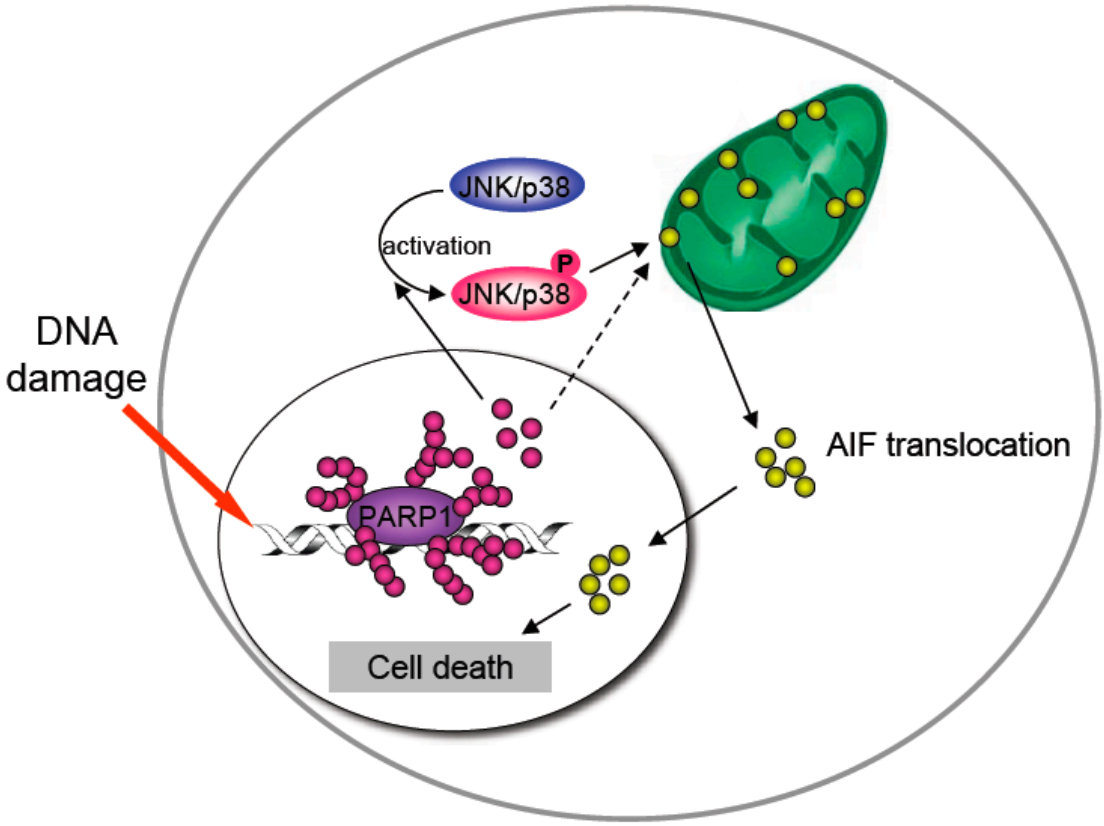

Figure 3.1. A proposed mechanism of PARP-1-mediated cell death.

PARP-1 hyperactivation mediates PAR formation and stimulates stress reponse kinases (JNK and p38 MAPK) activation, the activation of which signals the translocation of AIF from mitochondria to the nucleus, where it causes large-scale DNA fragmentation, chromatin margination, and ultimately cell death.

3.2. RESULTS

3.2.1. TGHQ induces time- and concentration-dependent increases in ROS generation and necrotic cell death.

TGHQ induced cytotoxicity in LLC-PK1 cells is dependent upon the formation of ROS (Mertens et al., 1995). It was therefore essential to determine the relative ability of TGHQ to generate ROS in HK-2 cells. Live cell imaging by confocal microscopy was used to visualize ROS generation with a fluorescent ROS indicator, H_2DCFDA. A significant time- and concentration-dependent increase in fluorescence intensity was observed in HK-2 cells (Figure 3.2A), and TGHQ-mediated ROS generation was completely inhibited by the scavenging of ROS by catalase (Figure 3.2B). At 800 μM TGHQ, increased generation of ROS was observed as early as 5 min after exposure. However at 400 μM TGHQ, there was a delay in the generation of fluorescence, perhaps reflective of the consumption of various reducing equivalents (GSH, NAD[P], etc) prior to overwhelming the cellular anti-oxidant response.

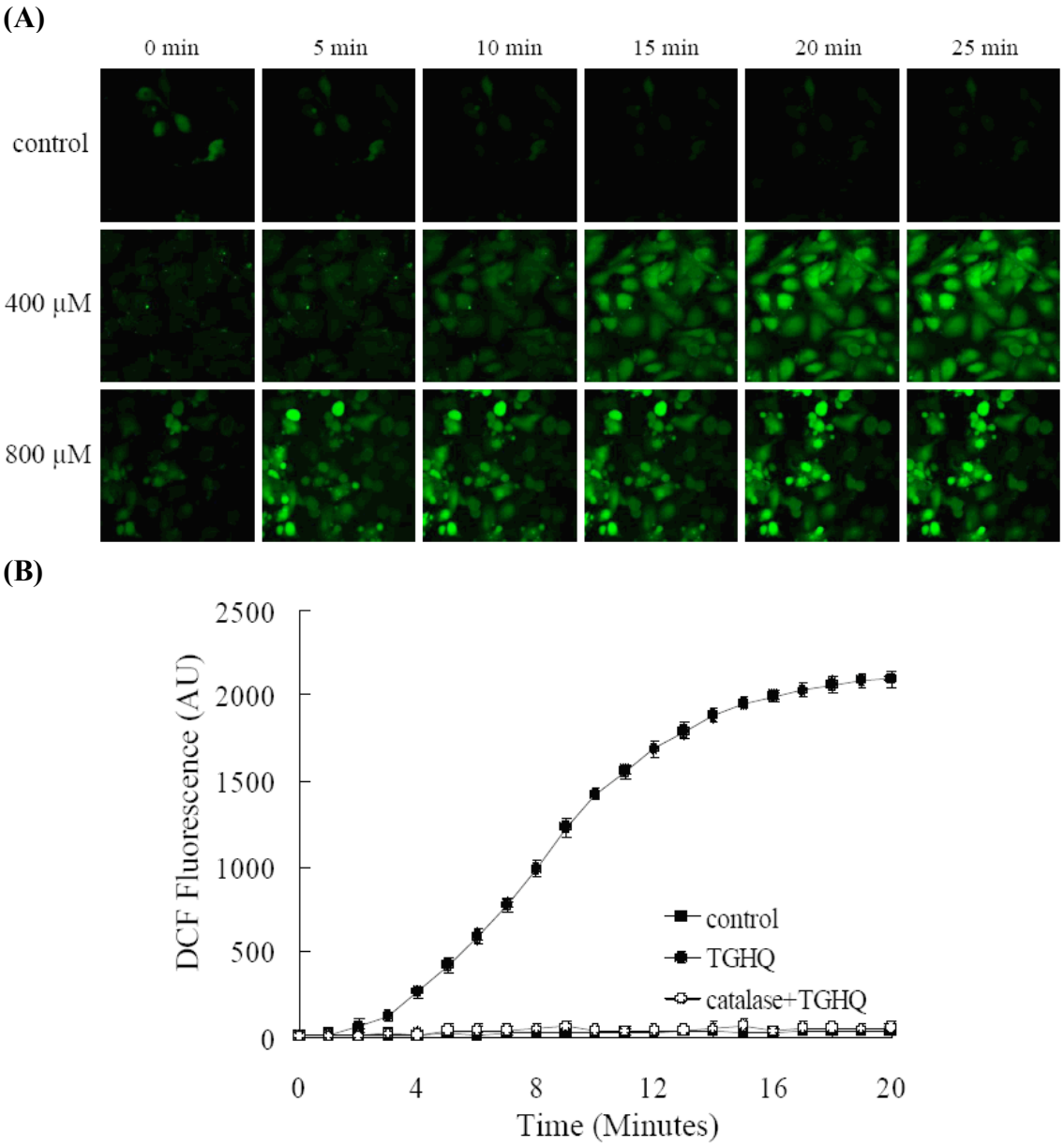

Figure 3.2. TGHQ induces ROS generation in HK-2 cells.

(A) Analysis of ROS was performed in the presence or absence of TGHQ. Cells were incubated with H_2DCFDA (10 µM) for 30 min at 37ºC. Cells were then treated with different concentrations of TGHQ and imaged by confocal microscopy. **(B)** To determine the level of ROS, cells were treated with 400 µM TGHQ in the presence of absence of catalase. An area of cells was selected and changes in fluorescence were recorded every 1 min during treatment, up to 20 min. Values represent the average of total cellular DCF fluorescence expressed as arbitrary units (AU). Data represent the mean ± standard deviation ($n \geq 3$).

TGHQ also induced a time-, and concentration-dependent decrease in HK-2 cell viability (Figure 3.3) determined by measuring mitochondrial dehydrogenase activity. In addition, TGHQ-mediated cell death was completely abrogated by the scavenging of ROS by catalase, suggesting that ROS was an essential factor for TGHQ-induced renal cell dath.

We subsequently investigated whether TGHQ (400 μM) induced apoptotic and/or necrotic cell death in HK-2 cells, as determined by flow cytometry (Annexin-V/PI staining) or Western blot analysis (caspase 3 activation). As a positive control for apoptosis, cells were treated with 50 μM cisplatin for 14 hr. Flow cytometric analysis permitted the resolution of apoptotic cells (Annexin-V^+/PI^-) from necrotic cells (Annexin-V^+/PI^+ and Annexin-V^-/PI^+). TGHQ-treated cell cultures exhibited a very low number of Annexin-V^+/PI^- cells (Figure 3.4) and no cleaved caspase 3 was detected in TGHQ-treated cells (Figure 3.5), indicating that there is no apoptotic HK-2 cell death associated with TGHQ treatment. In contrast, HK-2 cells treated with cisplatin for 14 hr exhibited significant levels of apoptosis, as indicated by both Annexin-V^+/PI^- staining (Figure 3.4) and caspase 3 cleavage (Figure 3.5).

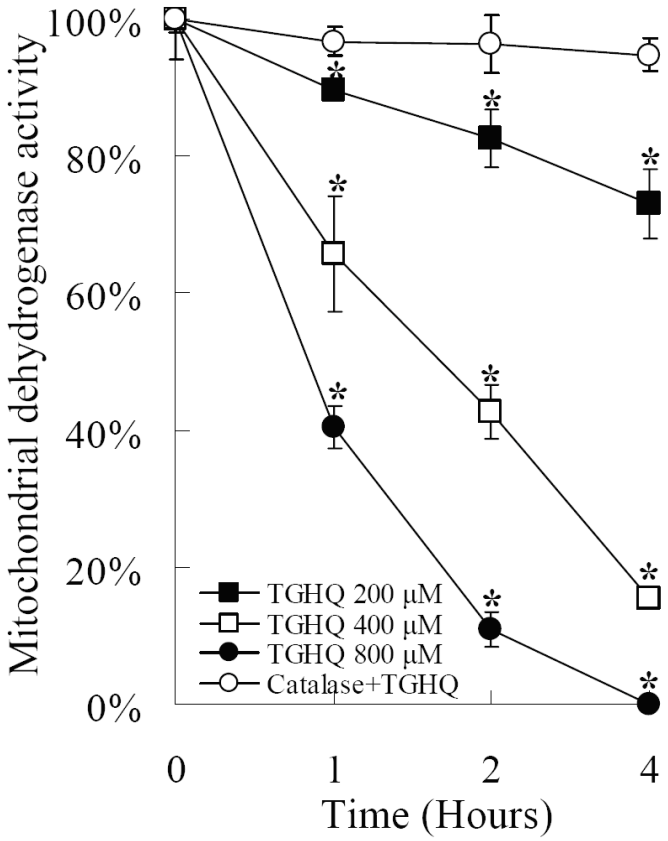

Figure 3.3. TGHQ induces cell death in HK-2 cells.

Cells were treated with different concentrations of TGHQ (200, 400, 800 μM) for different periods of time (1, 2, 4 hr) in the presence or absence of catalase (10 unit/ml). Cell viability was determined by measuring mitochondrial dehydrogenase enzyme activity in actively respiring cells. Formazan formation relative to untreated cells (% of control) represents cell viability after treatment. Data represent the mean ± standard deviation ($n \geq 3$). *: $p<0.05$.

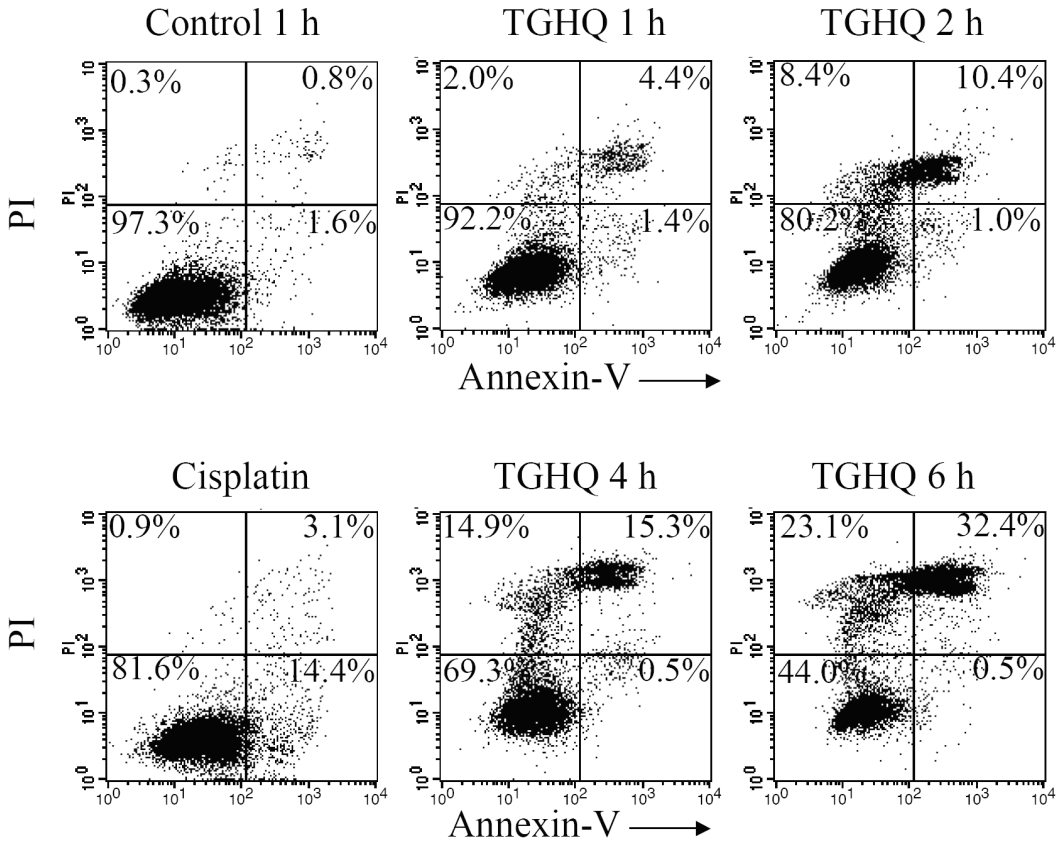

Figure 3.4. TGHQ mediates non-apoptotic cell death in HK-2 cells.

Flow cytometric analysis of necrotic and/or apoptotic cells was determined by Annexin-V/PI staining. Cells were exposed to cisplatin (50 μM) for 14 hr or TGHQ (400 μM) for various periods of time (1, 2, 4, 6 hr). Evaluation of both probes permitted the distinction of apoptotic cells (Annexin-V^+/PI^-) vs. necrotic cells (Annexin-V^+/PI^+ and Annexin-V^-/PI^+). Data shown are from a representative experiment.

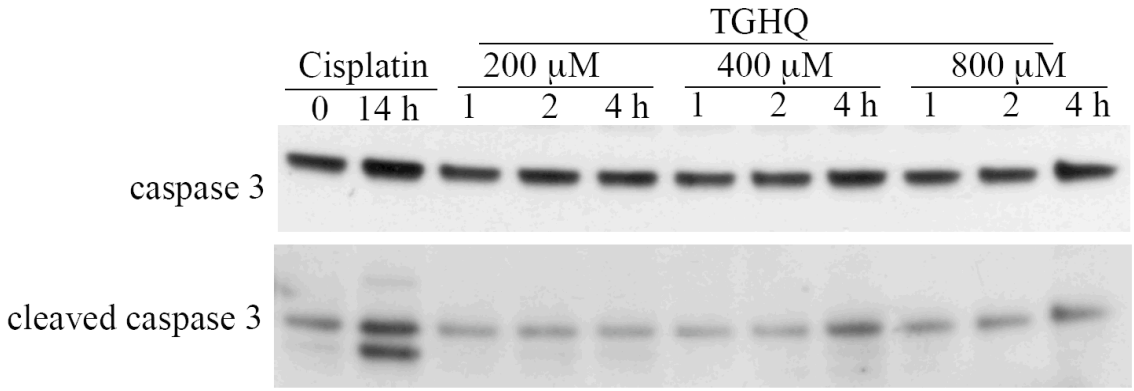

Figure 3.5. TGHQ mediates caspase-independent cell death in HK-2 cells.

Caspase 3 cleavage was not detected in cells treated with TGHQ. Cells were exposed to 50 μM cisplatin for 14 hr or various concentrations of TGHQ (200, 400 or 800 μM) for various periods of time (1, 2, 4 hr). Western blot analysis was performed using cleaved caspase 3 antibody. The illustrated blot is typical of at lease three independent experiments.

3.2.2. TGHQ induces DNA strand breaks.

ROS interact with DNA causing oxidative DNA base damage and DNA strand breaks. Histone H2AX S139 is rapidly phosphorylated (γ-H2AX) in the presence of DNA strand breaks (Rogakou et al., 1998). Therefore, TGHQ treated cells were monitored for γ-H2AX formation as an index of the presence of DNA strand breaks. Western blot analysis revealed an increase in γ-H2AX within 15 min of TGHQ treatment (Figure 3.6A), consistent with the generation of ROS (Figure 3.2), reaching maximal levels between 2-4 hr. Moreover, a significant increase in γ-H2AX foci formation was revealed by immunofluorescence staining of cells exposed to TGHQ (400 μM) for 30 min (Figure 3.6B). However, TGHQ-mediated H2AX phosphorylation was completely abrogated by the scavenging of ROS by catalase (Figure 3.6A) consistent with the inhibiton of ROS generation by catalase. The combined data suggest that TGHQ induces a persistent and gradual increase in ROS-dependent DNA damage.

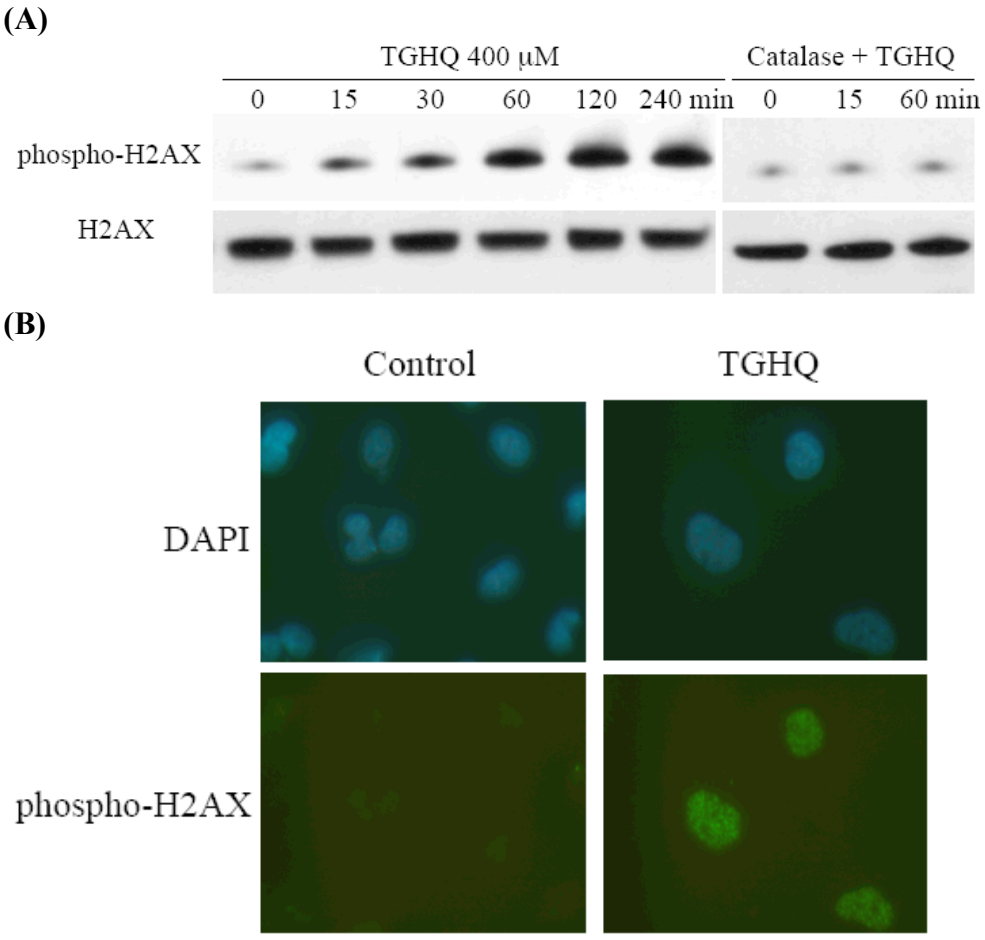

Figure 3.6. TGHQ-mediated DNA damage is dependent on the generation of ROS.

(A) Immnuoblot analyses of phosphorylated H2AX and total H2AX. Cells were treated with 400 μM TGHQ for various periods of time in the presence or in the absence of catalase (10 units/ml). Histones were acid-extracted and examined by Western blot analysis. The illustrated blot is typical of at lease three independent experiments. **(B)** γ-H2AX foci formation in HK-2 cells in response to TGHQ. Cells were treated with 400 μM TGHQ for 30 min. Untreated and treated cells were then fixed and immunostained with phospho-H2AX antibody for the direct analysis of γ-H2AX foci formation. Data shown are from a representative experiment.

3.2.3. TGHQ mediates PARP-1 hyperactivation and intracellular NAD depletion.

TGHQ-induced HK-2 cell death is accompanied by the rapid generation of ROS and DNA strand breaks. PARP-1, an enzyme implicated in DNA damage and repair mechanisms, is immediately activated following genotoxic stress, catalyzing the synthesis of PAR (Koh et al., 2005). Indeed, in LLC-PK1 cells, TGHQ induces the rapid (~5min) ribosylaiton of both core (H2, H3, H4) and linker (H1) histones (Monks et al., 2006). The ability of TGHQ to activate PARP-1 and promote the rapid accumulation of PAR in HK-2 cells was therefore investigated in log-phase cells treated with TGHQ. TGHQ-treated cells exhibited a time- and concentration-dependent increase in PAR accumulation (Figure 3.7A), consistent with the hyperactivation of PARP-1 in response to extreme DNA damage. PAR accumulation was evident at 10 min, and appeared to peak by 30 min. PAR formation requires the consumption of NAD, and PARP-1 hyperactivation depletes intracellular NAD content in a number of cell lines (Carson et al., 1986; Stubberfield and Cohen, 1988). We examined the effect of TGHQ on cellular NAD pools. TGHQ induced a rapid time- and dose-dependent depletion of total cellular NAD content (Figure 3.7B).

(A)

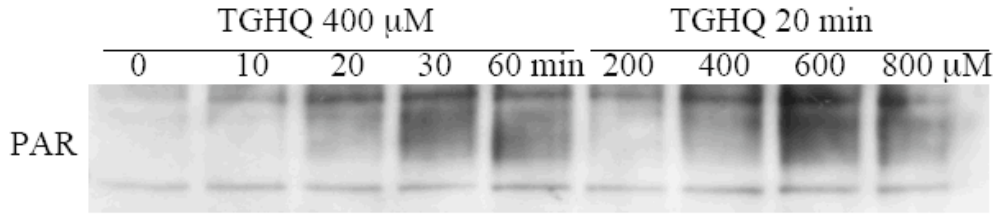

(B)

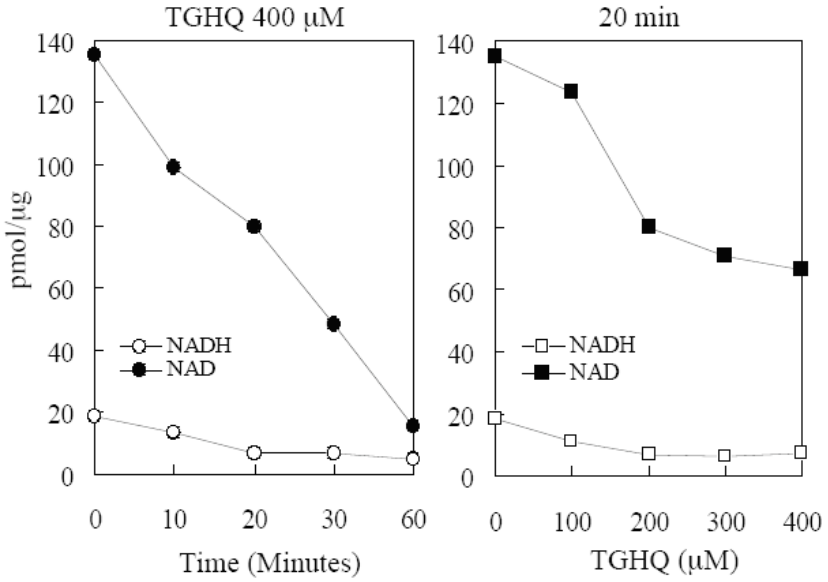

Figure 3.7. TGHQ mediated PARP-1 hyperactivation and intracellular NAD depletion.

Cells were treated with 400 μM TGHQ for various periods of time, as indicated, or treated with various concentrations of TGHQ for 20 min. **(A)** PAR accumulation was determined with a PAR antibody, SA-216. Equal loading was confirmed by Ponceau S staining (not shown). The illustrated blot is typical of at lease three independent experiments. **(B)** Total NAD content was determined using enzymatic cycling assays. Data represent the mean ± standard deviation ($n \geq 3$).

3.2.4. TGHQ-mediated HK-2 necrotic cell death is PARP-dependent.

PARP-1 hyperactivation has been coupled to cell death *via* the accompanying consumption of energy (ATP) and reducing equivalents (NAD). To determine whether PARP-1 hyperactivation and intracellular NAD loss contribute to TGHQ-mediated cytotoxicity, HK-2 cells were incubated with PJ34, a PARP inhibitor, prior to exposure to TGHQ. PJ34 pretreatment provided remarkable protection against TGHQ-induced necrotic cell death (Figure 3.8), with ~90% cell survival under conditions (800 μM, 2 hr) where TGHQ treatment alone caused 85% cell death. Cell survival in HK-2 cells pretreated with PJ34 was accompanied by the complete abrogation of TGHQ-mediated PAR accumulation (Figure 3.9A) and TGHQ-mediated NAD depletion (Figure 3.9B). Intriguingly, PJ34-stimulated cell survival occurred despite the continued generation of ROS (Figure 3.10). Consistent with the lack of effect of PJ34 on ROS generation, PJ34 also had no effect on DNA damage as assessed by γ-H2AX formation (Figure 3.11). Indeed, PJ34-stimulated cell survival appeared to occur in the face of increased amounts of γ-H2AX formation 4 hr after TGHQ treatment, perhaps reflecting decreases in the ability of PARP-1 to assist in the repair of DNA strand breaks and the consequent persistence of γ-H2AX-tagged foci.

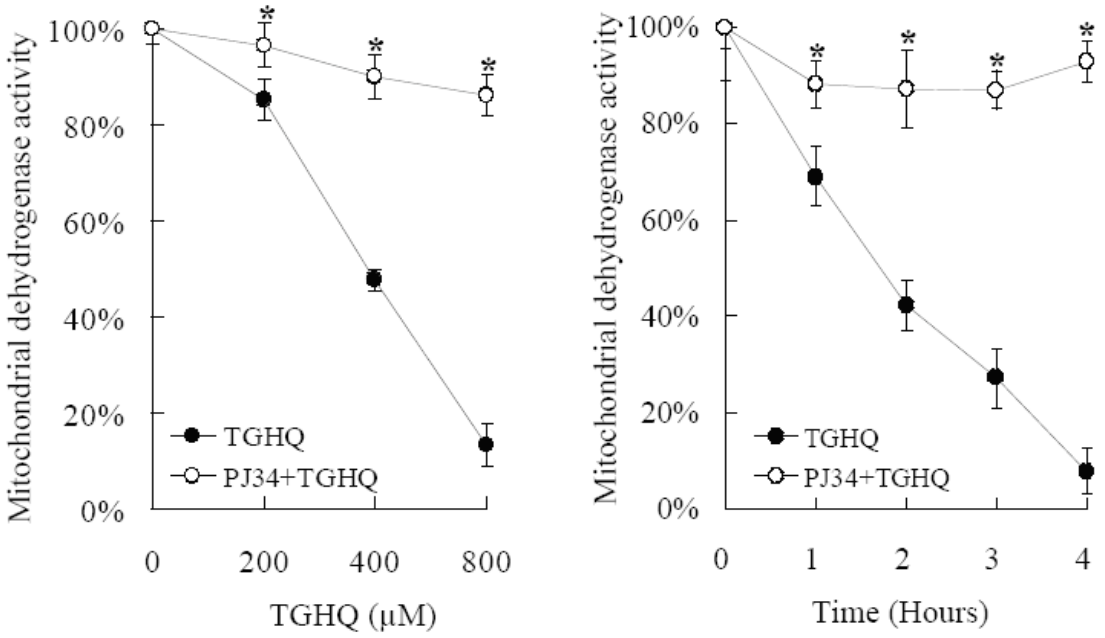

Figure 3.8. Inhibition of PARP attenuates TGHQ-mediated cell death.

Cells were pretreated with or without PJ34 (10 μM) for 30 min, and then exposed to TGHQ. **Left panel**; cells were treated with different concentrations of TGHQ (200, 400, 800 μM) for 2 hr. **Right panel**; cells were treated with 400 μM TGHQ for various periods of time (1, 2, 3, 4 hr). Cell viability was determined with the MTS based assay. Data represent the mean ± standard deviation ($n \geq 3$). *: $p<0.05$.

(A)

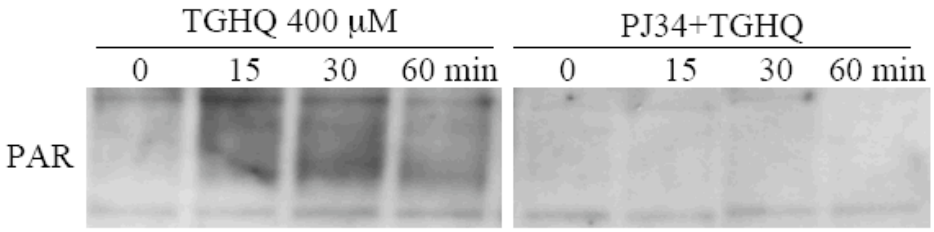

(B)

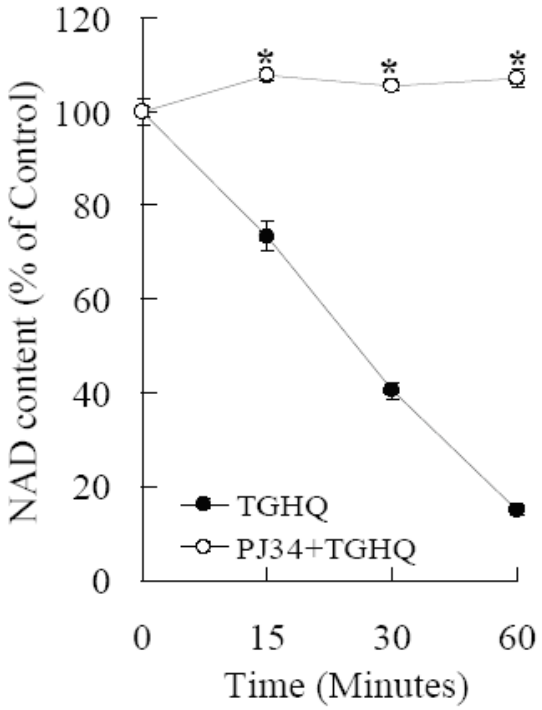

Figure 3.9. PJ34 inhibits PARP-1 hyperactivation and NAD depletion.

Cells were exposed to 400 μM TGHQ for various periods of time (15, 30, 60 min) with or without PJ34 pretreatment. **(A)** PAR accumulation is inhibited in the presence of PJ34. PAR accumulation was determined with a PAR antibody, SA-216. The blot illustrated is typical of at lease three independent experiments. **(B)** PARP-1 hyperactivation is necessary for NAD loss in response to TGHQ. Total NAD content was determined using enzymatic cycling assays. Data represent the mean ± standard deviation ($n \geq 3$).*: $p<0.05$.

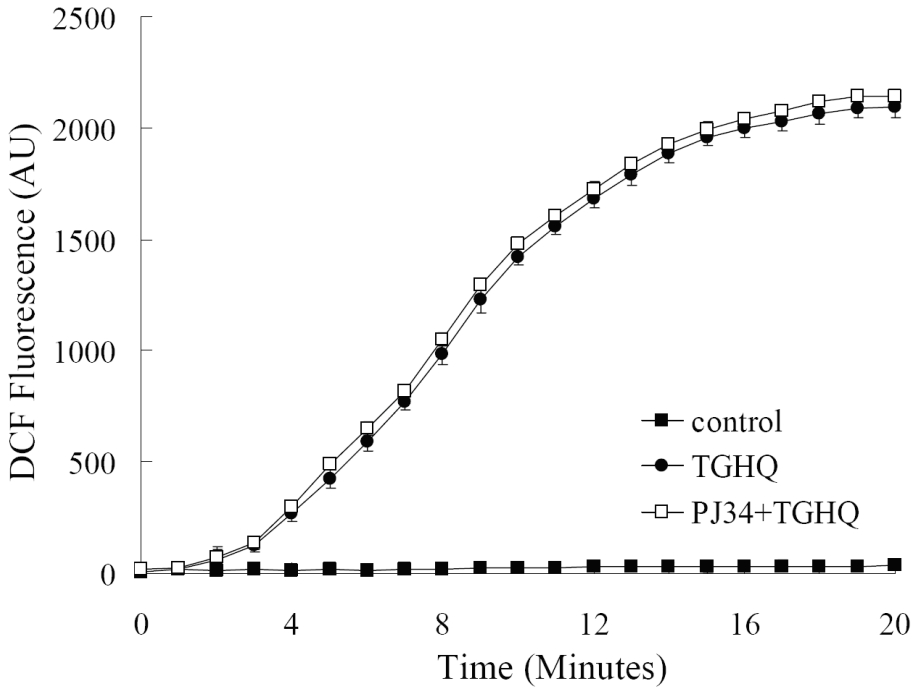

Figure 3.10. Modulation of TGHQ-mediated cytotoxicity by PJ34 is independent of TGHQ-mediated ROS generation.

PJ34 does not influence TGHQ-mediated ROS generation. Cells were pre-incubated with H_2DCFDA (10 μM) for 30 min, and then treated with 400 μM TGHQ in the presence or absence of PJ34. Images were collected via confocal microscopy. An area of cells was selected and changes in fluorescence were recorded every 1 min during treatment, up to 20 min. Values represent the average of total cellular DCF fluorescence expressed as arbitrary units (AU). Data represent the mean ± standard deviation ($n \geq 3$).

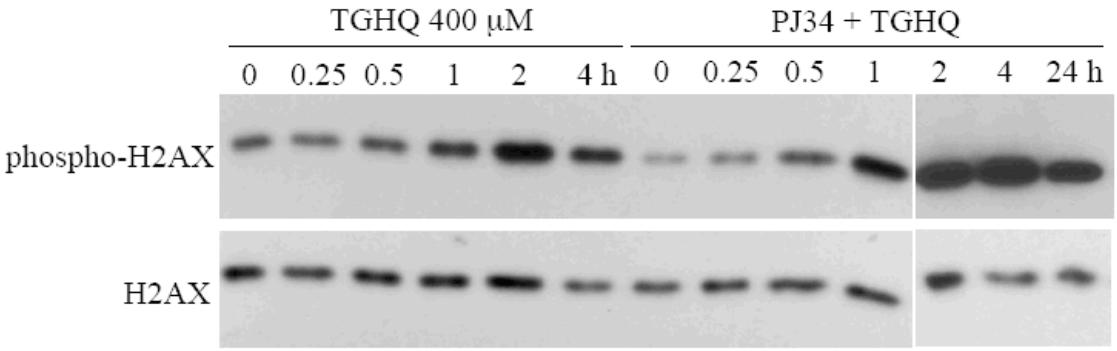

Figure 3.11. Modulation of TGHQ-mediated cytotoxicity by PJ34 is independent of TGHQ-mediated DNA damage.

Cells were treated with 400 μM TGHQ for different periods of time (0.25, 0.5, 1, 2, 4, 24 hr) in the presence or absence of PJ34. Histones were acid-extracted and examined by Western blot analysis. DNA strand breaks were determined using phospho-H2AX ser139 antibody (Top panel). For the 24 hr time point, medium containing TGHQ was replaced by normal culture medium after 4-hr TGHQ treatment and the phosphorylation of H2AX was determined 24 hr after initial TGHQ treatment. Equal loading was confirmed by immunoblot using histone H2AX antibody (Bottom panel). The illustrated blot is typical of at lease three independent experiments.

3.2.5. Hyperactivation of PARP-1 does not facilitate AIF translocation during necrotic cell death of HK-2 cells.

In normal cells, AIF is strictly confined to the mitochondrial inter-membrane space. However, under conditions of stress, the outer mitochondrial membrane becomes protein permeable and AIF translocates to the nucleus, causing DNA condensation and fragmentation, and cell death. The mitochondrial-nuclear redistribution of AIF is well defined in PARP-mediated cell death (Moubarak et al., 2007; Yu et al., 2002), is caspase-independent, and appears to be initiated by the depletion of NAD concomitant with PAR formation (Alano et al., 2004; van Wijk and Hageman, 2005). Since TGHQ-induced cell death in HK-2 cells occurs concomitant with PARP-1 activation and NAD depletion (Figure 3.7), and also appears caspase-independent (Figure 3.5), we next determined whether TGHQ mediates AIF translocation in HK-2. Cells were treated with TGHQ (400 μM) for various periods of time (0.5, 1, 2, 4 hr). Intracellular fractions, including mitochondria, cytoplasm, and nuclei, were isolated and analyzed to determine the relative distribution of AIF (Figure 3.12). Western blot analysis revealed no changes in the subcellular localization of AIF, suggesting that TGHQ-mediated PARP-1 hyperactivation is not accompanied by the translocation of AIF from mitochondria to the nucleus, a process usually associated with PARP-1 hyperactivation.

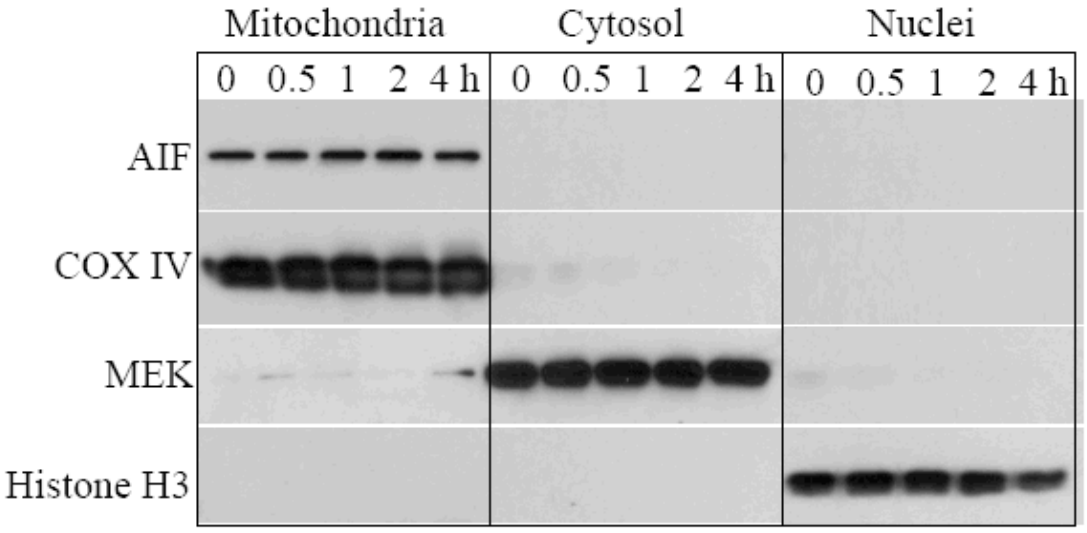

Figure 3.12. TGHQ-mediated cell death is AIF independent.

AIF protein is retained in mitochondria in response to TGHQ. Cells were treated with 400 μM TGHQ for various periods of time (0.5, 1, 2, 4 hr). The cytosolic, mitochondria, and nuclear fractions were recovered and examined with Western blot analysis using AIF antibody. COX IV, MEK and histone H3 were used as mitochondria, cytosolic and nuclear markers, respectively. The illustrated blot is typical of at lease three independent experiments.

3.2.6. The lack of AIF translocation is not due to the failure to engage JNK or p38 MAPK.

It has been suggested that during ischemia/reperfusion injury, c-jun NH(2)-terminal kinase (JNK) and/or p38 MAPK lie downstream of PARP activation, and may be required for PARP-mediated AIF translocation (Ho et al., 2006; Song et al., 2008). Indeed, ROS are known to activate various members of the MAPKs (Clerk et al., 1998; Cobb, 1999; Dong et al., 2004b). We therefore examined the response of the three major MAPK families to TGHQ. Interestingly, ERK1/2 were constitutively active in HK-2 cells, and exposure to TGHQ did not enhance ERK1/2 phosphorylation (Figure 3.13). In contrast, JNK1/2 and p38 MAPK were substantially, though only transiently (1-2 hr) activated in TGHQ-treated HK-2 cells (Figure 3.13). By 4 hr, JNK1/2 and p38 MAPK phosphorylation had returned to control levels. This decline in JNK1/2 and p38 MAPK phosphorylation was not due to degradation of either of these kinases, since protein levels remained unchanged. Thus, the lack of AIF translocation in HK-2 cells exposed to TGHQ is not due to their inability to activate either JNK1/2 or p38 MAPKs. Moreover, pharmacological inhibition of ERK1/2 (U0126), JNK1/2 (SP600125), or p38 MAPK (SB203580) had no effect on cell viability in TGHQ-treated HK-2 cells (Figure 3.14), further dissociating MAPK activation from PARP-1 hyperactivation in this model. In contrast, pretreatment of cells with PJ34 potentiated and prolonged TGHQ-mediated JNK1/2 and p38 MAPK activation (Figure 3.15).

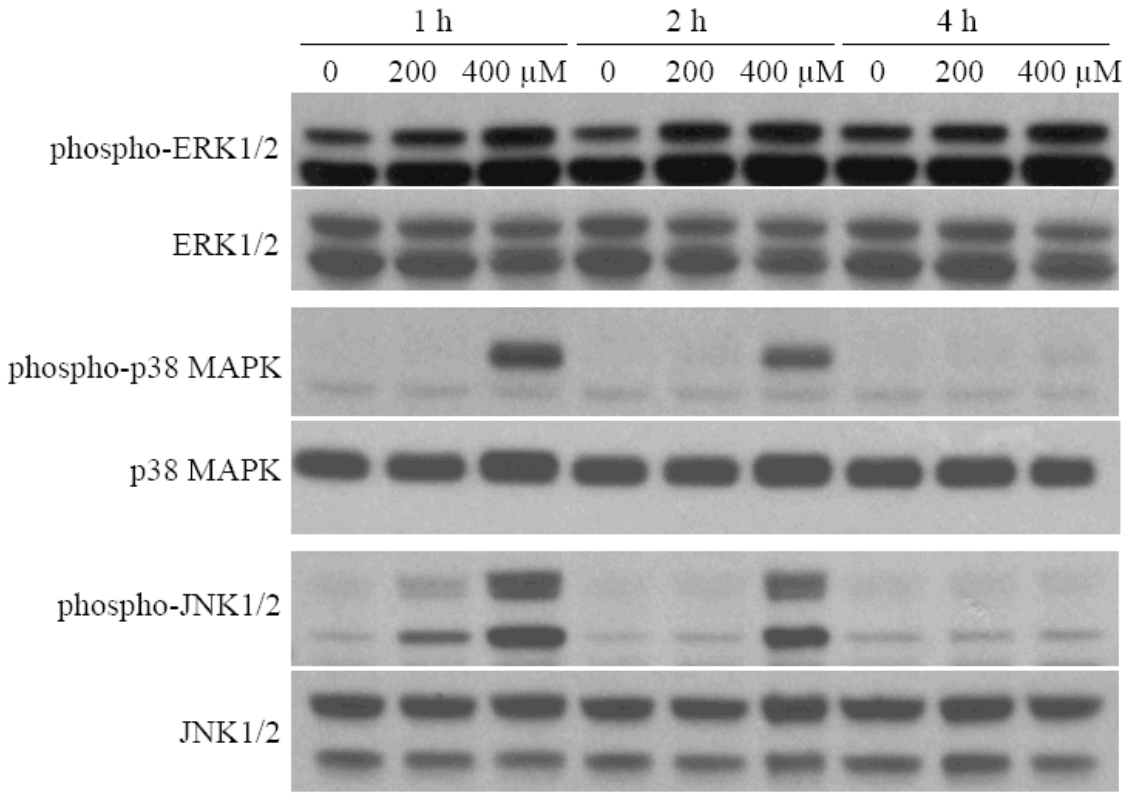

Figure 3.13. TGHQ mediated activation of MAPKs.

Cells were treated with different concentrations of TGHQ (200 or 400 μM) for different periods of time (1, 2, 4 hr). Total proteins were loaded and electrophoretically resolved on a 4-12% SDS-PAGE gel, followed by Western blot analysis for ERK1/2, phospho-ERK1/2, p38 MAPK, phospho-p38 MAPK, JNK1/2, and phospho-JNK1/2. The illustrated blot is typical of at lease three independent experiments.

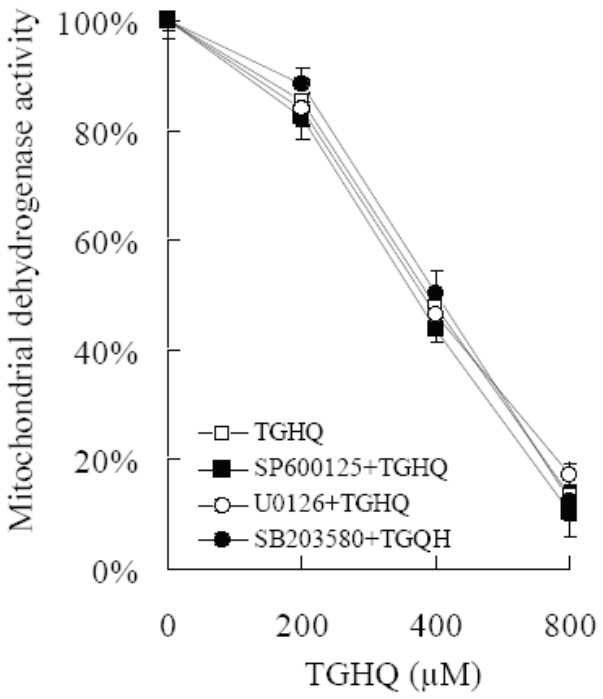

Figure 3.14. MAPK activation is independent of TGHQ-mediated cell death.

Cells were pretreated with or without an ERK inhibitor U0126 (10 μM), a p38 MAPK inhibitor SB203580 (50 μM) or a JNK1/2 inhibitor SP600125 (10 μM) for 1 hr, and then exposed to various concentrations of TGHQ (200, 400 or 800 μM) for 2 hr. Cell viability was determined using the MTS based assay. Data represent the mean ± standard deviation ($n \geq 3$).

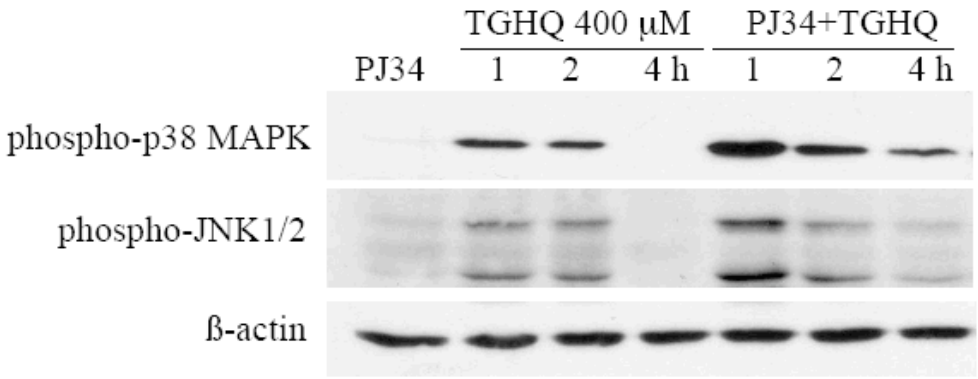

Figure 3.15. Inhibition of PARP-1 potentiates and prolongs TGHQ mediated activation of MAPKs.

Cells were pretreated with or without PJ34 for 30 min, and then exposed to TGHQ (400 μM) for different periods of time (1, 2, 4 hr). Total proteins were loaded and electrophoretically resolved on a 4-12% SDS-PAGE gel, followed by Western blot analysis using phospho-specific antibodies for p38 MAPK and phospho-JNK1/2. Equal loading was confirmed by assessing the protein level of β-actin. The illustrated blot is typical of at lease three independent experiments.

3.2.7. Inhibition of PARP delays but does not prevent TGHQ-mediated cell death.

In the ischemia/reperfusion model, administration of PARP inhibitors block NAD depletion, preserve cellular ATP, prevent necrosis and commit cells to apoptosis (Fiorillo et al., 2003). We therefore next investigated whether PJ34 was capable of sustaining HK-2 cell survival beyond 4-6 hr and whether or not PARP inhibition in TGHQ-treated HK-2 cells results in a similar switch in the mode of cell death, as seen during ischemia/reperfusion. Although ~45% of HK-2 cells remained viable 24 hr following treatment with 200 μM TGHQ, only about 15% remained viable after 48 hr (Figure 3.16A). The higher dose resulted in almost 100% cell death by 24 hr. Thus, inhibition of PARP with PJ34 only delays cell survival in response to TGHQ, even though PJ34 sustains cellular NAD concentrations for at least 4 hr (Figure 3.16B) and the viabile cells remain NAD content after 24 hr (Data not shows).

(A)

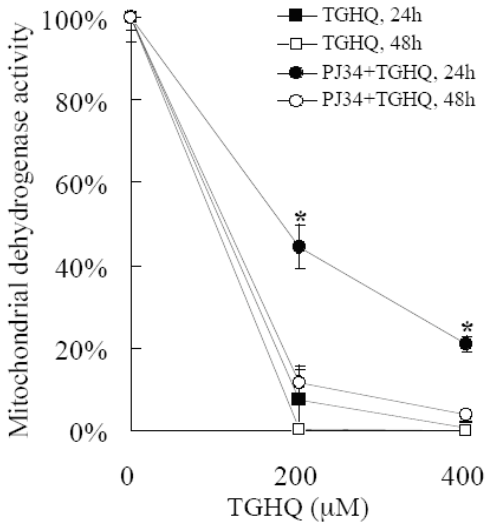

(B)

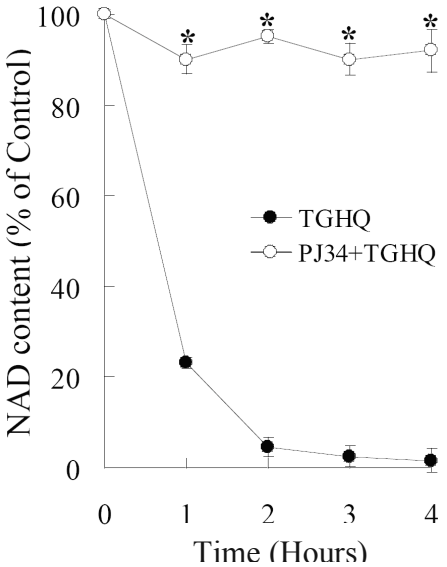

Figure 3.16. PARP-1 inhibition delays TGHQ-mediated cell death through the prevention of TGHQ-mediated rapid NAD depletions.

(A) Cells were treated with different concentrations of TGHQ (200, 400 μM) in the presence or in the absence of PJ34. After 4 hr treatment, medium containing TGHQ was replaced by normal culture medium. Cell viability was determined 24 or 48 hr post-treatment with TGHQ. **(B)** Cells were treated with 400 μM TGHQ in the presence or absence of PJ34. After 4 hr exposure, medium containing TGHQ was replaced by normal culture medium. NAD content was determined at different time points as indicated (1, 2, 3, 4 hr). Data represent the mean ± standard deviation ($n \geq 3$). *: $p<0.05$.

3.2.8. Inhibition of PARP does not alter the mode of TGHQ-induced cell death.

The next question was whether the delay in cell death, caused by PARP inhibition, was also accompanied by a change in the mode of cell death. Apoptotic cell death was measured *via* a DNA fragmentation assay and again cisplatin (50 μM) was used as a positive control. An increase in DNA fragmentation, reflected by the generation of oligonucleosomal ladders (Figure 3.17A), confirmed the ability of cisplatin to induce apoptosis in HK-2 cells. However, cells exposed to TGHQ following PJ34 pretreatment showed no fragmented DNA compared to cisplatin treated cultures. In addition, no cleavage of caspase 3 was detected in TGHQ treated cells pre-incubated with PJ34, whereas cells treated with cisplatin revealed significant amounts of cleaved caspase 3 (Figure 3.17B). These data reveal that at least in HK-2 cells, prevention of PARP-mediated NAD depletion following ROS-induced DNA damage does not trigger a transition from necrotic to apoptotic cell death.

(A)

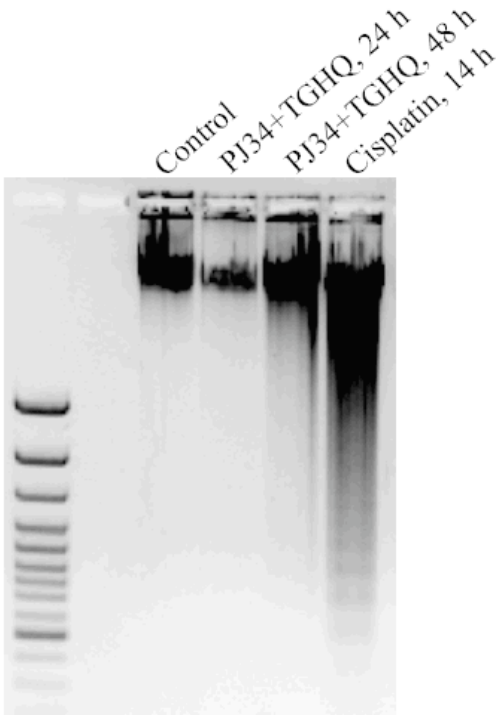

(B)

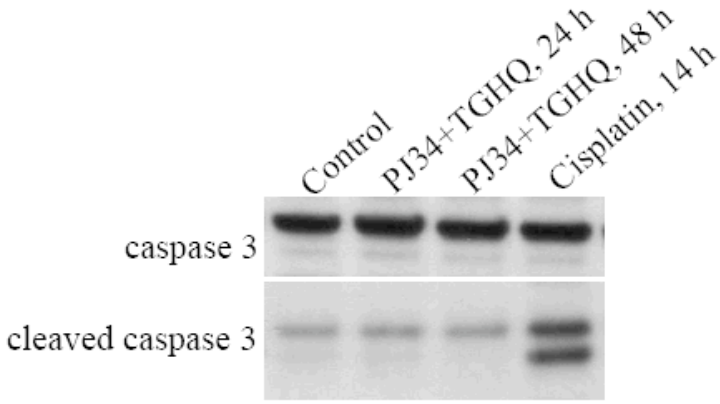

Figure 3.17. PARP-1 inhibition does not alter the mode of TGHQ-induced cell death.

Cells were treated with 50 μM cisplatin for 14 hr, or exposed to 400 μM TGHQ in the presence of PJ34 for 4 hr. Medium containing TGHQ was subsequently replaced by normal culture medium. Cells were collected 24 or 48 hr post-treatment with TGHQ. **(A)** Cellular DNA content was measured as described in Materials and Methods. **(B)** Western blot analysis was performed using cleaved caspase 3 antibody. The illustrated blot is typical of at lease three independent experiments.

3.3. DISCUSSION

The addition of TGHQ, a redox cycling metabolite of HQ, to HK-2 cells causes a time-, and concentration-dependent decrease in cell viability (Figure 3.3) that occurs in the absence of hallmarks of apoptosis (Figure 3.4 and 3.5). Cell death is associated with DNA damage (Figure 3.6) and the activation of PARP-1 (Figure 3.7). Moreover, inhibition of PARP prolongs survival of HK-2 cells exposed to TGHQ (Figure 3.8). The pathways coupling PARP-1 hyperactivation to cell death continue to be debated, but are likely to be context-dependent. PAR polymers have been implicated as a death signal, since in ischemia/reperfusion injury of the heart, transgenic mice overexpressing PAR glycohydrolase (PARG), the enzyme that degrades PAR polymers, have significantly reduced infarct size, whereas mice with reduced PARG have increased infarct size (Andrabi et al., 2006). In the majority of cases where PARP-1 hyperactivation contributes to cell death, it promotes the translocation of AIF from the mitochondria to the nucleus (Kang et al., 2004; Yu et al., 2006), causing DNA condensation and fragmentation, in an apparently caspase-independent fashion. However, in HK-2 cells PARP-1 hyperactivation was not accompanied by the translocation of AIF from mitochondrial to the nucleus (Figure 3.12).

In various models in which ROS activate PARP-dependent AIF translocation, p38 MAPK and/or JNK lie downstream of PARP-1 activation, and their activation appears required for PARP-mediated AIF translocation (Kwon et al., 2008; Song et al., 2008; Takada et al., 2008; Xu et al., 2006). Thus, dominant-negative JNK1 blocks AIF translocation, whereas constitutively active JNK1 promotes AIF translocation (Takada et

al., 2008). This raises the possibility that PARP-1 activation is uncoupled from subsequent p38 MAPK and/or JNK activation in HK-2 cells, thereby preventing AIF translocation. However, both p38 MAPK and JNK were activated in response to TGHQ (Figure 3.13) suggesting that at least in HK-2 cells, p38 MAPK and JNK activation is insufficient to couple PARP-1 activation to AIF translocation. The reason for this is unclear, but may be related to additional pathways coupling PARP-1 activation to AIF translocation. For example, PARP and AIF-dependent MNNG-induced necrosis requires calpains and Bax (Moubarak et al., 2007), with genetic ablation revealing that the latter is indispensable for AIF release from mitochondria. HK-2 cells do express Bax (Cuttle et al., 2001), which is presumably required to assist in permeabilization of the mitochondrial outer membrane, thereby facilitating AIF release. We are in the process of examining the regulation of the mitochondrial permeability transition in HK-2 cells in response to ROS as a possible factor contributing to the lack of AIF release in these cells. Finally, Zhang et al (2007) have suggested that JNK1 is an upstream regulator of PARP-1. Thus, either chemical inhibition of JNK1 activity or genetic deletion suppressed the "late-phase" PARP-1 activation by hydrogen peroxide, and *in vitro* kinase assays revealed that PARP-1 can serve as a direct substrate of JNK1 (Zhang et al., 2007b). These data suggest that the JNK1/PARP-1 interaction is likely to be more complex than initially considered.

Although the inhibition of PARP protected HK-2 cells from TGHQ-induced cell death, the cytoprotection occurred in the presence of an increase in γ-H2AX (Figure 3.6) an index of DNA strand breaks. Thus, when PARP-1 is inhibited, the ability to either

recognize the DNA damage, and/or to recruit DNA repair proteins to the sites of damage, is impaired. Consistent with this view, PAR formation is totally abrogated in PARP-inhibited HK-2 cells (Figure 3.9A) with a concomitant preservation of NAD concentrations (Figure 3.9B). How do HK-2 cells respond to an increase in DNA strand breaks when the DNA repair machinery is compromised? In the ischemia/reperfusion model, administration of PARP inhibitors blocks NAD depletion, preserves cellular ATP, prevents necrosis and commits cells to a caspase-dependent apoptotic pathway (Fiorillo et al., 2006). However, energy collapse is not the *de facto* cause of cell death during PARP-1 hyperactivation (Chiarugi, 2002; Fossati et al., 2007). Since NAD (and presumably ATP) concentrations are preserved in PARP-inhibited HK-2 cells, perhaps the cells initially surviving the ROS-induced DNA damage are similarly able to commit to cell death *via* apoptosis. However, the transition from necrotic to apoptotic cell death did not occur in HK-2 cells (Figure 3.17). Even though HK-2 cells clearly possess the machinery to engage apoptosis, cells that survive the initial ROS-induced DNA damage eventually succumb to necrotic cell death; inhibition of PARP-1 in HK-2 cells only seems to delay necrotic cell death.

In summary, ROS-induced PARP-dependent necrotic cell death of HK-2 cells occurs in the absence of AIF translocation from the mitochondria to the nucleus. The dissociation of PARP-dependent necrotic cell death from nuclear AIF translocation in HK-2 cells is not due to an inability to activate either JNK1/2 or p38 MAPK, but may be related differences in the mechanism by which HK-2 cells regulate the mitochondrial permeability transition. Finally, PARP-inhibited HK-2 cells that survive the initial ROS-

induced cell damage, eventually succumb to cell death. However, this cell death remains necrotic in nature, as HK-2 cells fail to transition into an apoptotic mode of cell death, despite possessing the necessary machinery with which to do so.

CHAPTER 4: ROS-INITIATED, PARP-MEDIATED NECROTIC CELL DEATH IS PREVENTED BY CALCIUM SEQUESTRATION

4.1. INTRODUCTION AND RATIONALE

We have been investigating the mode of TGHQ-driven ROS-induced cell death in renal proximal tubule epithelial HK-2 cells. ROS-induced necrotic cell death of HK-2 cells occurs in the presence of extensive DNA strand breaks (γ–H2AX), PARP-1 activation, and the concomitant depletion in cellular NAD concentrations (Chapter 3). However, PARP-1 activation is not coupled the translocation of AIF from mitochondria to the nucleus, or to the activation of p38 MAPK and JNK1/2, an early event prior to AIF translocation. Moreover, inhibition of PARP-1 with PJ34 only transiently protected HK-2 cells from ROS-induced necrotic cell death (Chapter 3), suggesting that other factors play an important role in modulating cell death within the context of PARP-1 hyperactivation. One such potential factor is intracellular Ca^{2+}.

Prior studies have shown that oxidative stress can disrupt intracellular Ca^{2+} homeostasis, leading to cell injury or even cell death (Bellomo et al., 1982; Richter and Kass, 1991). Oxidative stress mediates a rapid increase in cytosolic Ca^{2+} levels by triggering Ca^{2+} influx from the extracellular environment and/or from the ER (Waring, 2005). It has been revealed that rapidly rising cytosolic Ca^{2+} concentration leads to the activation of a number of Ca^{2+} sensitive proteins including calpain (Harriman et al., 2002). Calpains, a family of Ca^{2+}-activated cysteine proteases, are involved in necrotic cell death (Schanne et al., 1979). Calpain is activated upon elevation of intracellular Ca^{2+} levels. Activated calpain mediates disruption of lysosomal membrane integrity resulting

in the release of hydrolytic enzymes from lysosomes into the cytoplasm. These hydrolytic enzymes, such cathepsin, cause the degradation of cellular structures and subsequent cell death (Liu et al., 2004).

Another Ca^{2+} sensitive target is mitochondria (Bernardi and Rasola, 2007). Functioning mitochondria normally protect cells from Ca^{2+} overload by serving as a Ca^{2+} reservoir. Normally, mitochondrial Ca^{2+} concentrations are low, but when cytosolic Ca^{2+} concentrations increase, the mitochondrial uniporter transports Ca^{2+} into the mitochondrial matrix (Nicholls, 2005). At a certain point, mitochondrial Ca^{2+} concentrations increase to levels sufficient to trigger a process referred to as the mitochondrial permeability transition (MPT) (Dong et al., 2006). The formation of MPT pores results in mitochondrial membrane potential collapse, and the release of a number of cell death inducing factors into the cytosol (Hajnoczky et al., 2006). Although Ca^{2+} has been recognized as playing a key role in cell injury and cell death for many years (Bellomo et al., 1982; Ermak and Davies, 2002; Richter and Kass, 1991), the exact mechanisms by which Ca^{2+} contribute to cell death remain a subject of debate. In the present study we have investigated the role of Ca^{2+} in ROS-dependent, PARP-mediated necrotic cell death of HK-2 cells.

4.2. RESULTS

4.2.1. TGHQ induces intracellular Ca^{2+}elevation.

We examined changes in intracellular Ca^{2+} levels in response to TGHQ with a cell permeable intracellular Ca^{2+} indicator, Fura-2-AM. Cells were loaded with 5 μM Fura-2-AM and incubated for 45 min to allow for the dye to permeate cells. Cells were then incubated for an additional 20 min, in the presence or in the absence of 5 μM BAPTA-AM. Following TGHQ addition, images were collected every 15 seconds for 1 hr. Fold increases in fluorescence intensity were determined relative to basal intracellular Ca^{2+} levels. After exposure to TGHQ, HK-2 cells exhibited a time- and concentration- dependent increase in intracellular Ca^{2+} levels (Figure 4.1). HK-2 cells exhibited an increase in Fura-2 fluorescence from 30-40 min, after which time Ca^{2+} levels continue to elevate, with a 2-5 fold increase at 400 μM TGHQ and 5-10 fold increases at 800 μM TGHQ. Pretreatment of HK-2 cells with the Ca^{2+} chelator BAPTA-AM prevented the rise of intracellular Ca^{2+} levels mediated by TGHQ.

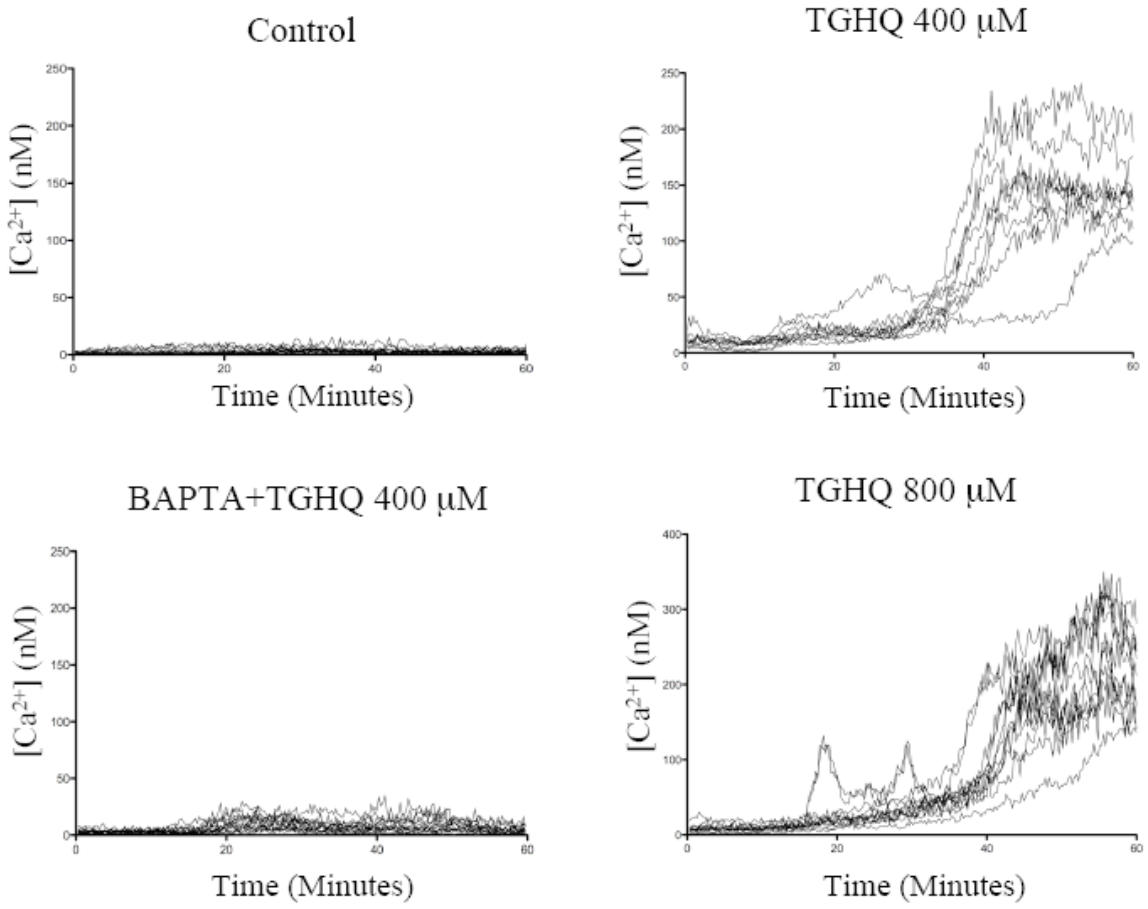

Figure 4.1. TGHQ induces intracellular Ca^{2+}elevations.

Intracellular Ca^{2+} concentrations were measured in live cells via fluorescence microscope using a cell permeable Ca^{2+} sensitive indicator Fura-2-AM. Cells were loaded with Fura-2-AM (5 μM) for 45 min, and incubated for an additional 20 min to allow for hydrolysis of the AM-ester. Cells were then exposed to 400 μM or 800 μM TGHQ in the presence or in the absence of BAPTA-AM (10 μM). Images were collected every 15 seconds for 1 hr, as indicated. Results are displayed in graphic form to illustrate fold changes in Fura-2 fluorescence in cells after TGHQ treatment. Each line represents the change in Fura-2 fluorescent intensity of individual cells overtime; each graph represents one of at least three independent experiments.

4.2.2. TGHQ-induced cell death is Ca^{2+} dependent.

Disruptions in intracellular Ca^{2+} homeostasis have been coupled to apoptotic and necrotic cell death. To determine whether increases in intracellular Ca^{2+} levels contribute to TGHQ-mediated cytotoxicity, HK-2 cells were incubated with a cell permeable Ca^{2+} chelator BAPTA-AM, prior to exposure to TGHQ. BAPTA-AM pretreatment provided significant protection against TGHQ-induced necrotic cell death (Figure 4.2), with ~100% cell survival under conditions (800 μM, 2 hr) where TGHQ treatment alone caused 85% cell death. Long term cell survival was also examined. BAPTA-pretreated cells exhibited 90% viability at 24 h and 85% viability at 48 h, compared to 95% cell death in cells treated with TGHQ alone (Figure 4.3). However, unlike the PJ34-mediated transient cytoprotection, BAPTA-mediated protective effects are retained for at least 48 hr. Indeed, BAPTA-stimulated cell survival appeared to occur in the fact of decreased amounts of γ-H2AX formation, 24 hr after TGHQ treatment (Figure 4.5), reflecting the enhanced ability of cells to repair DNA strand breaks, with the consequent decrease in γ-H2AX-tagged foci.

To ensure that the cytoprotective effects of BAPTA-AM were not related to an ability of BAPTA-AM to scavenge ROS, live cell imaging using confocal fluorescence microscopy was used, and revealed an increase in TGHQ-catalyzed ROS generation in HK-2 cells that was unaffected by BAPTA-AM (Figure 4.4). However, inconsistent with the lack of effect on ROS generation, BAPTA-AM delayed γ-H2AX formation (Figure 4.5). Increases in γ-H2AX formation occur within 1-2 hr of exposure of HK-2 cells to TGHQ. Pretreatment of HK-2 cells with BAPTA-AM prior to TGHQ exposure

significantly delayed the appearance of γ-H2AX. Whether Ca^{2+} chelation simply delays the onset of γ-H2AX formation (damage recognition), or actually influences (decreases) DNA damage is unclear. However, since BAPTA-AM has no effect on ROS generation it seems unlikely that the decrease in γ-H2AX formation is caused by a decrease in DNA damage.

4.2.3. Ca^{2+} is an initiating factor in TGHQ-mediated cell death.

Prior data demonstrated that intracellular Ca^{2+} increased within 30-40 min after TGHQ treatment. To examine whether Ca^{2+} is a required initiating factor in TGHQ-mediated cell death, HK-2 cells were exposed to various concentration of TGHQ. BAPTA-AM was added 30 min before or at various times thereafter, up to 2 hr (Figure 4.6). A time-dependent decrease in cell viability was observed with delayed addition of BAPTA-AM, indicating that Ca^{2+} elevation was a critical initiating event in ROS-induced necrotic cell death.

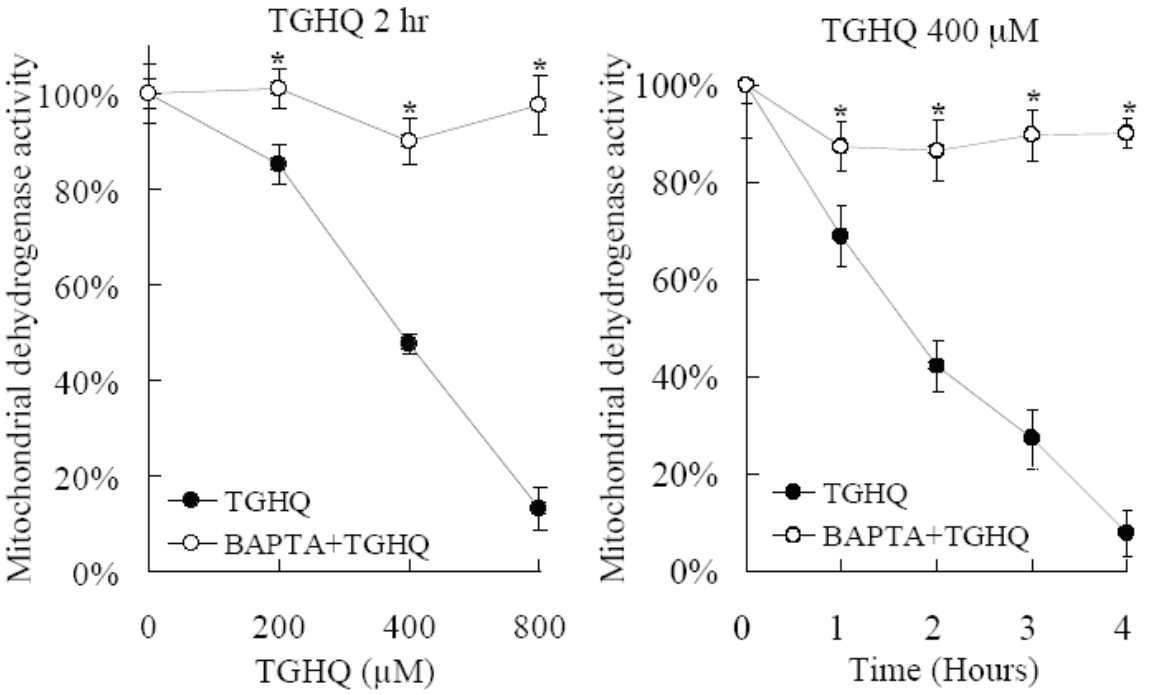

Figure 4.2. Ca^{2+} chelation attenuates TGHQ-mediated cell death.

Cells were pretreated with or without BAPTA-AM (5 μM) for 30 min, and then exposed to TGHQ. **Left panel;** cells were treated with different concentrations of TGHQ (200, 400, 800 μM) for 2 hr. **Right panel;** cells were treated with 400 μM TGHQ for various periods of time (1, 2, 3, 4 hr). Cell viability was determined by measuring mitochondrial dehydrogenase enzyme activity in actively respiring cells. Formazan formation relative to untreated cells (% of control) represents cell viability after treatment. Data represent the mean ± standard deviation ($n \geq 3$). *: $p<0.05$.

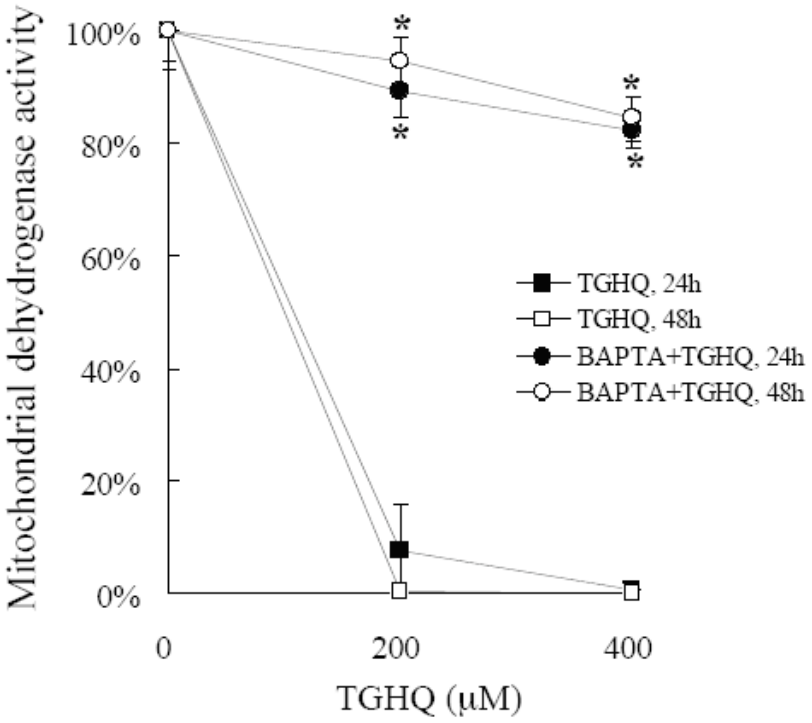

Figure 4.3. Ca^{2+} chelation completely prevents TGHQ-mediated cell death.

Cells were treated with different concentrations of TGHQ (200, 400 μM) in the presence or in the absence of BAPTA-AM (5 μM). After 4 h of exposure, medium containing TGHQ was replaced with normal culture medium. Cell viability was determined 24 or 48 h post-treatment with TGHQ. Data represent the mean ± standard deviation ($n \geq 3$). *: $p<0.05$.

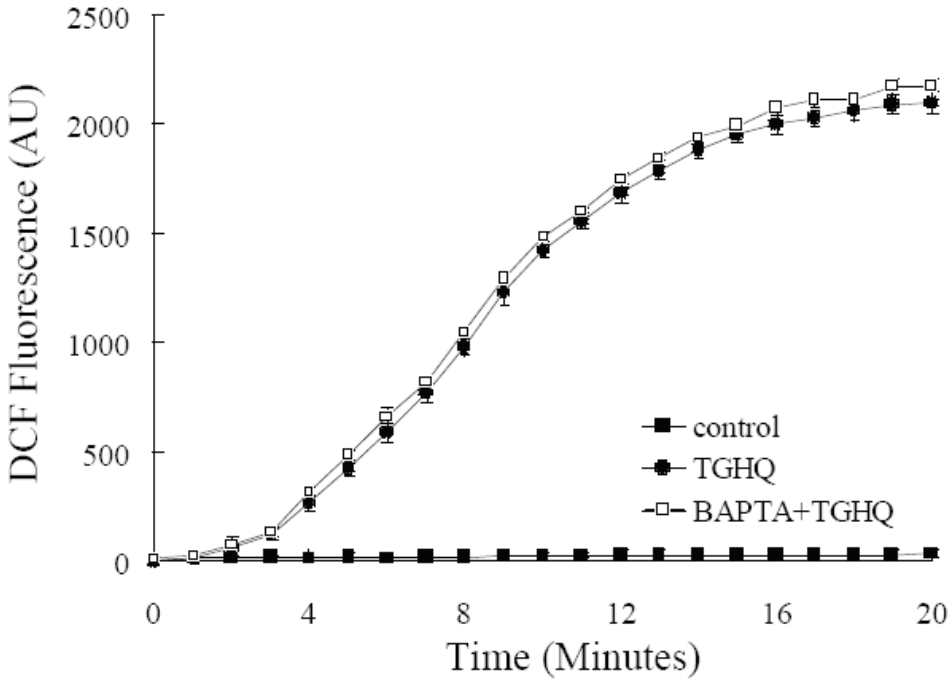

Figure 4.4. BAPTA-mediated cytoprotection does not modulate TGHQ-mediated ROS generation.

Cells were pre-incubated with 10 μM H_2DCFDA for 30 min, and then treated with 400 μM TGHQ in the presence or absence of BAPTA-AM (5 μM). Images were collected via confocal microscopy. An area of cells was selected and changes in fluorescence were recorded every 1 min during treatment up to 20 min. Values represent the average total cellular DCF fluorescence expressed as arbitrary units (AU). Data represent the mean ± standard deviation ($n \geq 3$).

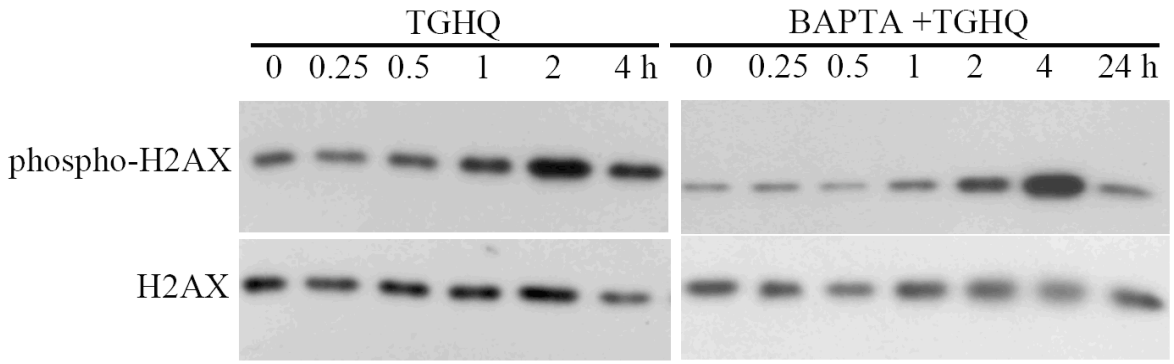

Figure 4.5. BAPTA-AM modulates TGHQ-induced γ-H2AX formation.

Cells were treated with 400 μM TGHQ for different periods of time (0.25, 0.5, 1, 2, 4 hr) in the presence or in the absence of BAPTA-AM (5 μM). Histones were acid-extracted and examined with Western blot analysis. DNA strand breaks were determined using phospho-H2AX ser139 antibody (Top panel). For the 24 hr treatment sample, medium containing TGHQ was replaced by normal culture medium after 4 hr TGHQ treatment and the phosphorylation of H2AX was determined 24 hr after initial TGHQ treatment. Equal loading was confirmed by immunoblot using histone H2AX antibody (Bottom panel). The illustrated blot is typical of at lease three independent experiments.

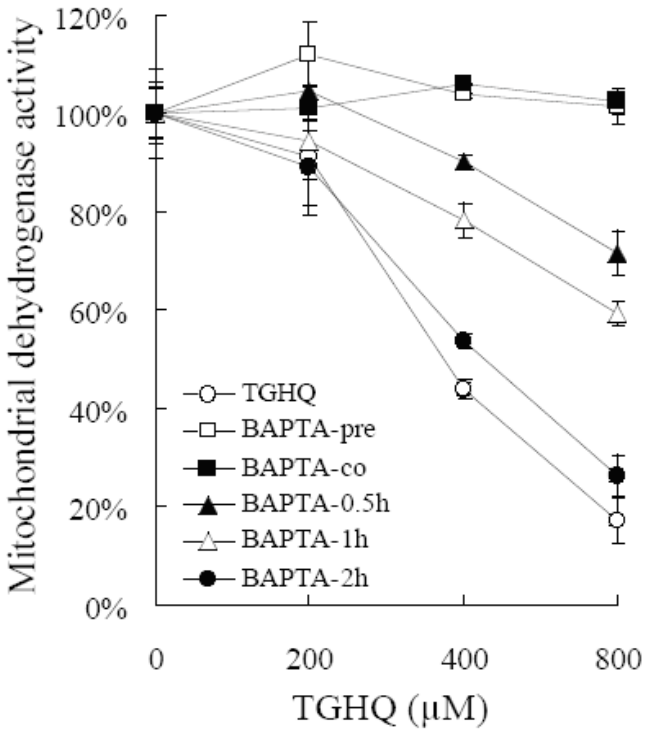

Figure 4.6. Ca^{2+} release is an initiating event in TGHQ-mediated cell death.

Cells were treated with various concentration (200, 400, 800 μM) of TGHQ alone or together with 5 μM BAPTA-AM which was **pre-**treated (30 min), **co**-treated, or added to TGHQ-treated cells at various times afterwards, as indicated (0.5, 1, 2 hr). Cell viability was determined with MTT based assay 2 hr post-treatment with TGHQ. Data represent the mean ± standard deviation ($n \geq 3$).

4.2.4. Inhibition of Ca^{2+}-activated calpain partially attenuates TGHQ-mediated cell death.

Although Ca^{2+} has been recognized as playing a key role in cellular injury, the exact mechanisms by which Ca^{2+} contributes to cell death remain a subject of debate. Rapidly rising cytosolic Ca^{2+} concentrations lead to activation of calpain, which mediates lysosomal membrane disruption. Lysosomes contain over 80 types of hydrolytic enzymes, release of which into the cytoplasm results in the degradation of cellular structures and cell death. We therefore investigated the role of calpain in TGHQ-mediated cell death. Pretreatment of cells with three different calpain inhibitors, PD15605 (5 μM), calpeptin (10 μM), calpain inhibitor III (10 μM), attenuated TGHQ induced-toxicity (Figure 4.7). However, unlike Ca^{2+} chelation with BAPTA-AM, inhibition of calpain only partially rescued TGHQ-induced cell death. Among all three calpain inhibitors, calpeptin is the most effective one, and the relative protection-mediated by calpeptin was only ~50% in cells treated with 400 μM TGHQ. Although inhibition of calpain led to a 60% to 70% survival of cells exposed to 400 μM TGHQ, only about 30% remained viable at 800μM TGHQ. Thus the higher dose resulted in less cytoprotection mediated by the inhibition of calpain. This may be due to the activation of additional Ca^{2+}-dependent proteases following excessive TGHQ-mediated disruption to the cell. These data suggest that calpain is not the only downstream mediator of Ca^{2+}-dependent cell death.

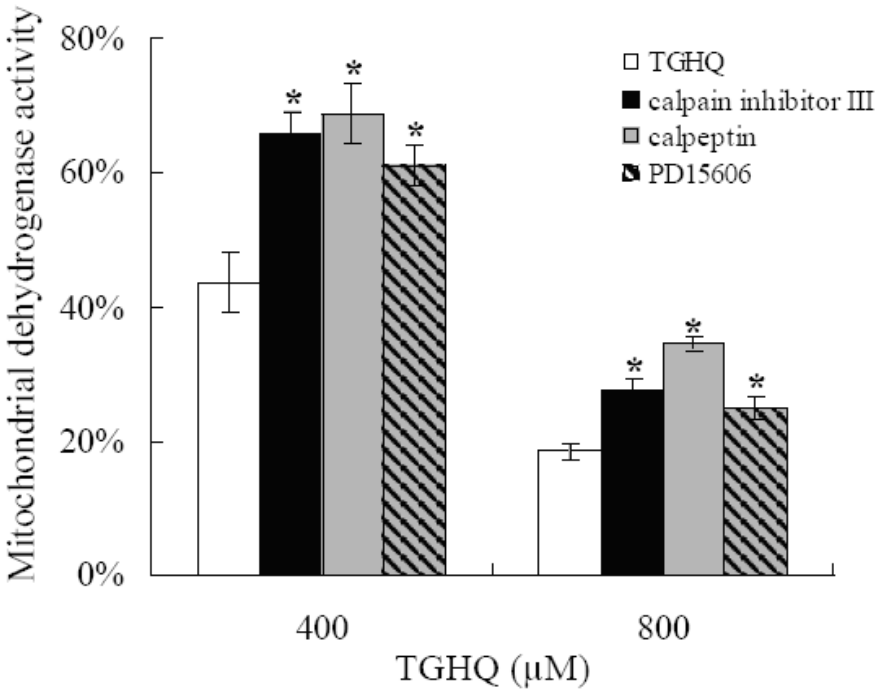

Figure 4.7. Calpain activation contributes to TGHQ-mediated cytotoxcity.

Cells were pretreated with or without three different calpain inhibitors, PD15605 (5 μM), calpeptin (10 μM), or calpain inhibitor III (10 μM) for 1 hr, and then exposed to various concentration (400 μM, 800 μM) of TGHQ for 2 hr. Cell viability was determined by measuring mitochondrial dehydrogenase enzyme activity in actively respiring cells. Formazan formation relative to untreated cells (% of control) represents cell viability after treatment. Data represent the mean ± standard deviation ($n \geq 3$). *: $p<0.05$.

4.2.5. Ca^{2+} depletion attenuates the loss of mitochondrial membrane potential.

Rapid elevations in cytosolic Ca^{2+} concentrations lead to mitochondria Ca^{2+} overload, activation of the mitochondrial permeability transition (MPT), and subsequently cell death. To explore whether changes in intracellular Ca^{2+} levels after TGHQ treatment could affect mitochondrial membrane integrity, cells were treated with TGHQ in the presence or absence of BAPTA-AM. Alterations in the mitochondrial membrane potential were monitored by flow cytometry, using the cationic dye, JC-1. In normal cells, JC-1 accumulates in the mitochondrial matrix as revealed by red fluorescence. When the mitochondrial membrane potential collapses, JC-1 is dispersed throughout the cell and is detected as green fluorescence. A decrease in the red/green fluorescence intensity ratio provides an index of mitochondrial depolarization. Untreated control HK-2 cells exhibit a high mitochondrial membrane potential and are hyperpolarized, whereas, cells treated with TGHQ become depolarized and exhibit a time-dependent decline in the mitochondrial membrane potential (Figure 4.8). Thus, after 4 h, 83% of TGHQ-treated HK-2 cells display a collapse in the mitochondrial membrane potential, whereas 94% of the BAPTA-AM pretreated cells maintain their mitochondrial membrane potential. Ca^{2+} chelation with BAPTA-AM alone caused a transient decrease in the mitochondrial membrane potential that was essentially completely restored by 2-4 hr. This may be due to the ability of BAPTA to alter intracellular Ca^{2+} homeostasis.

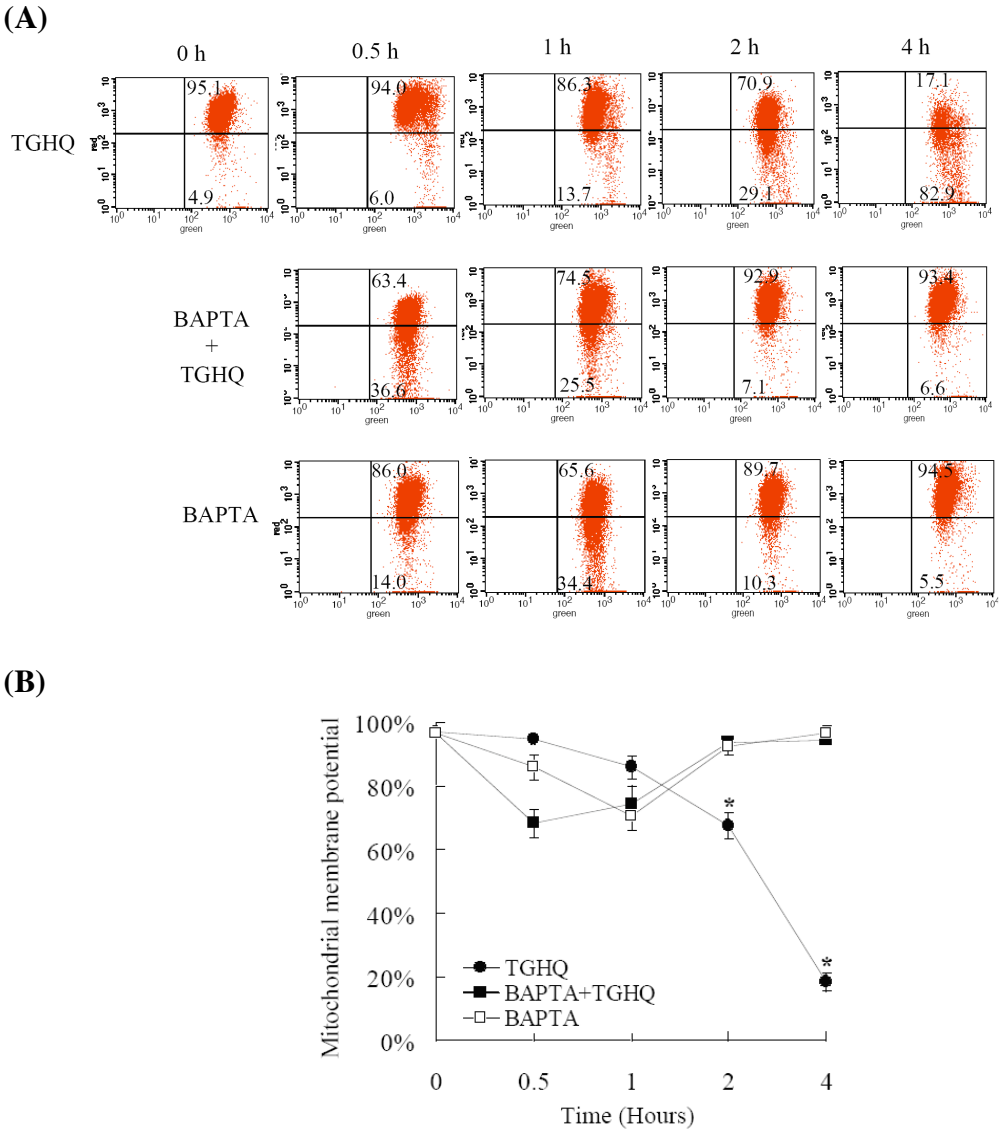

Figure 4.8. TGHQ-mediated loss of mitochondrial membrane potential is modulated by the alterations in intracellular Ca^{2+} homeostasis.

Mitochondrial membrane potential was measured with JC-1 using flow cytometry. Cells were treated with 400 µM TGHQ (top panel), or pretreated with 5 µM BAPTA-AM for 30 min followed by TGHQ (400 µM) exposure (central panel), or treated with 5 µM BAPTA-AM alone (bottom panel) overtime. Changes in mitochondrial membrane potential were determined at 0.5, 1, 2, and 4 hr post-treatment. **(A)** Cells in the upper right-hand quadrant exhibit high mitochondrial membrane potential, while cells in the lower right-hand quadrant exhibit loss of mitochondrial membrane potential. **(B)** Bar graph of the mitochondrial membrane potential shown in Figure 4.9A. Data represent the mean ± standard deviation ($n \geq 3$). *: $p<0.05$.

4.2.6. TGHQ-mediated loss of mitochondrial membrane potential is not completely dependent on ROS.

Because TGHQ-induced cell death was accompanied by a loss of the mitochondrial membrane potential, we suspected that formation of the mitochondrial permeability transition (MPT) played a role in TGHQ-mediated cell death. To investigate this, cells were pre-incubated with a MPT inhibitor, cyclosporine A (CsA) for 1 hr followed by 400 μM TGHQ treatment. After 2 hr incubation, the mitochondrial membrane potential was determined in CsA pretreated cells compared to cells treated with TGHQ alone. Fewer (14%) CsA pretreated cell sucoombed to mitochondrial membrane depolarization, compared to cells exposed to TGHQ alone (25%) (Figure 4.9). However, the manner of the loss of the mitochondrial membrane potential induced by TGHQ was different from that mediated by H_2O_2 or MNNG. H_2O_2, the ROS agent, and MNNG, a DNA alkylation agent, both caused a complete CsA-dependent mitochondrial membrane depolarization (Figure 4.9). In contrast, TGHQ-induced mitochondrial membrane depolarization was only attenuated by CsA. In addition, pretreatment with CsA significantly prevented cell death induced by H_2O_2 or MNNG, but had much less of an effect on TGHQ-mediated cytotoxicity (Figure 4.10). These combined data suggest that TGHQ-mediated ROS generation is necessary for the increase in intracellular Ca^{2+} concentrations, but not sufficient for the unique activation of MPT induced by TGHQ.

(A)

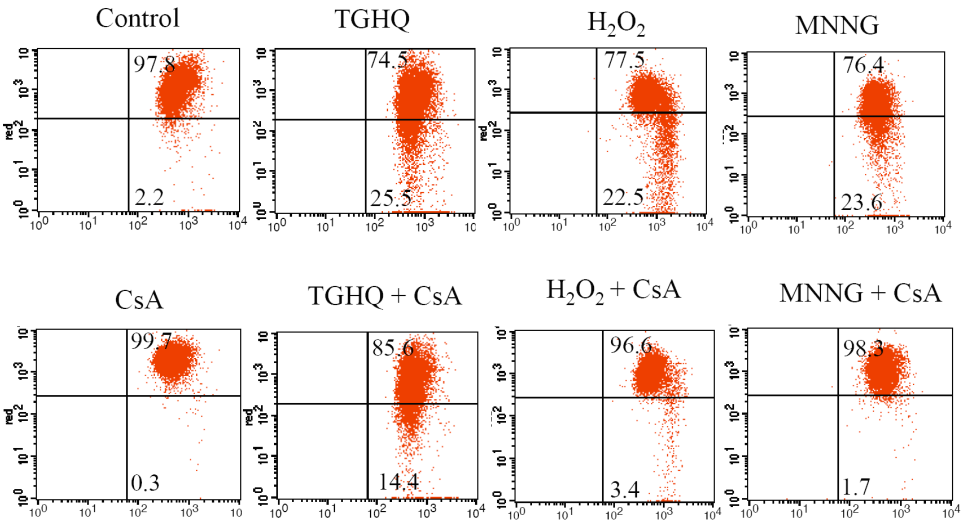

(B)

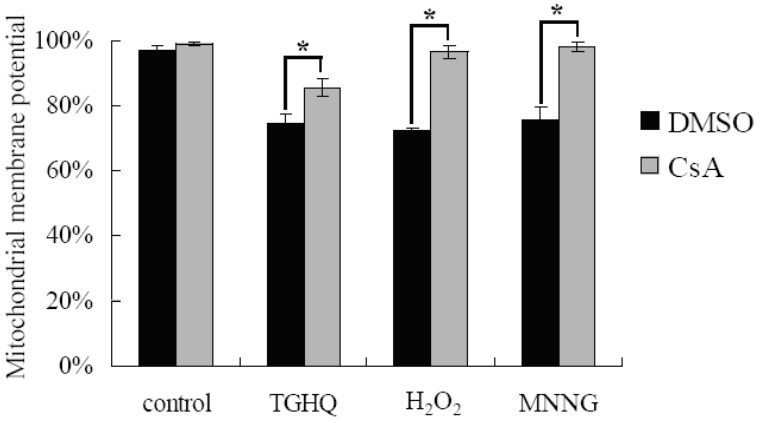

Figure 4.9. Cyclosporin A only partially attenuates TGHQ-mediated loss of mitochondrial membrane potential.

Mitochondrial membrane potential was measured in control or chemical treated cells. Cells were treated with TGHQ (400 µM), H_2O_2 (200 µM), MNNG (50 µM), in the presence or in the absence of 5µM CsA. 2 hr after treatment, cells were harvested for analyses of changes in mitochondrial membrane potential by flow cytometry with JC-1 staining. (A) Cells in the upper right-hand quadrant exhibit high mitochondrial membrane potential, while cells in the lower right-hand quadrant exhibit loss of mitochondrial membrane potential. (B) Bar graph of the mitochondrial membrane potential shown in Figure 4.9A. Data represent the mean ± standard deviation ($n \geq 3$). *: $p<0.05$.

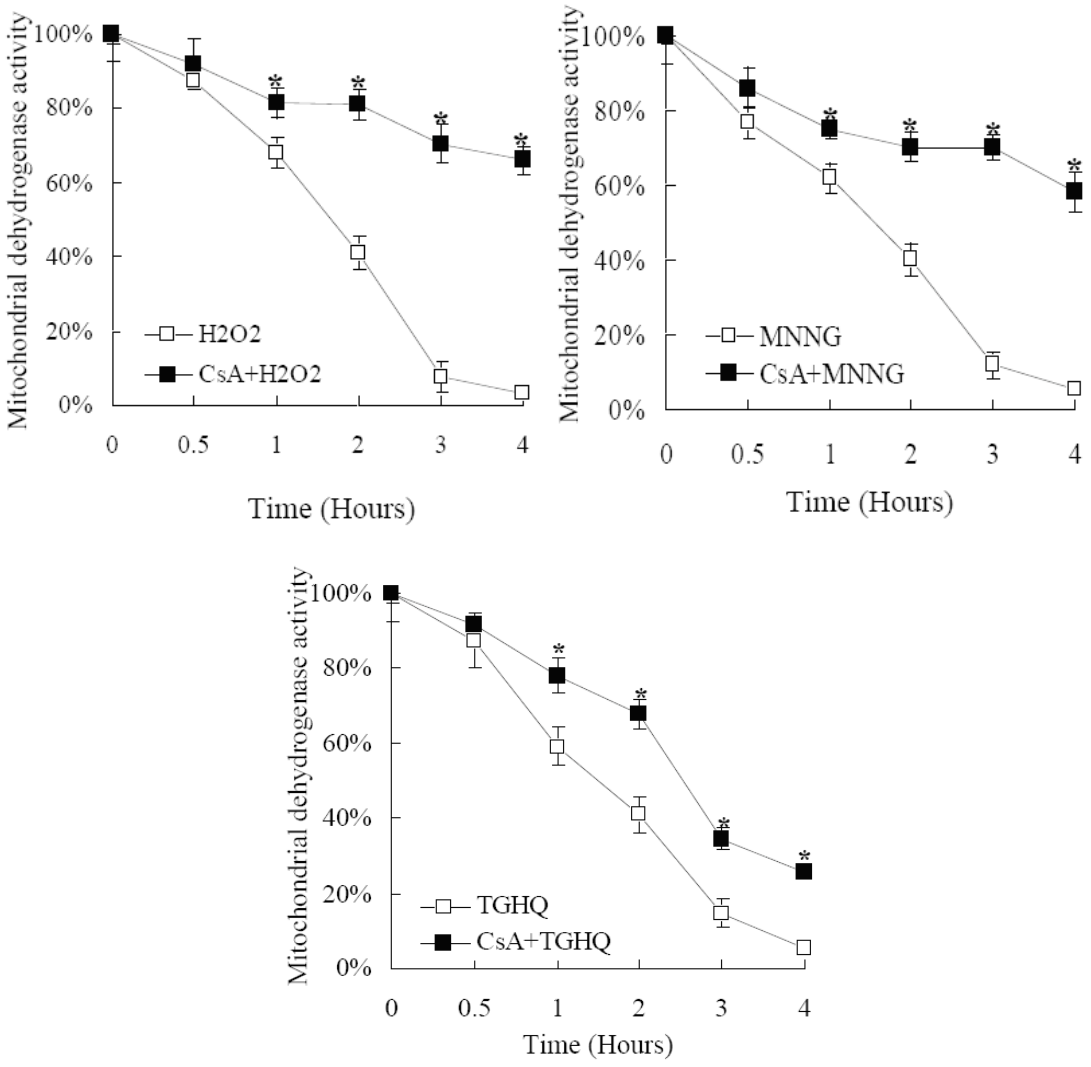

Figure 4.10. Cyclosporin A only partially attenuates TGHQ-mediated necrotic cell death.

Cells were pretreated with or without CsA (5 μM) for 1.5 hr, and then exposed to different chemicals (200 μM H_2O_2; 50 μM MNNG; or 400 μM TGHQ) for various periods of time (0.5, 1, 2, 3, 4 hr) Cell viability was determined with the MTS based assay. Data represent the mean ± standard deviation (n ≥ 3). *: $p<0.05$.

4.2.7. Ca^{2+} depletion attenuates PAR accumulation and NAD depletion.

As demonstrated in chapter 3, TGHQ-induced necrotic cell death of HK-2 cells is PARP-1-dependent. The finding that Ca^{2+} chelation also protected against TGHQ-induced cell death suggests that PARP-1 activation and changes in intracellular Ca^{2+} are coupled. We therefore determined the influence of Ca^{2+} chelation on PARP-1 activation and intracellular NAD levels. Increases in PAR levels in TGHQ-treated cells could be detected between 30-120 min, with maximal levels at ~45 min (Figure 4.11). PAR accumulation in HK-2 cells was accompanied by a parallel and rapid decline in NAD concentrations. Thus within 1 hr of exposure of HK-2 cells to TGHQ, NAD concentrations had declined to just 20% of untreated cells, and by 2 hr were essentially zero (Figure 4.12A). BAPTA-AM pre-treated HK-2 cells exhibited much less PAR accumulation than cells treated with TGHQ alone, (Figure 4.11). The attenuation of PAR formation by BAPTA-AM was accompanied by an initial (60 min) preservation of cellular NAD concentrations (Figure 4.12A), which subsequently reached a nadir between 3-5 hr, prior to rebounding to control levels by 12 hr. The transient decline in NAD content in BAPTA-AM pretreated HK-2 cells is apparently PARP-dependent, since inhibition of PARP with PJ34 abrogates the delayed consumption of NAD in a time-dependent manner (Figure 4.12B). In BAPTA-pretreated cells, intracellular NAD loss was completely prevented when PJ34 was added during the initial preservation period, as seen at 0, 0.5 and 1 hr (Figure 4.12B, grey bars). Afterward, a time-dependent loss of cytoprotection was observed with the delayed addition of PJ34. These data suggest that the BAPTA-modulated NAD loss is also PARP dependent.

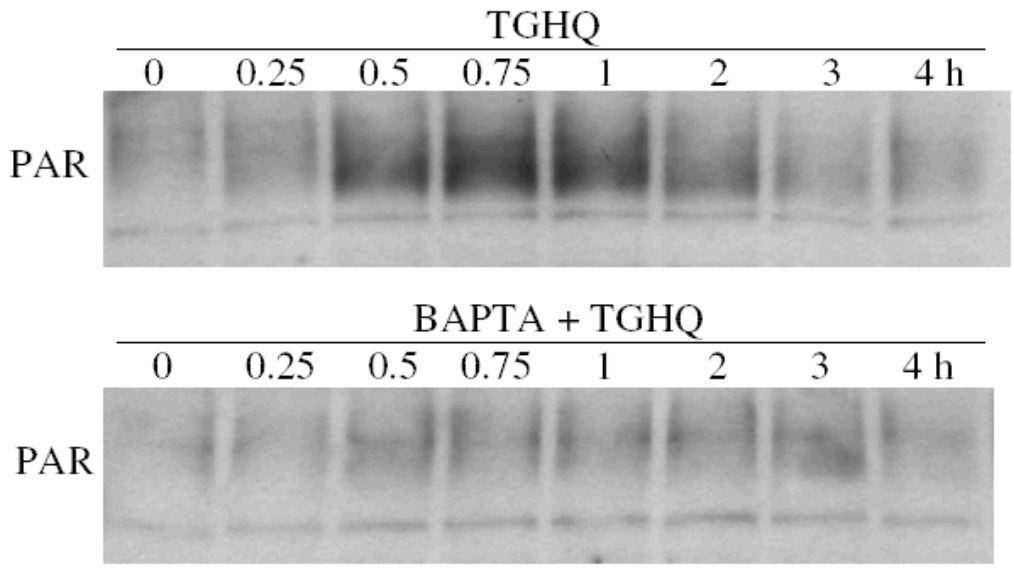

Figure 4.11. TGHQ-induced PAR accumulation is Ca^{2+} sensitive.

Cells were pretreated with or without 5 μM BAPTA-AM for 30 min, and then exposed to 400 μM TGHQ for various periods of time (0.25, 0.5, 0.75, 1, 2, 3, 4 hr). PAR accumulation was determined by Western blot analysis.

(A)

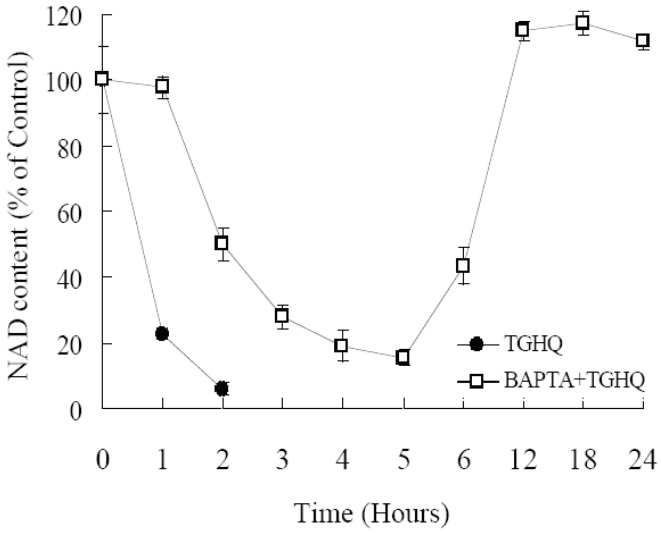

(B)

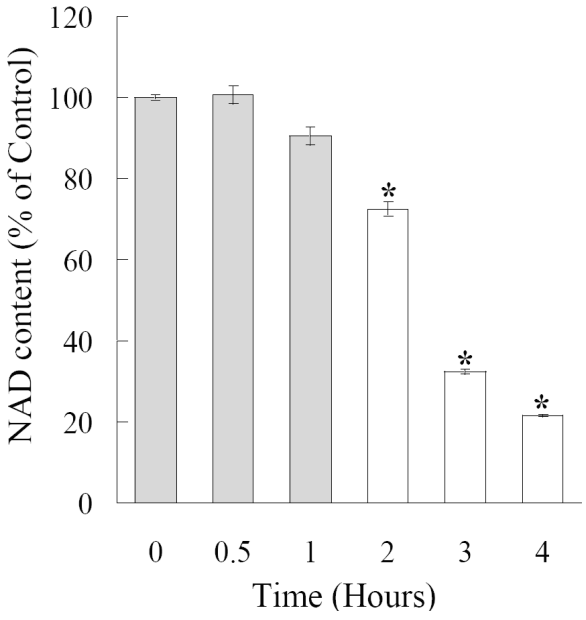

Figure 4.12. Ca^{2+} depletion delays TGHQ-mediated NAD loss, which is also PARP dependent.

(A) Cells were treated with 400 μM TGHQ in the presence or in the absence of BAPTA-AM. After 4 hr exposure, medium containing TGHQ was replaced by normal culture medium. NAD content was determined at different time points as indicated (1, 2, 3, 4, 5, 6, 12, 18, 24 hr). **(B)** BAPTA-AM pretreated (5 μM, 30 min) cells were exposed to 400 μM TGHQ. PJ34 was co-treated with TGHQ or added to TGHQ-treated cells at various times afterwards as indicated (0.5, 1, 2, 3, 4 hr). NAD content was measured 4 h after initial TGHQ treatment. *: $p<0.05$.

4.2.8. TGHQ-induced poly(ADP-ribosyl)ation alters intracellular Ca^{2+} release

We finally examined a possible connection between PARP-1 hyperactivation and intracellular Ca^{2+} levels in response to TGHQ. HK-2 cells were loaded with Fura-2-AM for 45 min, and then treated with 400 μM TGHQ in the presence or absence of 10 μM PJ34. An area of cells was selected and changes in fluorescence were recorded every 15 seconds up to 1 hr. After exposure to 400 μM TGHQ, HK-2 cells exhibited a 2-5 fold increase in Fura-2 fluorescence from 30 to 40 min (Figure 4.13). The rise in intracellular Ca^{2+} concentrations was inhibited in the presence of PJ34. However, not all TGHQ-treated cells were affected by the pretreatment with PJ34. 4 of 25 cells monitored, 4 exhibited a rise in intracellular Ca^{2+} concentration in response to TGHQ despite the presence of PJ34. In contrast to cells exposed to TGHQ alone, PJ34 pretreated cells which exhibited a rise in intracellular Ca^{2+} concentration showed a delayed (started from ~50 min) and attenuated (less than 1 fold) increase in intracellular Ca^{2+} levels. This may be due to the heterogeneity of the cell population. These data suggest a role for poly(ADP-ribosyl)ation in the modulation of intracellular Ca^{2+} release after TGHQ exposure.

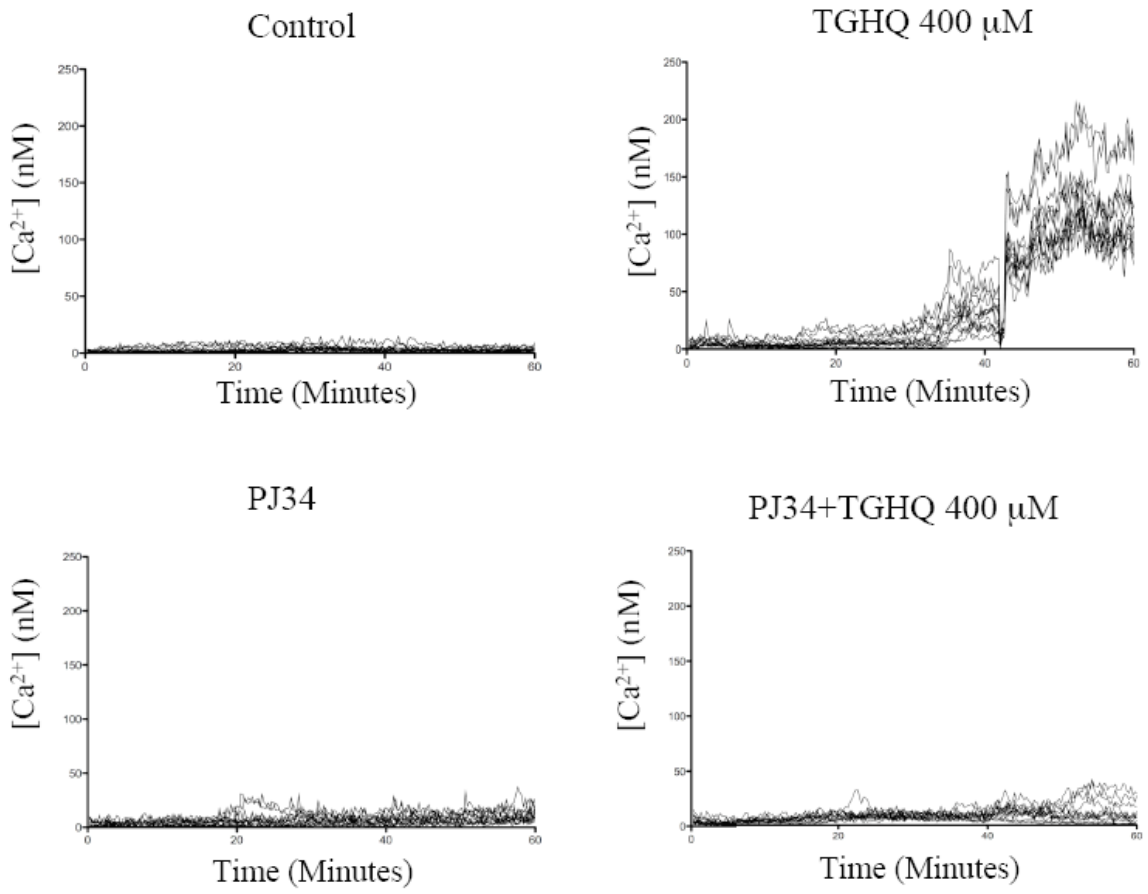

Figure 4.13. TGHQ-induced intracellular elevations in Ca^{2+} concentrations are PJ34 sensitive.

Analysis of intracellular Ca^{2+} concentration was performed using cell permeable Ca^{2+} sensitive indicator Fura-2-AM. Cells were loaded with Fura-2-AM (5 μM) for 45 min, and incubated for an additional 20 min to allow for hydrolysis of the AM-ester. Cells were then exposed to 400 μM TGHQ in the presence or in the absence of PJ34 (10 μM). Images were collected every 15 seconds for 1 hr, as indicated. These results are displayed in graphic form to illustrate fold changes in Fura-2 fluorescence in cells after TGHQ treatment. Each line represents the change in Fura-2 fluorescent intensity of individual cells overtime; each graph represents one of at least three independent experiments.

4.3. DISCUSSION

Disruption of cellular Ca^{2+} homeostasis contributes to cell death, TGHQ-induced cell death occurs in a Ca^{2+}-dependent manner (Figure 4.2). TGHQ-induced necrotic cell death of HK-2 cells is also PARP-1-dependent (Chapter 3). We propose that rapid activation of PARP-1, along with elevations in intracellular Ca^{2+} concentrations in response to TGHQ, activate a novel AIF-independent necrotic cell death pathway. Increases in intracellular Ca^{2+} concentrations are ROS-dependent, suggesting that Ca^{2+} plays a critical role in the signaling of ROS-induced necrosis. When increases in intracellular Ca^{2+} concentrations are directly blocked via BAPTA-AM pretreatment, downstream responses such as loss of mitochondrial membrane potential and cell death, were prevented. Our results also reveal that PARP-1 hyperactivation, NAD depletion, and mitochondrial membrane depolarization are all coupled to increases in intracellular Ca^{2+} concentrations.

Downstream events responsible for the execution of Ca^{2+}-mediated cell death remain poorly understood. One such downstream executor is the Ca^{2+}-dependent protease, calpain. Activation of calpain activity by rises in intracellular Ca^{2+} concentrations is a well characterized response of oxidative stress (Hill et al., 2008; van Wijk and Hageman, 2005). However, althouth inhibition of calpain attenuated TGHQ-induced cytotoxictiy (Figure 4.7), none of the calpain inhibitors could fully rescue TGHQ-mediated cell death, indicating activation of calpain was necessary but not sufficient for TGHQ-induced cytotoxicity.

In elucidating TGHQ-mediated necrotic cell death, the data reveal that Ca^{2+}-modulated PARP-1-hyperactivation commits cells to death in the absence of AIF translocation (Chapter 3). Moreover, ROS-induced, PARP-1-mediated necrotic cell death requires Ca^{2+} as a cofactor. Ca^{2+} chelation with BAPTA-AM not only attenuated PAR accumulation (Figure 4.11), but also altered the pattern of NAD depletion (Figure 4.12A). In vitro studies on poly(ADP-ribosyl)ation suggeste that Ca^{2+} is required for the activation of PARP-1 auto(ADP-ribosyl)ation (Kun et al., 2004). In addition, Ca^{2+} can hyperactivate PARP-1 in vivo in the absence of DNA strand breaks (Homburg et al., 2000). We speculate that ROS-induced elevations in intracellular Ca^{2+} concentrations might directly regulate PARP-1 activity. Thus, BAPTA-AM protects cells against TGHQ-mediated cytotoxicity by reducing intracellular free Ca^{2+} and preventing hyperactivation of PARP-1. More importantly, BAPTA-AM did not completely inhibit PARP-1 activation (Figure 4.11), which would be important for the ability of the residual PARP-1 activity to sufficiently repair TGHQ-mediated DNA strand breaks. This hypothesis is consistent with the finding that histone H2AX phosphorylation returns to control levels 24 hr post TGHQ exposure in BAPTA-AM pretreated cells (Figure 4.5). Furthermore, increases in Ca^{2+} levels can apparently inhibit PARG activity by up to 50% (Tanuma et al., 1986). Decreases in PARG activity will disrupt the normal turnover of PAR, resulting in PARP-1 self-inhibition. Therefore, BAPTA-AM mediated cytoprotection may be consequence of the maintenance of PARG function, releasing PARP-1 self-inhibition, and sustaining levels of DNA repair necessary for cell survival.

Although Ca^{2+} has been recognized as playing a key role in cell injury and cell

death for many years, the regulatory mechanisms by which intracellular Ca^{2+} promote cell death in response to ROS remain debatable. The complex manner in which intracellular Ca^{2+} homeostasis is maintained is a major reason for this inconstancy, particular the multiple channels, uniporters, exchangers, and ATP-dependent pumps that modulate the import, export, and intracellular redistribution of Ca^{2+} (Graier et al., 2007). Several adenine-containing second messengers including ADP-ribose, cyclic ADP-ribose, and nicotinic acid–adenine dinucleotide phosphate are involved in the regulation of Ca^{2+}-homeostasis (Fliegert et al., 2007). At least one such Ca^{2+}-influx pathway, the TRPM2 channel is regulated by free ADP-ribose (Kuhn et al., 2005; Naziroglu and Luckhoff, 2008). TRPM2 is a member of the transient receptor potential melastatin-related (TRPM) family of cation channel enabling influx of Na^{+} and Ca^{2+} (Eisfeld and Luckhoff, 2007; Harteneck, 2005). TRPM2 is activated upon oxidative stress leading to an increase in the cytosolic Ca^{2+} concentration (Hara et al., 2002; Wehage et al., 2002). Oxidative stress may act via the free ADP-ribose after poly(ADP-ribose) have been formed by PARP-1 and hydolysed by PARG (Fonfria et al., 2004). ADP-ribose regulates TRPM2 through binding to a Nudix box motif in the cytosolic C-terminus of the channel (Perraud et al., 2005). This is consistent with our data showing that inhibition of PARP-1 by PJ34 prevented the increase in intracellular Ca^{2+} concentrations (Figure 4.13). Thus Ca^{2+} modulates PARP-1 activity which in turn regulates Ca^{2+} homeostasis in the cells exposed to ROS. Rises in intracellular Ca^{2+} concentrations will accelerate TGHQ-induced PARP-1 activation, leading to PARP-1 hyperactivation, creating a feed-forward loop whereby the generation of free ADP-ribose favors more Ca^{2+} influx, resulting in a vicious cycle

(Figure 4.14).

In summary, our studies provide new insights into PARP-1-mediated necrotic cell death. We propose that changes in intracellular Ca^{2+} concentrations provide a connection between PARP-1-hyperactivation and subsequent cell death, during which AIF is retained in the mitochondria. The loss of cellular NAD, loss of the mitochondrial membrane potential, and Ca^{2+}-mediated activation of calpain, all contribute to the ROS-induced PARP-1-dependent cell death. The qualitative, quantitative, and temporal nature of the cell stress determines the nature of the cellular stress response. In other words, the nature, intensity, and duration of any particular stress will dictate the nature of the response and the outcome; whether the cell survives, or succumbs to death *via* necrosis or apoptosis. It is at the interface between the commitment to either necrosis or apoptosis that many opportunities exist and questions remain to be answered. For example, can interventions be made to the necrotic response in order that a more controlled form of cell death can be engaged, with less tissue threatening consequences? Our data indicate that responses to stress that usually result in necrotic cell death can indeed be manipulated, at the genetic and pharmacological level, to produce a potentially favorable (survivable) tissue response.

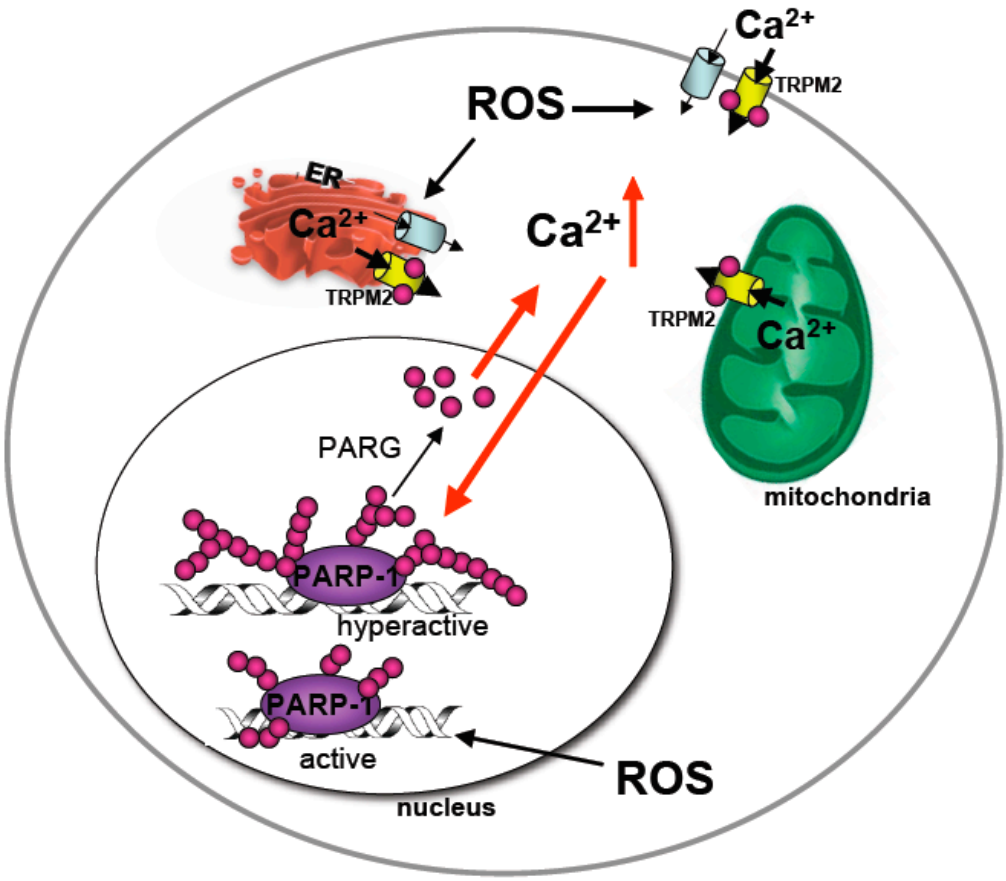

Figure 4.14. Inter-regulation between PARP-1 and intracellular Ca^{2+} in response to ROS.

ROS mediate DNA strand breaks leading to the activation of PARP-1. In addition, ROS oxidize Ca^{2+}-channel proteins resulting in Ca^{2+} influx into the cytosol. Rises in intracellular Ca^{2+} concentrations accelerate the activation of PARP-1, leading to PARP-1 hyperactivation. Meanwhile, free ADP-riboses, generated from the degradation of poly(ADP-ribose) by PARG, ativates Ca^{2+}-channel such as TRPM2 and favor more Ca^{2+} influx, resulting in a vicious cycle between hyperactivation of PARP-1 and elevation of intracellular Ca^{2+}. (●: ADP-ribose)

CHAPTER 5: PEROXIREDOXIN III: THE MITOCHONDRIA ANTIOXIDANT AND ITS ROLE IN MODULATING THE RESPONSE TO OXIDATIVE STRESS

5.1. INTRODUCTION AND RATIONALE

ROS are associated with a variety of human diseases such as tumorigenesis, atherosclerosis, diabetes mellitus, and with the aging process (Bolton et al., 2000). ROS initiate cell injury by interacting with selective cellular constituents. The redox active chemical, HQ exhibits an array of toxicological activity, behaving as both a nephrotoxicant and a nephrocarcinogen (Lau et al., 2001; Monks et al., 1991; Peters et al., 1997). HQ induces cellular toxicity by a combination of the generation of ROS and by covalently binding to cellular proteins. It is important to note that these two properties are not necessarily mutually exclusive, since covalently adducted quinones still retain the ability to redox cycle. This may lead to the local focusing of an oxidative stress. Sequential oxidation and addition of GSH to 1,4-benzoquinone leads to the formation of a number of GSH conjugates, including TGHQ (Lau et al., 1988a). TGHQ retains the ability to redox-cycle and to generate ROS (Monks and Lau, 1994). Although TGHQ induces ROS-dependent DNA damage and cell death in renal proximal tubule epithelial cells (LLC-PK1) (Jeong et al., 1996; Mertens et al., 1995; Ramachandiran et al., 2002), it remains unclear precisely how ROS generated by redox-active quinone metabolites initiate and promote renal cell death. The goal of the present studies therefore was to understand the molecular mechanisms whereby TGHQ-mediated ROS formation induces cellular toxicity in renal epithelial cells. In particular, previous studies in our laboratory

using two-dimensional gel electrophoresis and mass spectrometry revealed significant changes in peroxiredoxin III (PrxIII) proteins in response to TGHQ, and we therefore focused current efforts on elucidating the role of PrxIII in TGHQ-mediated cytotoxicity.

PrxIII belongs to a multifunctional family of thiol-specific peroxiredoxins (Prxs). In the presence of thioredoxin, Prxs behave as antioxidants by catalyzing the reduction of peroxides (Hofmann et al., 2002). Upon oxidative stress, the redox-sensitive cysteine of one subunit of Prxs is oxidized to Cys-SOH, which then reacts with a neighboring Cys-SH on the second subunit to form an intermolecular disulfide. Prxs can be "over-oxidized" to sulfinic ($PrxSO_2$) or sulfonic forms ($PrxSO_3$) which subsequently lose their peroxidase properties (Seo et al., 2000; Wagner et al., 2002; Wood et al., 2003b). In addition to their peroxidase activity, Prxs participate in redox-signal transduction pathways and act as "gatekeepers" for cell signaling in response to ROS (Wood et al., 2003a). In mammalian cells, the Prx family includes at least six isoforms (Chae et al., 1999b; Chae et al., 1994; Rhee et al., 2001). PrxI-IV possess two conserved cysteine residues, whereas PrxsV and VI possess only one of the cysteine residues that participate in catalyzing the peroxidase activity (Kang et al., 1998). Prxs are ubiquitously distributed and reside in the cytoplasm, nucleus, mitochondria, peroxisomes, endoplasmic reticulum and extracellular space. Of the various Prxs, PrxIII contains a mitochondrial localization sequence, and is exclusively localized to the mitochondria (Araki et al., 1999) where it is essential for mitochondrial homeostasis and inhibiting neoplastic transformation (Wonsey et al., 2002). PrxIII regulates physiological levels of H_2O_2 and plays an important role in the antioxidant defense system within mitochondria.

To further examine the role of PrxIII in TGHQ-mediated cellular toxicity, we transiently transfected wild-type or dominant negative PrxIII, respectively, into LLC-PK1 cells, and examined the functional effect of PrxIII on TGHQ-mediated cytotoxicigy. The reason to use pig cells instead of human cells in the this study is because we can obtain ~90% transfection efficiency in LLC-PK1 cells compared to ~10% transfection efficiency in HK-2 cells. In addition, previous studies which revealed the changes in PrxIII by 2-D gel electrophoresis followed by mass spectrometry were also conducted in LLC-PK1 cells.

5.2. RESULTS

5.2.1. PrxIII is modified by TGHQ in LLC-PK1 cells.

Total proteins from control and TGHQ treated (200 μM, 2 hr) cells were separated by 2-D gel electrophoresis and stained with SYPRO Ruby protein stains (Bio-Rad, Hercules, CA) (Figure 5.1A). After TGHQ treatment, the intensity of the spot with more acidic pI increased, and the intensity of the spot with more basic pI decreased compared to controls. This mode of change is likely due to a post-translational modification(s), such as an oxidation and/or phosphorylation. To confirm this acidic shift, we performed PrxIII immunoblot assays after 2-D gel electrophoresis, which revealed the same shifting pattern in TGHQ treated samples when compared to controls (Figure 5.1B, top pannel). To further investigate the putative post-translational modification causing these acidic shifts, proteins from control and TGHQ treated samples were again separated by 2-D gel electrophoresis followed by western blotting with a Prx-SO_3H antibody that reacts specifically with the sulfinic or sulfonic forms of Prxs (Figure 5.1B, bottom pannel).

Immunoblot analysis revealed that the second and third spots represented the oxidative form of PrxIII, and the observed decrease in the first PrxIII spot intensity was likely due to a shift of mobility of the protein after TGHQ treatment.

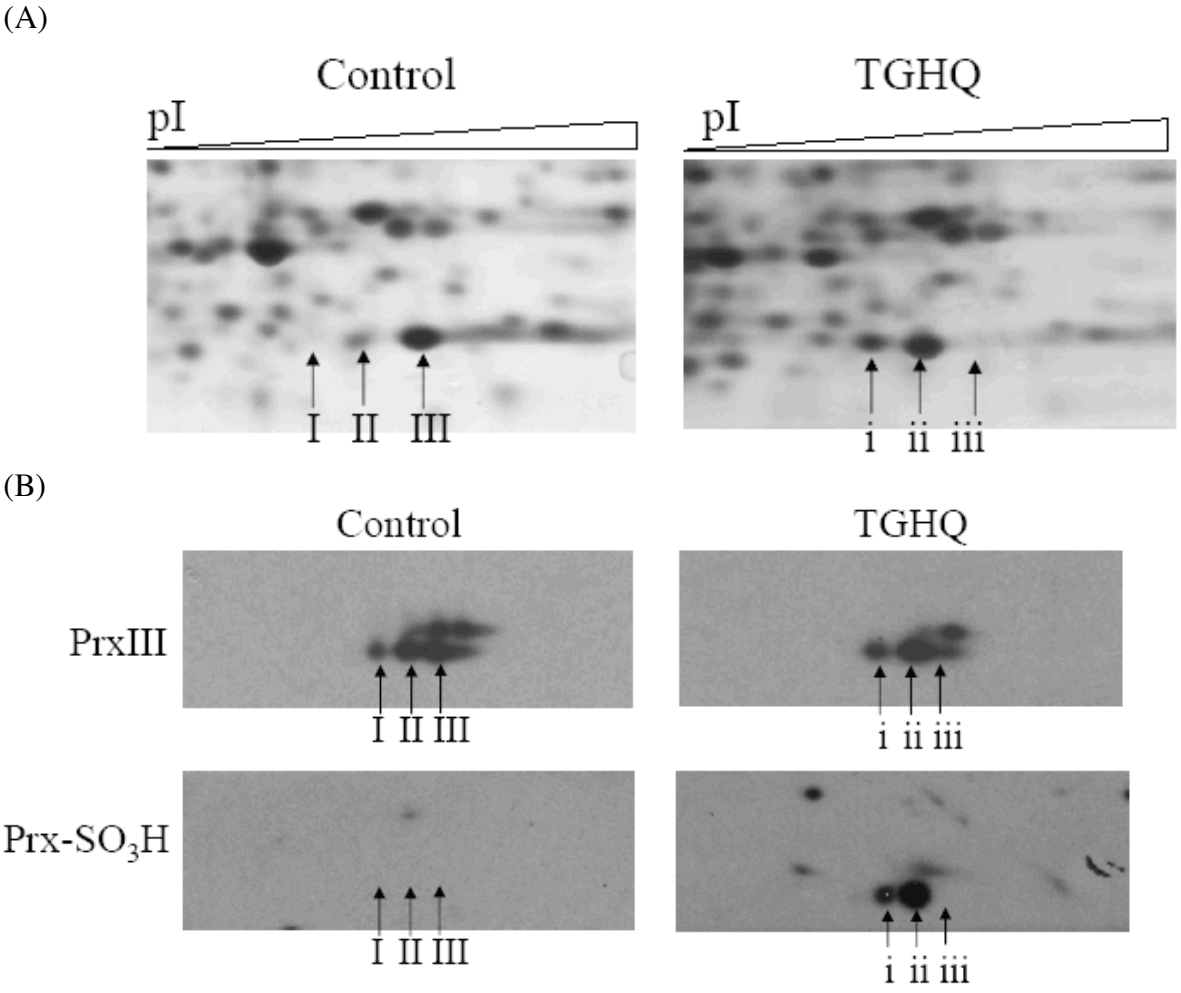

Figure 5.1. TGHQ induced modification of PrxIII revealed by 2-D gel analysis.

Total protein extract (100 μg) derived from either untreated cells (control) or cells treated with 200 μM TGHQ for 2 hr were subjected to 2-D gel electrophoresis. **(A)** Samples were separated by ICF using 3-10 IPG strips, followed by SDS-PAGE, and finally visualized by fluorescent staining. **(B)** The corresponding gels were subjected to western blot analysis using antibodies recognizing either PrxIII (upper blots) or Prx-SO_3H (lower blots). The corresponding spots on the control (I, II, III) or TGHQ-treated samples (i, ii, iii) are marked with the same numbers.

5.2.2. Oxidation of PrxIII.

Transitions between monomers and dimers of Prxs are governed by oxidation state (Moon et al., 2005). To study the oxidation state of PrxIII after TGHQ exposure, immunoblot analysis under reducing denaturing, or non-reducing denaturing conditions was devised to detect the relative amounts of reduced (Prx-SH), oxidized (Prx-S-S-Prx) or superoxidized (Prx-SO_2H/SO_3H) forms of PrxIII. Non-reducing SDS-PAGE revealed that only the PrxIII dimer was observed in control samples (Figure 5.2). With increasing TGHQ concentrations and exposure time, more PrxIII was oxidized to the sulfinic or sulfonic forms, which were present in the monomeric state. Complete conversion of dimeric PrxIII to oxidized PrxIII monomers was achieved with 400 μM TGHQ. At high TGHQ concentrations, the appearance of monomeric bands indicated that hyperoxidized PrxIII are no longer capable of dimer formation.

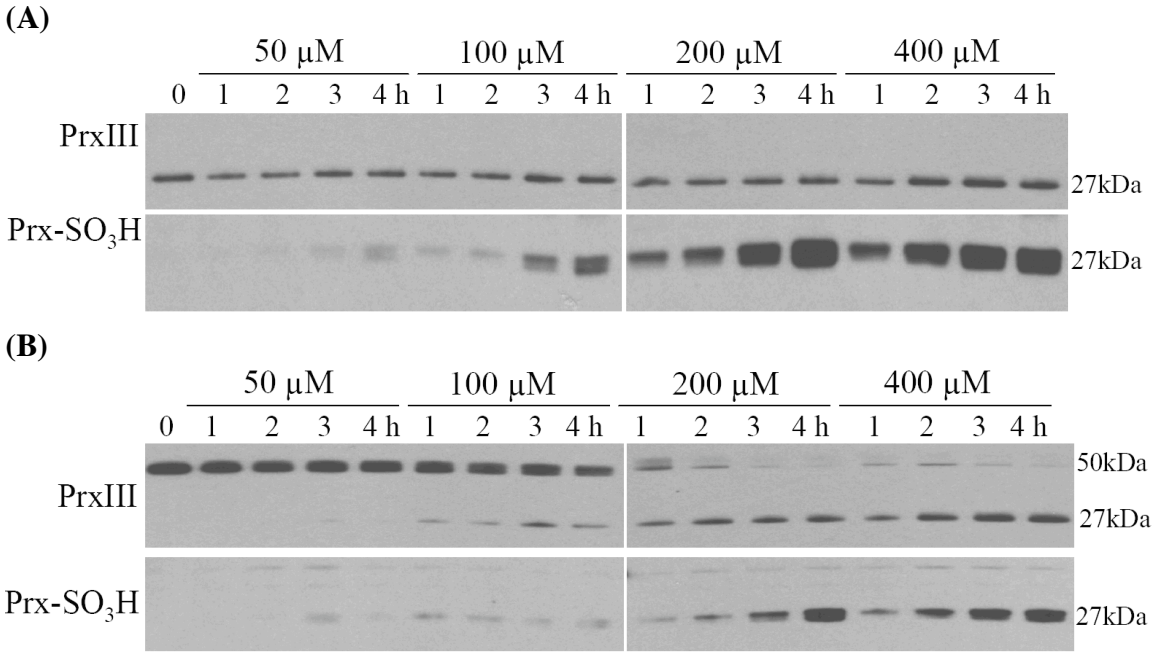

Figure 5.2. TGHQ mediated changes in PrxIII redox status revealed by western blot analysis.

TGHQ-treated cells were lysed and subject to western blot analysis under reducing **(A)** or non-reducing **(B)** denaturing conditions using specific antibodies against PrxIII (upper blots) or Prx-SO_3H (lower blots). Total protein extracts (5 μg) were loaded onto SDS-PAGE either from untreated cells or cells treated with different dose of TGHQ (50, 100, 200, 400 μM) for different periods of time (1, 2, 3, 4 hr).

5.2.3. TGHQ-mediated changes in the structure of PrxIII

We analyzed PrxIII protein structure on a native-PAGE gel under non-denaturing conditions. Native western blot analysis revealed a significant band shift after TGHQ treatment (Figure 5.3A). Before treatment, a single band was identified as native PrxIII by mass spectrometry. In the presence of TGHQ (200 μM or 400 μM, 2 hr) the intensity of the native PrxIII band decreased significantly, with the concomitant appearance of multiple forms of high molecular weight (HMW) protein complexes above the native PrxIII band. This mobility shift is most likely due to the formation of the Prx molecular chaperone structure, as reported by others for PrxI and PrxII (Jang et al., 2006; Moon et al., 2005). Interestingly, longer exposure (200 μM or 400 μM, 4 h) of LLC-PK1 cells to TGHQ resulted in a return of the HMW complexes to low molecular weight (LMW) protein species, which were observed as bands with even lower mobility than those associated with native PrxIII bands. Moreover, only the LMW protein species appeared to represent hyper-oxidized forms of Prxs, as indicated by the native western with $PrxSO_3H$ antibody (Figure 5.3B).

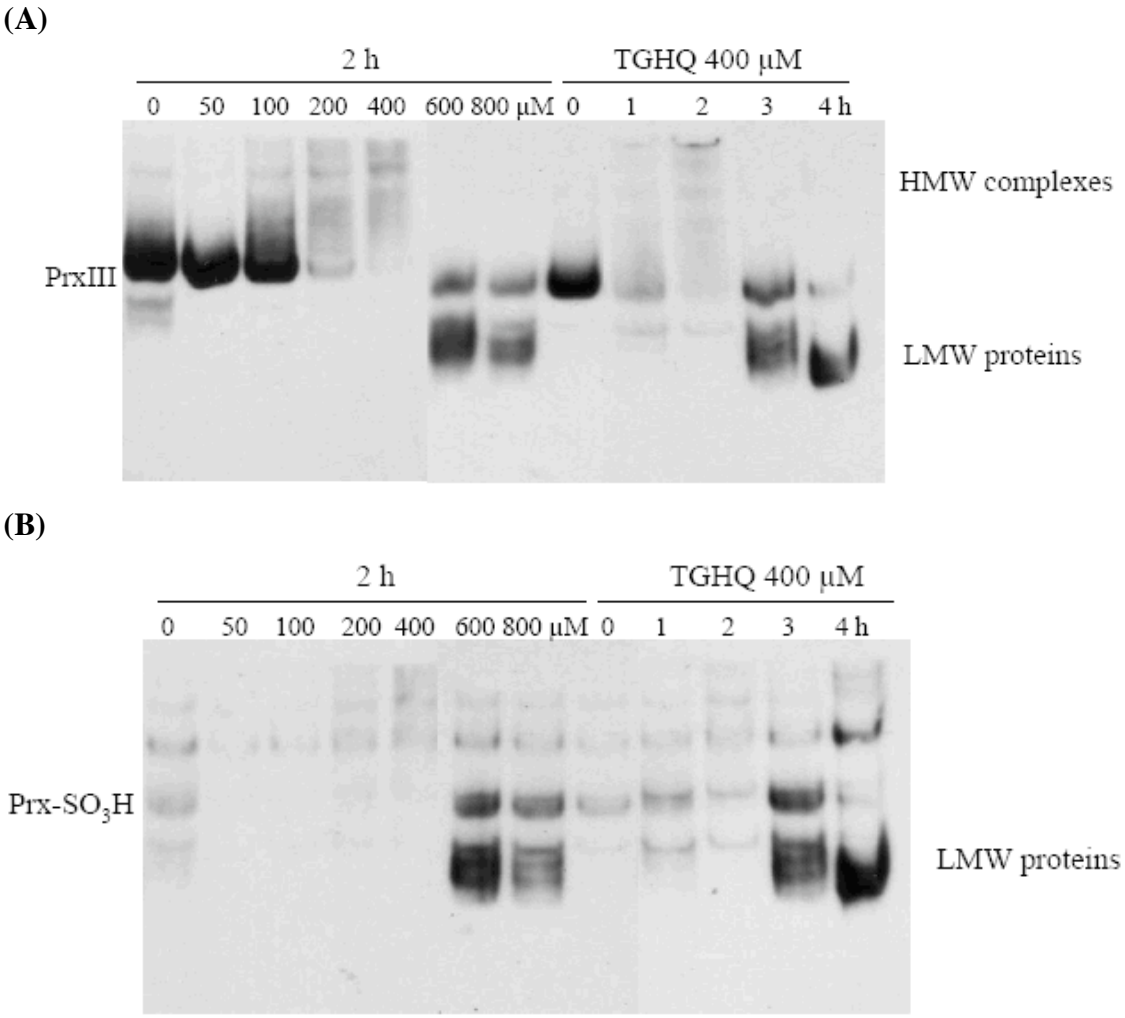

Figure 5.3. Effect of TGHQ on PrxIII protein conformation.

Cells were treated with different concentrations of TGHQ for various times (0.5, 1, 2, 3, 4 hr). Total protein extracts (5 µg) were prepared in the absence of reducing agents and revolved by native gel electrophoresis to preserve protein complexes. Native western blot with antibodies against PrxIII **(A)** or Prx-SO_3H **(B)** revealed HMW complexes of PrxIII.

5.2.4. Construction and expression of PrxIII and PrxIII mutants.

PrxIII contains two conserved redox-active sites, which exist at C108 and C229 in the translated precursor form prior to import into mitochondria (identical to C47 and C168 in processed mitochondrial form) (Kang et al., 2005). The putative catalytic cysteine residues, C47 and C168, are essential for PrxIII function (Cao et al., 2007). Site-directed mutagenesis was used to generate a dominant negative PrxIII (C108S, C229S) mutant containing a c-myc epitope tag on the N-terminal. Recombinant PrxIIIs were transiently transfected into LLC-PK1 cells. Protein expression was measured by immunoblotting, which demonstrated the expression of the proteins with correct mass (29 kDa) as predicted for the recombinant PrxIIIs containing the c-myc epitope tag (Figure 5.4A).

5.2.5. Effect of PrxIII mutant on cell death induced by TGHQ.

Exposure of LLC-PK1 cells to TGHQ is known to increase cellular ROS and subsequently to cause necrotic cell death. Overexpression of PrxIII was shown to influence cell viability and susceptibility to apoptosis (Chang et al., 2004a; Nonn et al., 2003). We examined the effect of dominant negative PrxIII (C108S, C229S) on TGHQ-induced cell death. Wild-type PrxIII transfected cells were protected against TGHQ-induced cell death, with a 15% increase in cell viability compared with empty vector-transfected cells (Figure 5.4B). In contrast, dominant negative PrxIII-C108, C229S transfected cells were more susceptible to TGHQ-mediated toxicity, with a 15 % decrease in cell viability compared to empty vector-transfected cells.

(A)

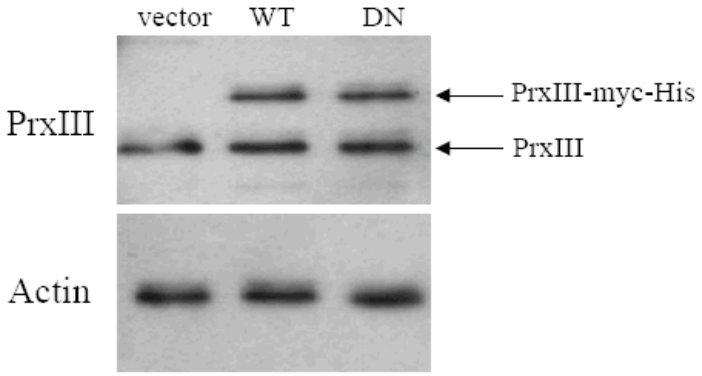

(B)

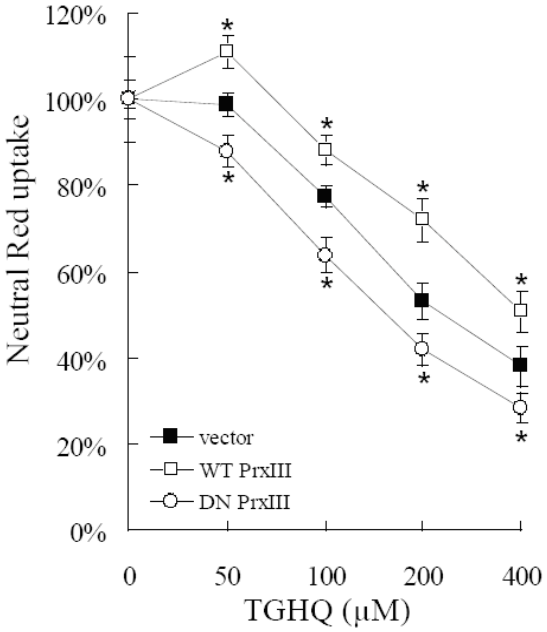

Figure 5.4. Dominant negative PrxIII (C108S, C229S) potentates TGHQ-induced cell death.

(A) Expression of recombinant PrxIII. Log phase cells were transiently transfected with wild-type PrxIII (WT), dominant negative (C108S, C229S) PrxIII (DN) or vector alone. 24 hr after transfection, cells were collected and subject to western blot analysis with anti-PrxIII antibody. Actin was used as a loading control. **(B)** TGHQ-mediated cytotoxicity in cells expressed recombinant PrxIII. WT, DN or vector transfected cells were treated with 200 μM TGHQ for 2 hr. Cell viability was measured using the neutral red assay. Differences between DN PrxIII and vector or WT PrxIII and vector transfected cells were significant at $p < 0.05$. Results are representative of three independent experiments, each analyzed in triplicate.

5.3. DISCUSSION

Three spots with altered mobility were identified by 2-D gel electrophoresis coupled to MALDI-TOF analysis, following treatment of LLC-PK1 cells with TGHQ. All three spots were identified as PrxIII. Others have reported the identification of only two spots on a 2-D gel as PrxIII, and observed similar changes in spot intensity after H_2O_2 treatment (Rabilloud et al., 2002). 2D-immnuoblot analysis with Prx-SO_3H antibody confirmed that those spots with a more acidic pI were in fact oxidized PrxIII (Figure 5.1). Thus, TGHQ-induced PrxIII modification involves oxidation of cysteine residues to sulfinic or sulfonic acid derivatives. The third spot definitively identified as oxidized PrxIII likely contains an additional post-translational modification, perhaps phosphorylation, which to date has only been reported for PrxI and PrxII (Chang et al., 2002; Jang et al., 2006; Przedborski, 2007). We are in the process of identifying the nature of this modification by LC-MS/MS.

Native western blot analysis revealed the presence of high molecular weight (HMW) forms of PrxIII following treatment with TGHQ (Figure 5.3). However, these HMW complexes were not hyper-oxidized PrxIII, with the sulfinic or sulfonic forms of PrxIII only being detected in the LMW protein species with longer exposure times (200 μM or 400 μM, 4h) or higher TGHQ dosage (600 or 800 μM) at 2h. HMW forms of PrxI and Prx II act as molecular chaperones, thereby exerting an additional cytoprotective function in response to heat-shock or oxidative stress (Jang et al., 2004; Moon et al., 2005). Indeed, the crystal structure of PrxIII reveals the presence of two catenated dodecameric toroids (Cao et al., 2007). However, the physiological relevance of this

structure remains to be demonstrated. Nonetheless, our results are the first to clearly indicate that HMW forms of mitochondrial PrxIII are formed under conditions of oxidative stress and appear to be devoid of hyper-oxidized cysteine sulfhydryls. Dose-dependent changes in the pattern and redox state of PrxIII might therefore serve as useful biomarkers of the extent of ROS-induced cell and tissue injury.

PrxIII also functions as a direct antioxidant by catalyzing the removal of H_2O_2. When cells are exposed to ROS, they possess a first line of defensive barriers to protect themselves against oxidative stress. In the presence of a small/physiological amount of intracellular ROS, PrxIII reduces H_2O_2 via the oxidation of the active cysteine sulfhydryl group to sulfenic acid (SOH), and subsequently disulfide bond formation with the second active cysteine residue on the accompanying monomer (Figure 5.5). Oxidation of these cysteine residues is quickly reversed by thioredoxin and thioredoxin reductase, and PrxIII regains its direct catalytic antioxidant function. In contrast, in the presence of an overwhelming amount of ROS, further oxidation of the PrxIII cysteine residues to sulfinic (SO_2H) and sulfonic acids (SO_3H) occurs, and this hyper-oxidation might be slowly reversible by sestrins and sulfiredoxin, in a manner similar to that reported for PrxI and PrxII (Biteau et al., 2003; Budanov et al., 2004). Because the turnover rate of the hyper-oxidation is kinetically slow ($3 \times 10^{-3}\,s^{-1}$) (Chang et al., 2004b), the catalytic antioxidant function of PrxIII is lost and ROS are available to interact with other cellular constituents and to mediate subsequent cellular toxicity. More interestingly, the oxidative stress results in a structural change in PrxIII and the formation of HMW complexes, which might function as molecular chaperones to

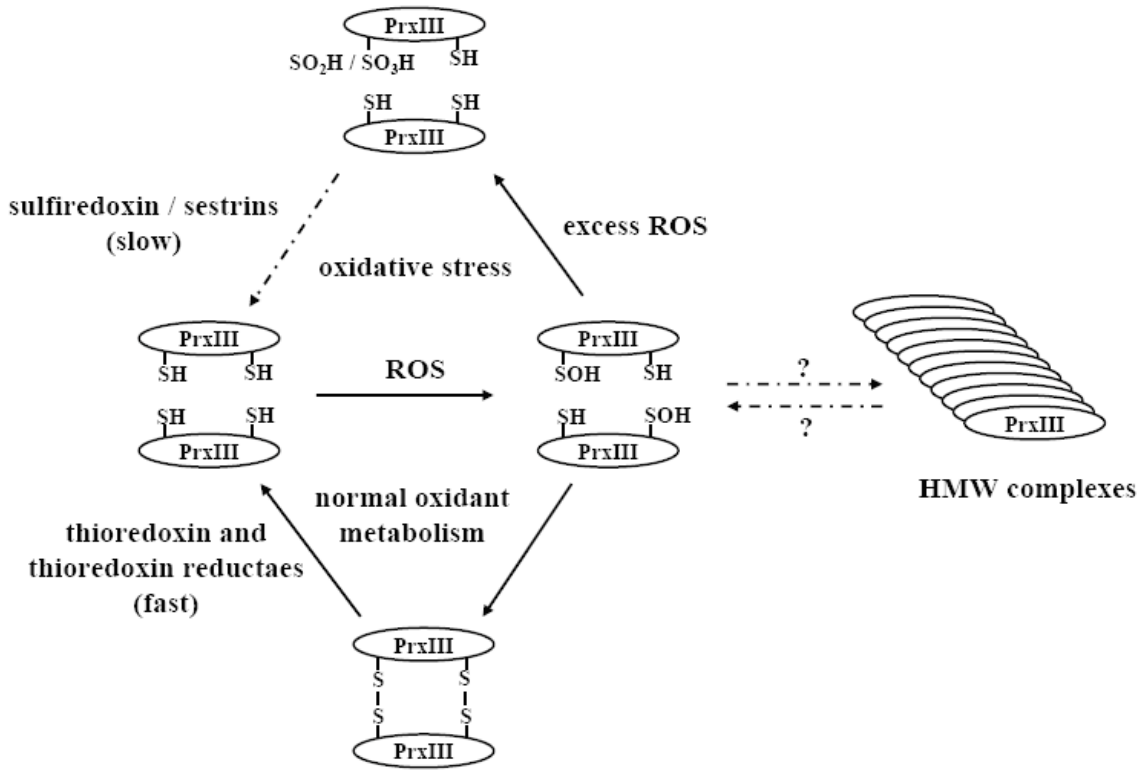

Figure 5.5. A schematic model for the cellular function of PrxIII.

Schematic representation of the proposed redox behavior for PrxIII.

prevent protein aggregation. It also appears that the hyper-oxidation of PrxIII promotes the reversion of HMW complexes back into LMW protein species. These hyper-oxidized LMW species of PrxIII are also incapable of performing the chaperoning function. Factors that regulate the conversion of mono/dimeric PrxIII into multimeric chaperone complexes as opposed to the hyper-oxidation of PrxIII are not known, and form the basis of additional ongoing investigations. Utilization of the PrxIII Cys mutants will enable us to determine whether or not the formation of HMW PrxIII complexes is dependent on their hyper-oxidation state.

TGHQ catalyzes the formation of ROS within renal epithelial LLC-PK1 cells, and inhibiting the accumulation of ROS by the addition of exogenous catalase prevents TGHQ-induced necrotic cell death (Jeong et al., 1997a). We have now shown that PrxIII overexpression is able to alter sensitivity of the cells to TGHQ. Cells overexpressing wild-type PrxIII exhibit an increased tolerance to TGHQ-meditated cytotoxicity (Figure 5.4B). In contrast, cells expressing a dominant-negative mutated PrxIII were more susceptible to TGHQ (Figure 5.4B). The data clearly reveal an important role for mitochondrial PrxIII in modulating the cellular response to TGHQ-induced ROS generation. Because transient transfection of both the wild-type and dominant-negative forms of PrxIII were relatively modest (~30 % transfection efficiency), we are in the process of developing lenti-viral infection of LLC-PK1 cells which should provide a more striking response to TGHQ-induced cytotoxicity. Establishment of stably transfected cell lines was hampered by the low level of expression both the wild-type and mutant forms of PrxIII. Nonetheless, the results of our study are consistent with findings

that overexpression of PrxIII efficiently prevents apoptosis induced by platelet-derived growth factor or tumor necrosis factor-α (Zhang et al., 2007a), and depletion of PrxIII with RNAi enhanced the effects of staurosporine on apoptosis (Chang et al., 2004a).

In summary, the present study reveals that mitochondrial PrxIII plays an important role in modulating the response to quinone-generated ROS, and we have demonstrated for the first time that the catalytic sites of PrxIII, C108 and C229, are physically involved in the oxidative stress response in culture cells. Utilization of these mutant forms of PrxIII will permit us to determine the role that these critical cysteine residues play in regulating the transition from monomeric/dimeric to multimeric PrxIII and their role in the chaperone function of PrXIII.

CHAPTER 6: CONCLUDING REMARKS

Although the ability of HQ to act as either an electrophile or redox cycling agent is well established, the complex mechanisms of action of chemical toxicants makes it extremely difficult to evaluate the precise mechanism of toxicity. Studies from our laboratory show that TGHQ induces rapid ROS generation, DNA single strand breaks, cell cycle arrest, and ROS-dependent necrotic cell death in porcine renal proximal tubule epithelial cells LLC-PK1. Although the LLC-PK1 cell line is a well established *in vitro* model to study chemical-induced renal cell death, LLC-PK1 cells originate from the New Hampshire Mini-pig. Thus, to assess the contribution of ROS in TGHQ-mediated nephrotoxicity, we investigated the oxidative stress response signaling pathways in a human proximal tubular epithelial line, HK-2. Activation of multiple stress-signaling pathways was demonstrated in LLC-PK1 cells exposed to TGHQ, including EGFR, MAPKs (ERKs, p38 MAPKs and JNKs), and histone H3 phosphorylatio.

In the current studies, I focused on two signaling pathways involved in ROS-mediated necrotic cell death in HK-2 cells. Figure 6.1 summarizes the conclusions from these investigations and illustrates potential future directions of research into ROS-mediated necrotic cell death. I first characterized the cytotoxic effects of TGHQ in HK-2 cells. TGHQ induced rapid ROS generation, massive DNA damage and necrotic cell death in HK-2 cells, which is consistent with findings in the LLC-PK1 cell model. Catalase completely prevented ROS generation, γ-H2AX foci formation, and subsequent cell death, indicating that ROS also play an essential role in TGHQ-mediated renal cell death in HK-2 cells. Upon TGHQ-mediated DNA damage, a time- and concentration-

dependent accumulation of PAR and depletion of cellular NAD were observed, suggesting that TGHQ induces hyperactivation of PARP-1 in HK-2 cells (Chapter 3).

In the majority of cases where PARP-1 hyperactivation contributes to cell death, it promotes the translocation of AIF from the mitochondria to the nucleus, inhibition of which abrogates PARP-1-mediated cell death (Kang et al., 2004; Yu et al., 2006). However, TGHQ-induced PARP-1 activation is dissociated from AIF translocation (Chapter 3). The pathways coupling PARP-1 hyperactivation to AIF translocation may be context-dependent, and more rigorous experiments are required to address this issue. For example, other ROS- and DNA damage-inducing agents could be utilized to determine the role of AIF in HK-2 cells. Alternatively, the ability of TGHQ to induce AIF translocation in other renal cell lines could be investigated. In addition, the mode of cell death would also be determined under each treatment condition in order to determine the influence of AIF translocation in apoptotic and necrotic cell death. Such experiments could ascertain whether the lack of AIF translocation in TGHQ-mediated necrotic cell death is cell type specific, treatment specific, or cell fate specific.

Pharmacological inhibition of PARP-1 with PJ34 blocked TGHQ-mediated PAR accumulation, NAD depletion, and subsequently necrotic cell death (Chapter 3). However, PJ34 only seems to delay necrotic cell death in HK-2 cells, which is probably a consequence of the lack of PARP-1-dependent DNA repair processes. Since NAD concentrations are preserved in PARP-inhibited HK-2 cells, cells may initially survive, regardless of the presence of DNA damage. Although inhibition of PARP preserves cellular energy, which is required for cells to commit to apoptosis, the transition from

necrotic to apoptotic cell death did not occur in HK-2 cells. Whether introduction of other apoptosis releasing factors into the experimental system would modify the mode of cell death in PARP-inhibited HK-2 cells is not known. Introduction of an active form of AIF, under tetracycline control, followed by a determination of cell death pathways in the PARP-inhibited HK-2 cells could answer this question.

In addition to activating PARP-1, TGHQ also induces a rapid elevation in intracellular Ca^{2+} levels (Chapter 4). Rises in intracellular Ca^{2+} concentrations lead to an activation of hydrolytic enzyme, such as calpain, and the collapse of the mitochondrial membrane potential. This sequence of events is replicated during TGHQ-mediated necrotic cell death. The Ca^{2+} chelator BAPTA, prevents increases in intracellular Ca^{2+} levels, the loss of mitochondrial membrane potential, and subsequent cell death. However, in contrast to the inhibition of PARP, chelation of intracellular Ca^{2+} completely abrogates TGHQ-induced necrotic cell death. Moreover, BAPTA-stimulated cell survival occurs concomitant with a decrease in DNA damage, reflecting the enhanced ability of cells to repair DNA strand breaks. More interestingly, BAPTA protects cells against TGHQ-mediated toxicity not only by modulating intracellular Ca^{2+} concentrations, but by interferencing with PARP-1 activation. Thus, in the presence of BAPTA, TGHQ-induced PARP-1 hyperactivation is significantly attenuated, and the kinetics of cellular NAD is also altered. The residual PARP-1 activity may be important for the repair of TGHQ-mediated DNA strand breaks, and contributes to the overall protective effects of BAPTA. Our findings suggest that intracellular Ca^{2+} levels may directly or indirectly regulate PARP activation. *In vivo* studies have demonstrated that

Ca^{2+} can hyperactivate PARP-1 in the absence of DNA strand breaks (Homburg et al., 2000). In addition, Ca^{2+} may interfere with PARP activation by regulating PARG activity. Indeed, increases in Ca^{2+} levels can inhibit PARG activity (Tanuma et al., 1986). Although there are no pharmacological inhibitors specifically targeting PARG, we could introduce a dominant negative mutant of PARG in HK-2 cells, and examine their susceptibility to TGHQ. If PARG plays a role in TGHQ-mediated cell death, overexpression of dominant negative PARG might lead to a loss of BAPTA-mediated cytoprotection.

Intracellular Ca^{2+} modulates TGHQ-stimulated PARP-1 activation. In the meanwhile, PARP-1 activity also interfere intracellular Ca^{2+} homeostasis. We demonstrate that inhibition of PARP with PJ34 significantly attenuates TGHQ-mediated elevation of intracellular Ca^{2+} levels, suggesting that PARP activation may exacerbate TGHQ-stimulated disruption of Ca^{2+} homeostasis by activating certain Ca^{2+} channels or transporters. One such Ca^{2+}-channel, TRPM2, is regulated by ADP-ribose (Kuhn et al., 2005; Naziroglu and Luckhoff, 2008).

We have shown that TGHQ induces an increase in intracellular Ca^{2+} concentrations (Chapter 4), without identifying the source of this Ca^{2+}. One such potential source is the endoplasmic reticulum (ER). Intracellular Ca^{2+} changes could be monitored in response to TGHQ by confocal microscopy, and combining an ER tracker with the fluorescence Ca^{2+} indicator. After identification of the specific sources of Ca^{2+}, we could pinpoint particular Ca^{2+} channels involved in TGHQ-mediated Ca^{2+} influx with specific Ca^{2+} channel blockers. In addition, the identity of certain post-translational

modifications on these Ca^{2+} channels, particularly by protein ADP-ribosylation and TGHQ-mediated covalent protein adducts, might assist in revealing Ca^{2+}-channel proteins modulated following exposure to TGHQ.

In addition to its redox ability, TGHQ also retains the ability to form covalent adducts with a variety of cellular macromolecules, which can cause a loss of normal cellular function. One such molecule may be cyclophilin D. H_2O_2-mediated loss of the mitochondrial membrane potential is completely abrogated by the cyclophilin D inhibitor CsA. In contrast, CsA only attenuates TGHQ-induced mitochondrial membrane depolarization (Chapter 4), suggesting that other effects mediated TGHQ, in addition to ROS generation, may contribute to the formation of MPT. In addition, pretreatment with CsA significantly prevents H_2O_2-mediated cell death, but had much less of an effect on TGHQ-mediated cytotoxicity. These combined data suggest that TGHQ-mediated covalent adduction also contributes to the activation of the MPT induced by TGHQ. TGHQ may directly target molecules that comprise the formation of MPT pores. Several proteins, including the adenine nucleotide translocase (ANT), voltage-dependent anion channel (VDAC) and cyclophilin D have been implicated in the formation of MPT pores (Crompton et al., 1998). Therefore, we could apply the different pharmacological inhibitors which target VDAC and ANT, respectively, and examine their effects on TGHQ-mediated loss of mitochondrial membrane potential. In addition, we might also identify specific covalent adducts on these molecules in cells exposed to TGHQ by mass spectrometry.

ROS have been implicated in both apoptosis and necrosis. Although the roles of ROS in apoptotic cell death signaling pathways have been intensively studied, relatively less information is available on ROS-mediated signaling pathways during necrosis. Apoptosis is a generally controlled process which encompasses active signaling pathways. In contrast to apoptosis, necrotic cell death is usually considered to be a passive process. ROS-mediated necrotic injury frequently elicits an inflammatory response, and is associated with a number of human diseases. Therefore understanding the precise molecular mechanisms by which ROS regulate necrotic cell death will not only assists in uncovering ways to manipulate these processes, but also discovering potential therapeutic targets. Overall, this dissertation provides novel research findings that contribute to the understanding of TGHQ-driven ROS-mediated necrotic cell death. The discovery of the inter-regulation between PARP-1 and intracellular Ca^{2+} could have important implications for the manipulation of necrosis.

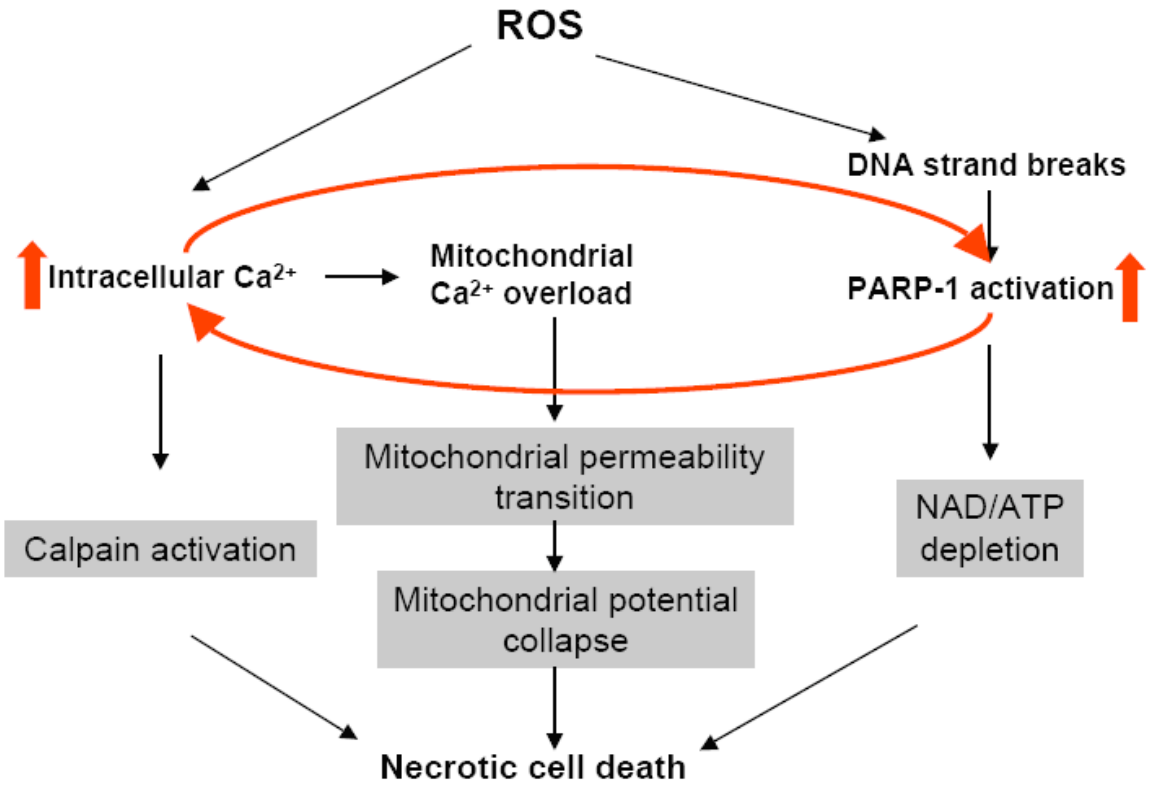

Figure 6.1. Summary of stress-signaling pathways in ROS-mediated necrotic cell death.

Activation of both PARP-1 and Ca^{2+} signaling pathways contributes to ROS-induced necrotic cell death. ROS induce DNA strand breaks leading to activation of PARP-1 and rapid depletion of NAD/ATP. ROS also mediate the elevation of intracellular Ca^{2+} concentrations resulting in activation of the Ca^{2+} sensitve proeases and collapse of the mitochondrial membrane potential. Meanwhile, accumulation of intracellular Ca^{2+} accelerates ROS-induced PARP-1 activation, leading to PARP-1 hyperactivation, creating a feed-forward loop whereby the generation of ADP-ribose favors more Ca^{2+} influx, resulting in a vicious cycle.

APPENDIX-CHAPTER 7:

HISTONE MODIFICATIONS RESPONSE TO DNA DAMAGE

7.1. INTRODUCTION

Exposure to physical and chemical agents such as ionizing radiation and ROS causes DNA damage. Although mechanisms of DNA repair are well established, the relationship between chromatin remodeling and the DNA damage response remains unclear. Signal transduction from cell surface to the nucleus often involves phosphorylation cascades culminating in the modification of chromatin structure. Indeed, complex combinations of post-translational modifications of N-terminal tails of core histones within nucleosomes contribute to the regulation of transcription, mitosis, and programmed cell death (Fischle et al., 2003; Hake et al., 2004; Wang et al., 2004b). Thus, histones are downstream targets of many signaling cascades and the post-translational modification of histones, including methylation, acetylation, phosphorylation, ubiquitination, sumoylation, citrullination and ADP-ribosylation, alter chromatin structure, subsequently dictating the specific biological outcome (Jenuwein and Allis, 2001). Histone phosphorylation is often linked with chromatin condensation involved in mitosis and meiosis, regulated by different histone kinases and phosphatases. For example, histone H3 is rapidly phosphorylated on serine 10 and serine 28 during mitosis (Goto et al., 1999; Wei et al., 1999). In contrast, histone phosphorylation also correlates with chromatin relaxation concomitant with activation of immediate-early response genes, such as *c-fos* and *c-jun* during mitogen stimulation.

Comparatively little is known about how changes in chromatin structure contribute to and facilitate the DNA damage stress response. Although phosphorylation of histone H2AX on serine 139 is one of the earliest responses to DNA double strand breaks, and is important for promoting efficient repair, the coordination of histone modifications and DNA damage remains unclear. Our laboratory has shown an increase in ^{32}P incorporation into histone H3 in response to TGHQ-induced DNA damage (Tikoo et al., 2001), and this modification occurs concomitant with premature chromatin condensation (PCC) and cell death. Moreover, ^{32}P incorporation only occurred on serine residues and not threonine or tyrosine (Palmer, 2004). However, western blot analysis revealed *decreases* in phosphorylation of histone H3 at both S10 and S28, both of which are well-established sites of serine phosphorylation during mitotic chromosomal condensation (Palmer, 2004). Moreover, TGHQ-induced phosphorylation only occurred on the histone H3.3 isoform, and not on histone H3 isoforms H3.1 and H3.2. Comparing the amino acid sequence of all three histone H3 variants, histone H3.3 contains a unique S site at position 31 in the highly modified N-terminal tail region (Figure 7.1), suggesting that S31 might be an alternate site of histone H3 phosphorylation in response to TGHQ-induced DNA damage. To ascertain whether S31 is indeed a novel site of phosphorylation in response to TGHQ, a specific histone H3.3 antibody that only recognizes the phosphorylated H3.3 S31 site was generated. In addition, to determine the role of H3.3 S31 phosphorylation in response to TGHQ, wild-type and histone H3.3 serine to alanine mutants (S31A) were constructed and TGHQ-mediated cytotoxicity determined in cells transiently transfected with wild-type or mutant H3.3.

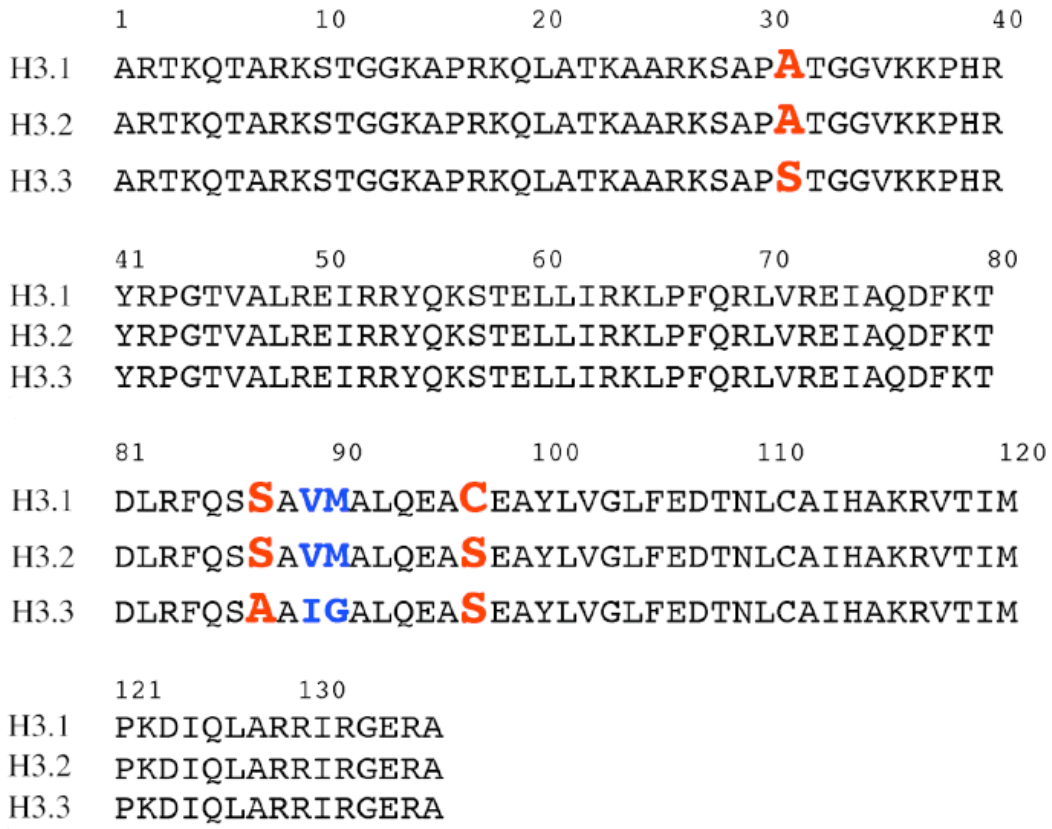

Figure 7.1. Protein sequence alignment showing the N-terminal tail of histone H3 variants.

Three mammalian H3 subtypes have been defined. H3.1 and H3.2 are major histones, which are expressed only during the S-phase of the cell cycle.The replication-independent histone H3.3 is expressed in none dividing quiescent or terminally differentiated cells (Ahmad and Henikoff, 2002a; Ahmad and Henikoff, 2002b).

7.2. MATERIALS AND METHODS

7.2.1. Chemicals, Reagents and Antibodies.

N-methyl-N-nitro-N-nitrosoguanidine (MNNG), H_2O_2, 12-O-tetradecanoyl-phorbol-13-acetate (TPA), paclitaxel, nocodazole, vinblastine, and demecolcine were purchased from Sigma (St. Louis, MO). 4′,6-diamidino-2-phenylindole, dihydro-chloride (DAPI) and ProLong® Gold antifade reagent were purchased from Invitrogen (Carlsbad, CA). Antibodies were: H3 (CT, pan, rabbit polyclonal, Upstate Biotechnology, Lake Placid, NY); H3 S10P (rabbit polyclonal, Upstate Biotechnology); H3 S28P (rabbit polyclonal, Upstate Biotechnology); H3.3 S31P (rabbit polyclonal); alpha-tubulin (monoclonal, Invitrogen); Alexa Fluor 488-conjugated IgG (donkey anti-rabbit, Invitrogen); Alexa Fluor 594-conjugated IgG_1 (goat anti-mouse, Invitrogen). All other secondary antibodies were from Santa Cruz Biotechnology, Inc. (Santa Cruz, CA).

7.2.2. Peptide Synthesis and Production of Antibodies.

Histone H3.3 phosphopeptide PH31 (AARKSAPpS^{31}TGGVKK-C) and non-phosphopeptide H31 (AARKSAPSTGGVKK-C), where pS represents phosphoserine, were chemically synthesized by Macromolecular Resources (Colorado State University). Rabbit polyclonal antibody H3.3-P-ser31 was produced by Sigma and purified using SulfoLink Coupling Gel (Pierce). Crude antiserum was first passed through an affinity column to which the phosphopeptide PH31 was attached. Antibodies binding to the phosphorylated column were eluted and affinity purified on a column containing the non phosphopeptide H31, to remove antibodies to epitopes outside the phosphorylation domain. Flow through, which contained the H3.3 phosphor-ser31 antibody, was

concentrated and antibody specificity was analyzed by peptide blocking using different phosphopeptides.

7.2.3. Immunoblotting.

Acid-extracted proteins were dissolved in 0.1 N NaOH and measured for protein concentrations with the Bradford assay (Biorad, CA). Protein (2 μg) was loaded onto a 15% SDS-polyacrylamide gel, electrophoresed, and transferred onto poly(vinylidene difluoride) membranes, which were subsequently incubated with 5% BSA in 0.1% Tween 20-PBS blocking buffer, followed by an overnight incubation with primary antibodies that recognized histone H3 or specific modified forms of histone H3. After incubation with HRP-conjugated anti-rabbit secondary antibodies, membranes were incubated with ECL substrate (Amersham Pharmacia) and visualized on chemiluminescence film.

7.2.4. Immunofluorescence Staining.

LLC-PK1 cells (2×10^5) were cultured overnight on coverslips and treated with or without agents that induce mitotic catastrophe for 16 hours. Cells were washed in PBS, fixed in 4% parafomaldehyde-PBS solution for 10 min and then permeabilized with cold acetone at -20˚C for 5 min. After several washes in PBS, cells were blocked with 10% goat serum in 1% BSA-PBS blocking solution and then incubated with alpha-tubulin (1 μg/ml) together with H3 S10P (1:100) or H3.3 S31P (1:50). Following 1-hr incubation with primary antibodies, cells were incubated with Alexa Fluor 488-conjugated IgG (1:1,000) and Alexa Fluor 596-conjugated IgG_1 (1:1,000) for 1 hour. After 10-min DAPI

(1 μg/ml) staining, cells were mounted with prolong gold anti-fade reagent. Stained cells were analyzed on an Olympus IX70 microscope. Image processing was carried out with MagnaFire 2.1 acquisition software and Adobe Photoshop software.

7.2.5. Plasmid Construction.

The coding region of human histone H3.3 was subcloned in the vector pBudCE4.1, which was inserted with a green fluorescence protein (GFP) under the human elongation promoter, as a PCR fragment under the pCMV promoter. This recombinant plasmid was used as a template for site directed mutagenesis. A series of H3.3 mutants (S10A, S28A, S31A, S57A, S86A, and S96A) were generated using QuikChange® II Site-Directed mutagenesis kit (Stratagene, La Jolla, CA). Clones containing the desired mutations were confirmed by DNA sequencing.

7.2.6. Transient Transfection.

LLC-PK1 cells were seeded in 100 mm tissue culture plates, and grown for 18 hr, followed by transient transfection with native H3.3, S10A, S28A, S31A, S57A, S86A, and S96A, and empty vectors (pBudCE4.1), using Lipofectamine^{TM} 2000 Reagent.

7.3. RESULTS AND DISCUSSION

7.3.1. Generation and characterization of H3.3 phospho-S31 antibodies.

To ascertain whether S31 was phosphorylated in response of TGHQ, an anti-H3.3 phospho-S31 antibody was generated using a specific phosphorylated peptide which was synthesized to incorporate the phosphorylation on S31 of histone H3.3 (Figure 7.2A). After double affinity purification, these antibodies exhibited high specificity toward H3.3 phospho-S31 in the peptide blocking assay (Figure 7.2B). Immunofluorescence microscopy demonstrated that H3.3 S31 phosphorylation was observed only in late pro-metaphase and metaphase, and was absent in anaphase (Figure 7.3). The H3.3 phosphorylation pattern with the H3 phospho-S10 mitosis marker was different to that of the phospho-S31 pattern, with H3 S10 initially becoming phosphorylated in prophase and being sustained through anaphase.

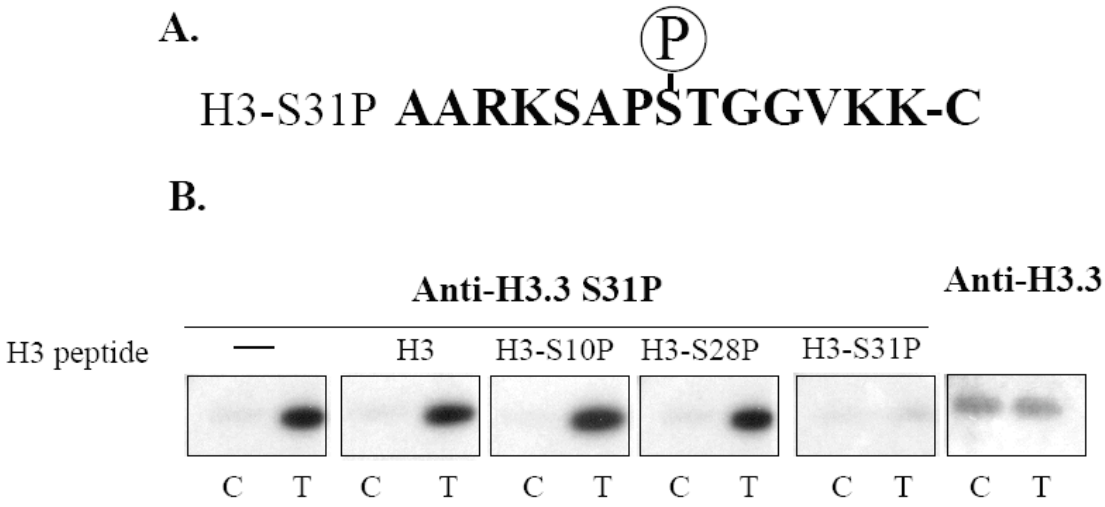

Figure 7.2. Specificity of H3.3 phospho-S31 antibodies.

(A) Amino acid sequence of the synthetic phospho-peptide H3-S31P, corresponding to the phosphorylation of H3.3 at S31. A phospho-residue is indicated by an amino acid residue and P within a circle. **(B)** Reactivity of H3.3 phospho-S31 antibody to untreated (C) and demecolcine (300 nM, 16 hr)-treated samples (T). H3.3-S31P antibody was pre-incubated in the presence of in the absence (—) of various H3 peptides (H3-S10P, H3-S28P, and H3-S31P corresponding to the phospho-peptides of H3.3 at S10, S28 and S31, respectively; H3 corresponding to non-phospho-peptide with the same sequence as the synthetic phospho-peptide H3-S31P) at room temperature for 30 min. The pre-absorbed H3.3 phospho-S31 antibody was then subjected to Western blot analysis. Equal loading is indicated with anti-histone H3.3.

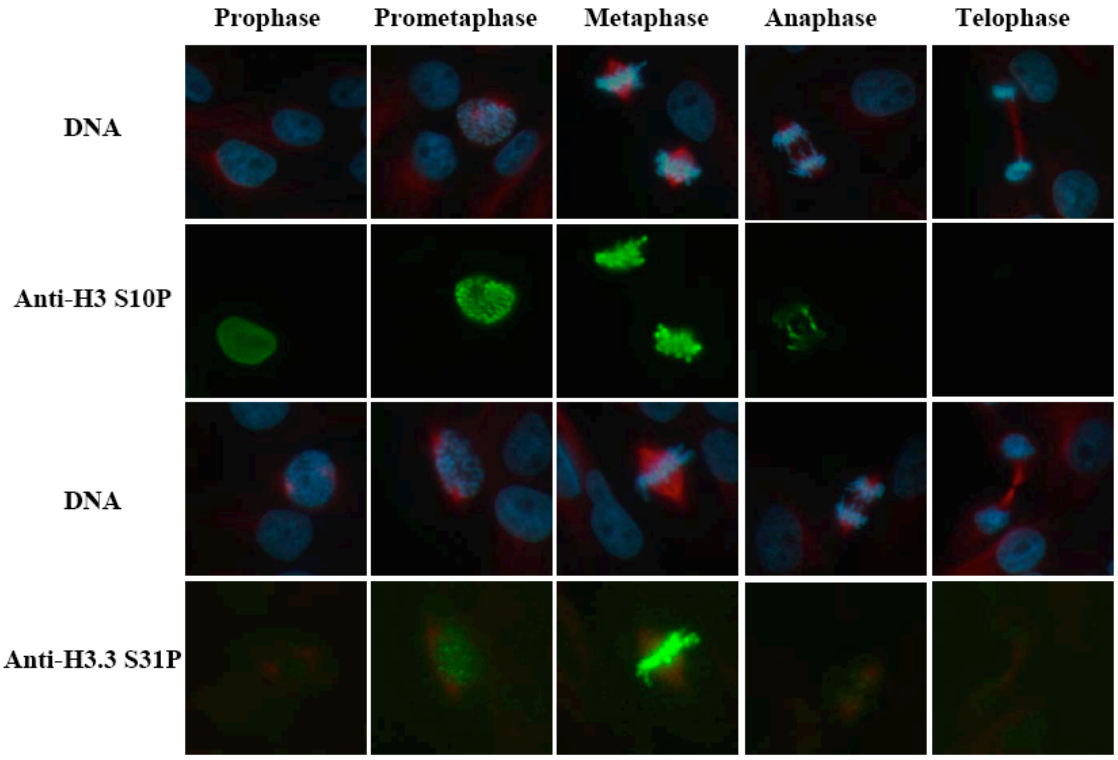

Figure 7.3. H3.3 S31 phosphorylation occurs in late prometaphase and metaphase.

Immunofluorescence staining of different mitotic stages of LLC-PK1 cells with antibodies against phospho-H3 S10 and phospho-H3.3 S31. DNA was stained with DAPI (blue) and microtubules were stained with α-tubulin antibody (red). Columns represent cells at the indicated stages of the cell cycle.

7.3.2. Phosphorylation of H3.3 S31 is increased during mitotic catastrophe.

Since microtubule-disrupting agents arrest cells in metaphase, we first determined whether various microtubule-disrupting agents could induce phosphorylation of H3.3 on S31. LLC-PK1 cells exposed to different microtubule-disrupting agents, including paclitaxel (100 nM), nocodazole (150 nM), vinblastine (50 nM) and demecolcine (300 nM), respectively, exhibited significant induction of histone H3.3 S31 phosphorylation, as well as S10 and S28 phosphorylation (Figure 7.4A). The latter two sites are associated with chromatin condensation during mitosis. Moreover, a significant increase in phospho-H3.3 S31 was revealed by immunofluorescence staining of cells exposed to paclitaxel (100 nM), or demecolcine (300 nM) for 16 hr (Figure 7.4B).

Previous studies demonstrated that TGHQ-mediated DNA-damage induces the phosphorylation of a novel site on histone H3.3 in LLC-PK1 cells. Moreover, TGHQ induced a decrease in S10 and S28 phosphorylation on histone H3. We therefore examined the H3.3 S31 phosphorylation pattern using the specific anti-H3.3 phospho-S31 antibody. Surprisingly, no changes in H3.3 S31 phosphorylation were detected following TGHQ treatment (Figure 7.5A). The overall phosphorylation pattern of histone H3 was also examined in cells exposed to a variety of DNA damaging agents. Another ROS generating agent, H_2O_2, caused a decrease in both S10 and S28 phosphorylation, but had no effect on H3.3 S31 phosphorylation (Figure 7.5B), and neither did the DNA alkylating agent, MNNG, (Figure 7.5B). Moreover, no phosphorylation of H3.3 S31 was detected in cells treated with (i) a telomerase inhibitor, 3'-azido-3'-dexoythymidine (AZT), (ii) a poly(ADP-ribose) polymerase inhibitor (PJ34), (iii) a topoisomerase inhibitor (etoposide)

or (iv) a DNA polymerase inhibitor, (aphidicolin) (Figure 7.8). The tumor promoter 12-O-tetradecanoyl- phorbol-13-acetate (TPA), a known mitogen, stimulated S10 and S28 histone H3 phosphorylation but did not induce phosphorylation of H3.3 at S31 (Figure 7.8). Thus, patterns of histone H3 phosphorylation vary dependent upon the stimulus, and S31 histone H3.3 phosphorylation appears to be restricted to metaphase, since immunofluorescence experiments confirmed that histone H3.3 S31 phosphorylation is present in late prometaphase and dramatically diminishes at early anaphase. The results also suggest that H3.3 S31 phosphorylation may serve as a marker for cells undergoing cell death *via* mitotic catastrophe.

(A)

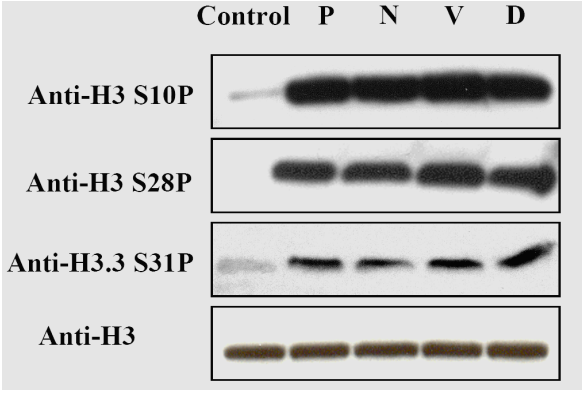

(B)

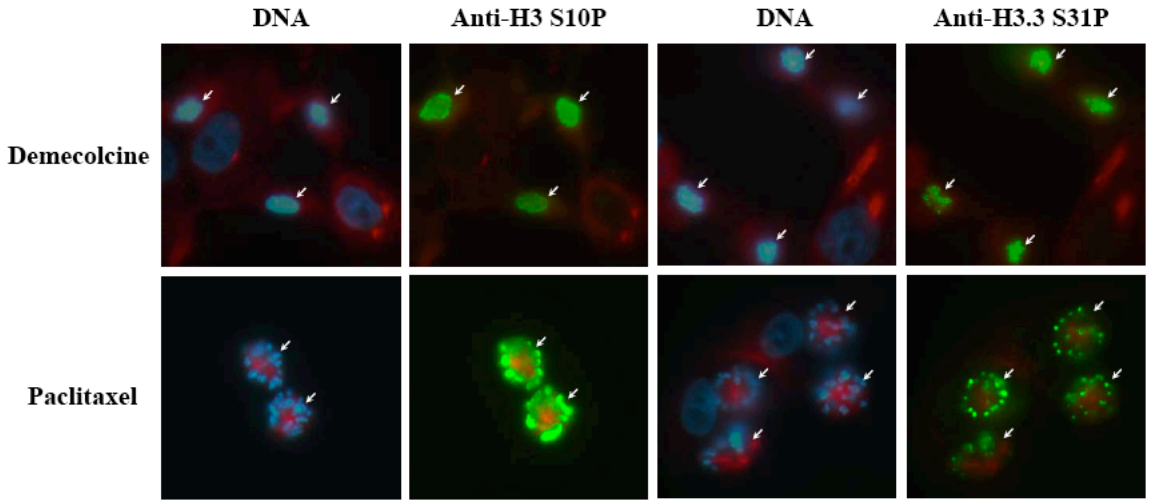

Figure 7.4. Histone H3.3 S31 phosphorylation is enhanced by different microtubule disrupting agents.

LLC-PK1 cells were treated with Pacilitaxel (100 nM), Nocadazol (150 nM), Vinblastine (50 nM) or Demecolcine (300 nM) for 16 hr. Histones were extracted and electrophoretically resolved on 18% SDS-PAGE gels. **(A)** Representative blots of histone H3 phosphorylation at S10, S28, and S31. Equal loading is indicated with anti-histone H3. **(B)** LLC-PK1 cells were treated with Pacilitaxel (100 nM), or Demecolcine (300 nM) for 16 hr. Cells were then fixed and immunostained with phospho-H3 S10 or phospho-H3.3 S31 antibody (green) for the direct analysis of histone H3 phosphorylation. DNA was stained with DAPI (blue) and microtubule was stained with α-tubulin antibody (red).

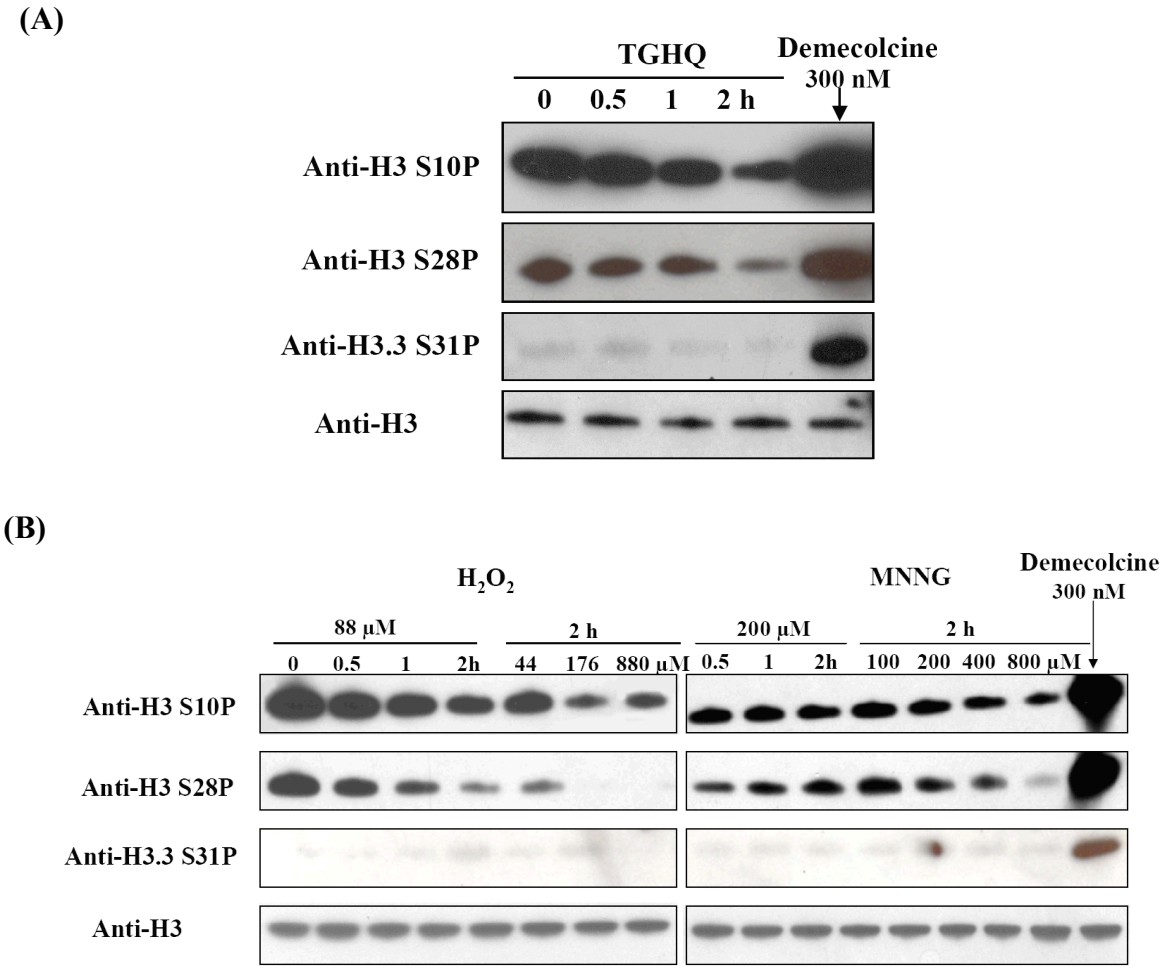

Figure 7.5. Differential histone H3 phosphorylation induced by TGHQ and various DNA damaging agents.

(A) LLC-PK1 cells were treated with TGHQ (200 µM) for different periods of time (1, 2, 4 hr). **(B)** Cells were treated with H_2O_2 (88 µM) or MNNG (200 µM) for various periods of time (0.25, 0.5, 1, 2 hr), or different doses of H_2O_2 (44, 88, 176, 880 µM) or MNNG (100, 200, 400, 800 µM) for 2 hr. Histones were then extracted and electrophoretically resolved on the 18% SDS-PAGE gels. Representative blots of histone H3 phosphorylation at S10, S28, and S31. Equal loading is indicated with anti-histone H3.

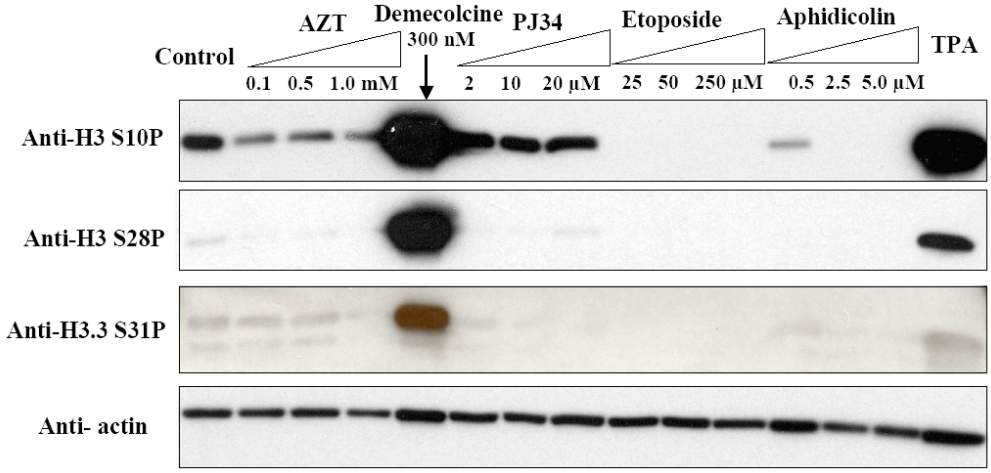

Figure 7.6. Different DNA damaging agents are unable to induce H3.3 S31 phosphorylation.

LLC-PK1 cells were treated with increasing doses of (i) the telomerase inhibitor, 3'-azido-3'-dexoythymidine (AZT), (ii) the poly(ADP-ribose) polymerase inhibitor, PJ34, (iii) the topoisomerase inhibitor, etoposide, (iv) the DNA polymerase inhibitor, aphidicolin for 16 hr, or treated with (v) 300 nM demecolcine or (vi) 100 nM TPA for 16 hr. Histones were extracted and electrophoretically resolved on the 18% SDS-PAGE gels. Representative blots of histone H3 phosphorylation at S10, S28, and S31. Equal loading is indicated with anti-actin.

7.3.3. Generation of a series of H3.3 alanine substitution mutants.

To probe the potential phosphorylation sites of H3.3 in response to TGHQ, a C-terminal H3.3-HA chimera and its corresponding mutants were constructed with a mammalian expression vector, pBudCE4.1, which contains a GFP under a different promoter (Figure 7.7A). Various serine to alanine histone H3.3 mutants, S10A, S28A, S31A, S57A, S86A, and S96A, were constructed (Figure 7.7B). Transient transfection of LLC-PK1 cells with wild-type histone H3.3-HA resulted in the expression of a HA-tagged H3.3 protein which was capable of being phosphorylated in response to the presence of a microtubule-disrupting agent (Figure 7.8A). In addition, the recombinant H3.3-HA functioned in a similar fashion to native histone proteins, with appropriate incorporation into chromatin (Figure 7.8B). To investigate whether any of these H3.3 serine sites might participate in the response to TGHQ induced DNA damage and cell death, LLC-PK1 cells were transiently transfected with one of the six different H3.3 mutants, prior to TGHQ exposure. Neutral red analysis revealed no changes in TGHQ-induced toxicity in cells transfected with the various mutants when compared to the empty vector transfected controls (Figure 9). This lack of effect on the response to TGHQ may, at least in part, be due to the dominant expression of endogenous histone H3.3 and the low transfection efficiencies (~50% transfection efficiency). To identify the precise phosphorylation sites, [^{32}P]-orthophosphate incorporation could be performed in TGHQ-treated cells expressing the various H3.3 mutants. HA immunoprecipitation of the [^{32}P]-labelled H3.3-HA mutants would subsequently identify which serine site is phosphorylated in response to TGHQ.

(A)

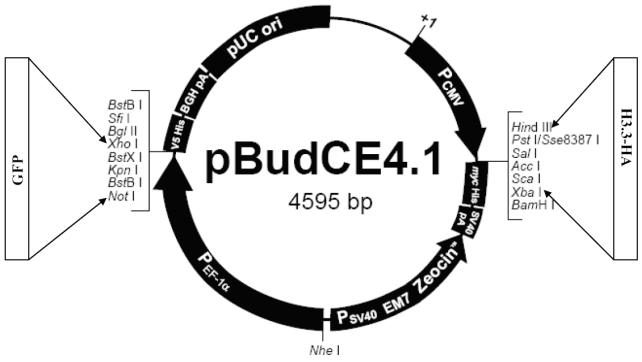

(B)

Histone	H3.1	1	ARTKQTARKS	TGGKAPRKQL	ATKAARKSAP	ATGGVKKPHR	YRPGTVALRE
Histone	H3.2	1	ARTKQTARKS	TGGKAPRKQL	ATKAARKSAP	ATGGVKKPHR	YRPGTVALRE
Histone	H3.3	1	ARTKQTARKS	TGGKAPRKQL	ATKAARKSAP	STGGVKKPHR	YRPGTVALRE
Histone	H3.1	51	IRRYQKSTEL	LIRKLPFQRL	VREIAQDFKT	DLRFQSSAVM	ALQEACEAYL
Histone	H3.2	51	IRRYQKSTEL	LIRKLPFQRL	VREIAQDFKT	DLRFQSSAVM	ALQEASEAYL
Histone	H3.3	51	IRRYQKSTEL	LIRKLPFQRL	VREIAQDFKT	DLRFQSAAIG	ALQEASEAYL
Histone	H3.1	101	VGLFEDTNLC	AIHAKRVTIM	PKDIQLARRI	RGERA	
Histone	H3.2	101	VGLFEDTNLC	AIHAKRVTIM	PKDIQLARRI	RGERA	
Histone	H3.3	101	VGLFEDTNLC	AIHAKRVTIM	PKDIQLARRI	RGERA	

10…28…31…57…86…96	H3.3-HA-GFP mutant
A… S… S… S… S… S	S10A
S… A… S… S… S… S	S28A
S… S… A… S… S… S	S31A
S… S… S… A… S… S	S57A
S… S… S… S… A… S	S86A
S… S… S… S… S… A	S96A

Figure 7.7. Construction of HA-tagged histone H3.3.

(A) A full-length human wild-type histone H3.3 cDNA was obtained from American Type Culture Collection. The HA-tag sequence was added to its C-terminal by PCR. HA-tagged H3.3 was then sub-cloned into the mammalian expression vector pBudCE4.1 which contains GFP under a different promoter. **(B)** To create mutant histone H3.3 lacking the serine phosphorylation sites, the codon for S10, S28, S31, S57, S86, and S96 of H3.3 were changed to encode alanine by site-directed mutagenesis.

(A)

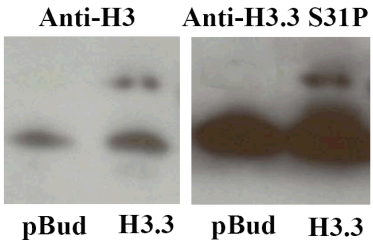

(B)

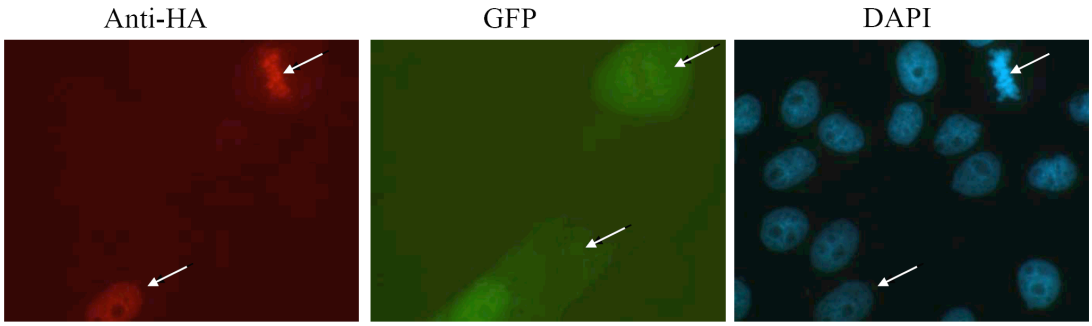

Figure 7.8. Expression of HA-tagged H3.3 wild-type proteins.

(A) Recombinant HA-tagged wild-type H3.3 was capable of being phosphorylated in response to a microtubule-disrupting agent. Cells were transiently transfected with recombinant H3.3-HA-GFP. 24 hr after transfection, cells were incubated with 300 nM demecolcine for an additional 16 hr. Histones were acid extracted and analyzed by Western blot analysis with antibodies to histone H3 and phospho-H3.3 S31. pBud represents empty vector transfection. **(B)** Recombinant HA-tagged H3.3 was incorporated into chromatin during normal cell mitosis. Cells were transiently transfected with recombinant H3.3-HA-GFP. 24 hr after transfection, cells were fixed and immunostained with HA-tagged antibody (red). DNA was stained with DAPI (blue). Transfected cells were indicated by the expression of GFP (green).

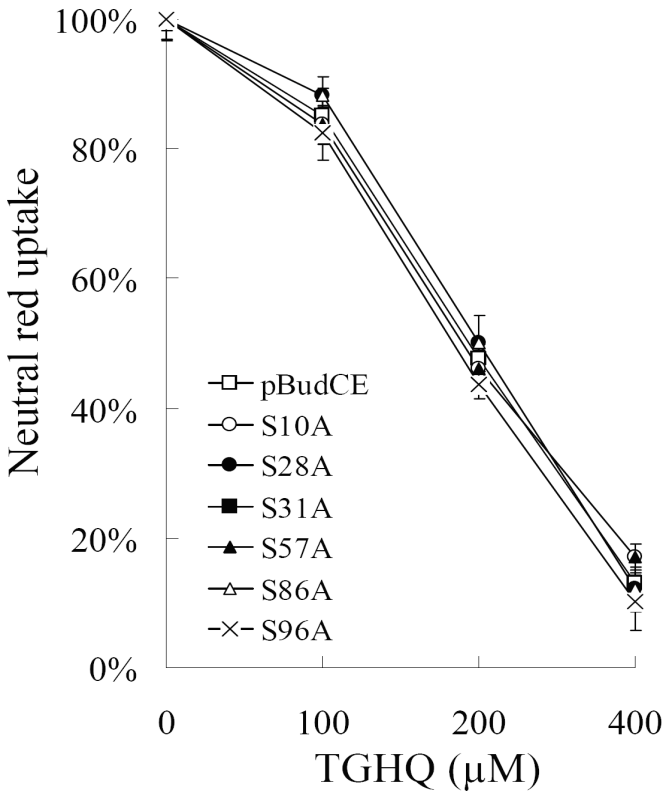

Figure 7.9. Viability of LLC-PK1 cells transiently transfected with mutant H3.3 cells exposed to TGHQ.

LLC-PK1 cells transiently transfected with empty vector pBudCE or various H3.3 mutants, including S10A, S28A, S31A, S57A, S86A, and S96A, were treated with different concentrations of TGHQ (100, 200, 400 μM) for 2 hr. Cell viability was determined by measuring lysosomal neutral red uptake by live cells, and is expressed as % control (untreated cells).

REFERENCES

Ahmad, K., and Henikoff, S. (2002a). Histone H3 variants specify modes of chromatin assembly. Proc Natl Acad Sci U S A *99 Suppl 4*, 16477-16484.

Ahmad, K., and Henikoff, S. (2002b). The histone variant H3.3 marks active chromatin by replication-independent nucleosome assembly. Mol Cell *9*, 1191-1200.

Alano, C. C., Ying, W., and Swanson, R. A. (2004). Poly(ADP-ribose) polymerase-1-mediated cell death in astrocytes requires NAD+ depletion and mitochondrial permeability transition. J Biol Chem *279*, 18895-18902.

Ame, J. C., Spenlehauer, C., and de Murcia, G. (2004). The PARP superfamily. Bioessays *26*, 882-893.

Andrabi, S. A., Kim, N. S., Yu, S. W., Wang, H., Koh, D. W., Sasaki, M., Klaus, J. A., Otsuka, T., Zhang, Z., Koehler, R. C.*, et al.* (2006). Poly(ADP-ribose) (PAR) polymer is a death signal. Proc Natl Acad Sci U S A *103*, 18308-18313.

Andreyev, A. Y., Kushnareva, Y. E., and Starkov, A. A. (2005). Mitochondrial metabolism of reactive oxygen species. Biochemistry (Mosc) *70*, 200-214.

Ankarcrona, M., Dypbukt, J. M., Bonfoco, E., Zhivotovsky, B., Orrenius, S., Lipton, S. A., and Nicotera, P. (1995). Glutamate-induced neuronal death: a succession of necrosis or apoptosis depending on mitochondrial function. Neuron *15*, 961-973.

Araki, M., Nanri, H., Ejima, K., Murasato, Y., Fujiwara, T., Nakashima, Y., and Ikeda, M. (1999). Antioxidant function of the mitochondrial protein SP-22 in the cardiovascular system. J Biol Chem *274*, 2271-2278.

Arner, E. S., and Holmgren, A. (2000). Physiological functions of thioredoxin and thioredoxin reductase. Eur J Biochem *267*, 6102-6109.

Bathori, G., Csordas, G., Garcia-Perez, C., Davies, E., and Hajnoczky, G. (2006). Ca2+-dependent control of the permeability properties of the mitochondrial outer membrane and voltage-dependent anion-selective channel (VDAC). J Biol Chem *281*, 17347-17358.

Bellomo, G., Jewell, S. A., Thor, H., and Orrenius, S. (1982). Regulation of intracellular calcium compartmentation: studies with isolated hepatocytes and t-butyl hydroperoxide. Proc Natl Acad Sci U S A *79*, 6842-6846.

Bernardi, P. (1999). Mitochondrial transport of cations: channels, exchangers, and permeability transition. Physiol Rev *79*, 1127-1155.

Bernardi, P., and Rasola, A. (2007). Calcium and cell death: the mitochondrial connection. Subcell Biochem *45*, 481-506.

Berridge, M. J., Bootman, M. D., and Roderick, H. L. (2003). Calcium signalling: dynamics, homeostasis and remodelling. Nat Rev Mol Cell Biol *4*, 517-529.

Biteau, B., Labarre, J., and Toledano, M. B. (2003). ATP-dependent reduction of cysteine-sulphinic acid by S. cerevisiae sulphiredoxin. Nature *425*, 980-984.

Bolton, J. L., Trush, M. A., Penning, T. M., Dryhurst, G., and Monks, T. J. (2000). Role of quinones in toxicology. Chem Res Toxicol *13*, 135-160.

Borst, P., and Rottenberg, S. (2004). Cancer cell death by programmed necrosis? Drug Resist Updat *7*, 321-324.

Bowes, J., McDonald, M. C., Piper, J., and Thiemermann, C. (1999). Inhibitors of poly (ADP-ribose) synthetase protect rat cardiomyocytes against oxidant stress. Cardiovasc Res *41*, 126-134.

Bratton, S. B., Lau, S. S., and Monks, T. J. (1997). Identification of quinol thioethers in bone marrow of hydroquinone/phenol-treated rats and mice and their potential role in benzene-mediated hematotoxicity. Chem Res Toxicol *10*, 859-865.

Bratton, S. B., Lau, S. S., and Monks, T. J. (2000). The putative benzene metabolite 2,3, 5-tris(glutathion-S-yl)hydroquinone depletes glutathione, stimulates sphingomyelin turnover, and induces apoptosis in HL-60 cells. Chem Res Toxicol *13*, 550-556.

Brookes, P. S., Yoon, Y., Robotham, J. L., Anders, M. W., and Sheu, S. S. (2004). Calcium, ATP, and ROS: a mitochondrial love-hate triangle. Am J Physiol Cell Physiol *287*, C817-833.

Bucks, D. A., McMaster, J. R., Guy, R. H., and Maibach, H. I. (1988). Percutaneous absorption of hydroquinone in humans: effect of 1-dodecylazacycloheptan-2-one (azone) and the 2-ethylhexyl ester of 4-(dimethylamino)benzoic acid (Escalol 507). J Toxicol Environ Health *24*, 279-289.

Budanov, A. V., Sablina, A. A., Feinstein, E., Koonin, E. V., and Chumakov, P. M. (2004). Regeneration of peroxiredoxins by p53-regulated sestrins, homologs of bacterial AhpD. Science *304*, 596-600.

Burkart, V., Wang, Z. Q., Radons, J., Heller, B., Herceg, Z., Stingl, L., Wagner, E. F., and Kolb, H. (1999). Mice lacking the poly(ADP-ribose) polymerase gene are resistant to pancreatic beta-cell destruction and diabetes development induced by streptozocin. Nat Med *5*, 314-319.

Burkle, A., Beneke, S., Brabeck, C., Leake, A., Meyer, R., Muiras, M. L., and Pfeiffer, R. (2002). Poly(ADP-ribose) polymerase-1, DNA repair and mammalian longevity. Exp Gerontol *37*, 1203-1205.

Camhi, S. L., Lee, P., and Choi, A. M. (1995). The oxidative stress response. New Horiz *3*, 170-182.

Cao, Z., Bhella, D., and Lindsay, J. G. (2007). Reconstitution of the mitochondrial PrxIII antioxidant defence pathway: general properties and factors affecting PrxIII activity and oligomeric state. J Mol Biol *372*, 1022-1033.

Carson, D. A., Seto, S., Wasson, D. B., and Carrera, C. J. (1986). DNA strand breaks, NAD metabolism, and programmed cell death. Exp Cell Res *164*, 273-281.

Chae, H. Z., Kang, S. W., and Rhee, S. G. (1999a). Isoforms of mammalian peroxiredoxin that reduce peroxides in presence of thioredoxin. Methods Enzymol *300*, 219-226.

Chae, H. Z., Kim, H. J., Kang, S. W., and Rhee, S. G. (1999b). Characterization of three isoforms of mammalian peroxiredoxin that reduce peroxides in the presence of thioredoxin. Diabetes Res Clin Pract *45*, 101-112.

Chae, H. Z., Robison, K., Poole, L. B., Church, G., Storz, G., and Rhee, S. G. (1994). Cloning and sequencing of thiol-specific antioxidant from mammalian brain: alkyl hydroperoxide reductase and thiol-specific antioxidant define a large family of antioxidant enzymes. Proc Natl Acad Sci U S A *91*, 7017-7021.

Chang, T. S., Cho, C. S., Park, S., Yu, S., Kang, S. W., and Rhee, S. G. (2004a). Peroxiredoxin III, a mitochondrion-specific peroxidase, regulates apoptotic signaling by mitochondria. J Biol Chem *279*, 41975-41984.

Chang, T. S., Jeong, W., Choi, S. Y., Yu, S., Kang, S. W., and Rhee, S. G. (2002). Regulation of peroxiredoxin I activity by Cdc2-mediated phosphorylation. J Biol Chem *277*, 25370-25376.

Chang, T. S., Jeong, W., Woo, H. A., Lee, S. M., Park, S., and Rhee, S. G. (2004b). Characterization of mammalian sulfiredoxin and its reactivation of hyperoxidized peroxiredoxin through reduction of cysteine sulfinic acid in the active site to cysteine. J Biol Chem *279*, 50994-51001.

Chatterjee, P. K., and Thiemermann, C. (1998). Inhibitors of poly (ADP-ribose) synthetase protect rat renal proximal tubular cells against oxidant stress. Biochem Soc Trans *26*, S318.

Chiarugi, A. (2002). Poly(ADP-ribose) polymerase: killer or conspirator? The 'suicide hypothesis' revisited. Trends Pharmacol Sci *23*, 122-129.

Clerk, A., Fuller, S. J., Michael, A., and Sugden, P. H. (1998). Stimulation of "stress-regulated" mitogen-activated protein kinases (stress-activated protein kinases/c-Jun N-terminal kinases and p38-mitogen-activated protein kinases) in perfused rat hearts by oxidative and other stresses. J Biol Chem *273*, 7228-7234.

Cobb, M. H. (1999). MAP kinase pathways. Prog Biophys Mol Biol *71*, 479-500.

Cosi, C., and Marien, M. (1999). Implication of poly (ADP-ribose) polymerase (PARP) in neurodegeneration and brain energy metabolism. Decreases in mouse brain NAD+ and ATP caused by MPTP are prevented by the PARP inhibitor benzamide. Ann N Y Acad Sci *890*, 227-239.

Cristovao, L., and Rueff, J. (1996). Effect of a poly(ADP-ribose) polymerase inhibitor on DNA breakage and cytotoxicity induced by hydrogen peroxide and gamma-radiation. Teratog Carcinog Mutagen *16*, 219-227.

Crompton, M. (1999). The mitochondrial permeability transition pore and its role in cell death. Biochem J *341 (Pt 2)*, 233-249.

Crompton, M., Virji, S., Doyle, V., Johnson, N., and Ward, J. M. (1999). The mitochondrial permeability transition pore. Biochem Soc Symp *66*, 167-179.

Crompton, M., Virji, S., and Ward, J. M. (1998). Cyclophilin-D binds strongly to complexes of the voltage-dependent anion channel and the adenine nucleotide translocase to form the permeability transition pore. Eur J Biochem *258*, 729-735.

Cuttle, L., Zhang, X. J., Endre, Z. H., Winterford, C., and Gobe, G. C. (2001). Bcl-X(L) translocation in renal tubular epithelial cells in vitro protects distal cells from oxidative stress. Kidney Int *59*, 1779-1788.

Dantzer, F., Ame, J. C., Schreiber, V., Nakamura, J., Menissier-de Murcia, J., and de Murcia, G. (2006). Poly(ADP-ribose) polymerase-1 activation during DNA damage and repair. Methods Enzymol *409*, 493-510.

Daugas, E., Susin, S. A., Zamzami, N., Ferri, K. F., Irinopoulou, T., Larochette, N., Prevost, M. C., Leber, B., Andrews, D., Penninger, J., and Kroemer, G. (2000). Mitochondrio-nuclear translocation of AIF in apoptosis and necrosis. Faseb J *14*, 729-739.

DeCaprio, A. P. (1999). The toxicology of hydroquinone--relevance to occupational and environmental exposure. Crit Rev Toxicol *29*, 283-330.

Degterev, A., Huang, Z., Boyce, M., Li, Y., Jagtap, P., Mizushima, N., Cuny, G. D., Mitchison, T. J., Moskowitz, M. A., and Yuan, J. (2005). Chemical inhibitor of nonapoptotic cell death with therapeutic potential for ischemic brain injury. Nat Chem Biol *1*, 112-119.

Degterev, A., and Yuan, J. (2008). Expansion and evolution of cell death programmes. Nat Rev Mol Cell Biol *9*, 378-390.

Deisinger, P. J., Hill, T. S., and English, J. C. (1996). Human exposure to naturally occurring hydroquinone. J Toxicol Environ Health *47*, 31-46.

Deryabina, Y. I., Isakova, E. P., and Zvyagilskaya, R. A. (2004). Mitochondrial calcium transport systems: properties, regulation, and taxonomic features. Biochemistry (Mosc) *69*, 91-102.

Devillers, J., Boule, P., Vasseur, P., Prevot, P., Steiman, R., Seigle-Murandi, F., Benoit-Guyod, J. L., Nendza, M., Grioni, C., Dive, D., and et al. (1990). Environmental and health risks of hydroquinone. Ecotoxicol Environ Saf *19*, 327-354.

Ding, R., Pommier, Y., Kang, V. H., and Smulson, M. (1992). Depletion of poly(ADP-ribose) polymerase by antisense RNA expression results in a delay in DNA strand break rejoining. J Biol Chem *267*, 12804-12812.

Divincenzo, G. D., Hamilton, M. L., Reynolds, R. C., and Ziegler, D. A. (1984). Metabolic fate and disposition of [14C]hydroquinone given orally to Sprague-Dawley rats. Toxicology *33*, 9-18.

Dong, J. (2004) Molecular Dissection of Reactive Oxygen Species-Mediated Oncotic Cell Death, The University of Texas at Austin.

Dong, J., Everitt, J. I., Lau, S. S., and Monks, T. J. (2004a). Induction of ERK1/2 and histone H3 phosphorylation within the outer stripe of the outer medulla of the Eker rat by 2,3,5-tris-(glutathion-S-yl)hydroquinone. Toxicol Sci *80*, 350-357.

Dong, J., Ramachandiran, S., Tikoo, K., Jia, Z., Lau, S. S., and Monks, T. J. (2004b). EGFR-independent activation of p38 MAPK and EGFR-dependent activation of ERK1/2 are required for ROS-induced renal cell death. Am J Physiol Renal Physiol *287*, F1049-1058.

Dong, Z., Saikumar, P., Weinberg, J. M., and Venkatachalam, M. A. (2006). Calcium in cell injury and death. Annu Rev Pathol *1*, 405-434.

Droge, W. (2002). Free radicals in the physiological control of cell function. Physiol Rev *82*, 47-95.

Duchen, M. R. (2000). Mitochondria and calcium: from cell signalling to cell death. J Physiol *529 Pt 1*, 57-68.

Eisfeld, J., and Luckhoff, A. (2007). Trpm2. Handb Exp Pharmacol, 237-252.

El-Khamisy, S. F., Masutani, M., Suzuki, H., and Caldecott, K. W. (2003). A requirement for PARP-1 for the assembly or stability of XRCC1 nuclear foci at sites of oxidative DNA damage. Nucleic Acids Res *31*, 5526-5533.

Eliasson, M. J., Sampei, K., Mandir, A. S., Hurn, P. D., Traystman, R. J., Bao, J., Pieper, A., Wang, Z. Q., Dawson, T. M., Snyder, S. H., and Dawson, V. L. (1997). Poly(ADP-ribose) polymerase gene disruption renders mice resistant to cerebral ischemia. Nat Med *3*, 1089-1095.

Endres, M., Wang, Z. Q., Namura, S., Waeber, C., and Moskowitz, M. A. (1997). Ischemic brain injury is mediated by the activation of poly(ADP-ribose)polymerase. J Cereb Blood Flow Metab *17*, 1143-1151.

Engasser, P. G., and Maibach, H. I. (1981). Cosmetic and dermatology: bleaching creams. J Am Acad Dermatol *5*, 143-147.

English, J. C., Deisinger, P. J., Perry, L. G., Schum, D. B., and Guest, D. (1988). Toxicokinetics studies with hydroquinone in male and female Fischer 344 rats: Part I. R&D Report pf Eastman Kodak Co, Rochester, NY.

Ermak, G., and Davies, K. J. (2002). Calcium and oxidative stress: from cell signaling to cell death. Mol Immunol *38*, 713-721.

Esposito, C., Parrilla, B., Cornacchia, F., Grosjean, F., Mangione, F., Serpieri, N., Valentino, R., Villa, L., Arra, M., Esposito, V., and Canton, A. D. (2009). The antifibrogenic effect of hepatocyte growth factor (HGF) on renal tubular (HK-2) cells is dependent on cell growth. Growth Factors, 1.

Feissner, R. F., Skalska, J., Gaum, W. E., and Sheu, S. S. (2009). Crosstalk signaling between mitochondrial Ca2+ and ROS. Front Biosci *14*, 1197-1218.

Filipovic, D. M., Meng, X., and Reeves, W. B. (1999). Inhibition of PARP prevents oxidant-induced necrosis but not apoptosis in LLC-PK1 cells. Am J Physiol *277*, F428-436.

Fiorillo, C., Ponziani, V., Giannini, L., Cecchi, C., Celli, A., Nassi, N., Lanzilao, L., Caporale, R., and Nassi, P. (2006). Protective effects of the PARP-1 inhibitor PJ34 in hypoxic-reoxygenated cardiomyoblasts. Cell Mol Life Sci *63*, 3061-3071.

Fiorillo, C., Ponziani, V., Giannini, L., Cecchi, C., Celli, A., Nediani, C., Perna, A. M., Liguori, P., Nassi, N., Formigli, L.*, et al.* (2003). Beneficial effects of poly (ADP-ribose) polymerase inhibition against the reperfusion injury in heart transplantation. Free Radic Res *37*, 331-339.

Fischle, W., Wang, Y., and Allis, C. D. (2003). Histone and chromatin cross-talk. Curr Opin Cell Biol *15*, 172-183.

Fisher, A. A., Labenski, M. T., Malladi, S., Gokhale, V., Bowen, M. E., Milleron, R. S., Bratton, S. B., Monks, T. J., and Lau, S. S. (2007). Quinone electrophiles selectively adduct "electrophile binding motifs" within cytochrome c. Biochemistry *46*, 11090-11100.

Fonfria, E., Marshall, I. C., Benham, C. D., Boyfield, I., Brown, J. D., Hill, K., Hughes, J. P., Skaper, S. D., and McNulty, S. (2004). TRPM2 channel opening in response to oxidative stress is dependent on activation of poly(ADP-ribose) polymerase. Br J Pharmacol *143*, 186-192.

Forman, H. J., and Torres, M. (2002). Reactive oxygen species and cell signaling: respiratory burst in macrophage signaling. Am J Respir Crit Care Med *166*, S4-8.

Forman, H. J., Torres, M., and Fukuto, J. (2002). Redox signaling. Mol Cell Biochem *234-235*, 49-62.

Fossati, S., Cipriani, G., Moroni, F., and Chiarugi, A. (2007). Neither energy collapse nor transcription underlie in vitro neurotoxicity of poly(ADP-ribose) polymerase hyper-activation. Neurochem Int *50*, 203-210.

Fridovich, I. (1978a). The biology of oxygen radicals. Science *201*, 875-880.

Fridovich, I. (1978b). Oxygen free radicals and tissue damage: chairman's introduction. Ciba Found Symp, 1-4.

Fridovich, I. (1978c). Superoxide dismutases: defence against endogenous superoxide radical. Ciba Found Symp, 77-93.

Fridovich, I. (1999). Fundamental aspects of reactive oxygen species, or what's the matter with oxygen? Ann N Y Acad Sci *893*, 13-18.

Fujii, J., and Ikeda, Y. (2002). Advances in our understanding of peroxiredoxin, a multifunctional, mammalian redox protein. Redox Rep *7*, 123-130.

Glatt, H., Padykula, R., Berchtold, G. A., Ludewig, G., Platt, K. L., Klein, J., and Oesch, F. (1989). Multiple activation pathways of benzene leading to products with varying genotoxic characteristics. Environ Health Perspect *82*, 81-89.

Goldman, M. P. (2000). The use of hydroquinone with facial laser resurfacing. J Cutan Laser Ther *2*, 73-77.

Golstein, P., and Kroemer, G. (2007). Cell death by necrosis: towards a molecular definition. Trends Biochem Sci *32*, 37-43.

Goto, H., Tomono, Y., Ajiro, K., Kosako, H., Fujita, M., Sakurai, M., Okawa, K., Iwamatsu, A., Okigaki, T., Takahashi, T., and Inagaki, M. (1999). Identification of a novel phosphorylation site on histone H3 coupled with mitotic chromosome condensation. J Biol Chem *274*, 25543-25549.

Greenlee, W. F., Gross, E. A., and Irons, R. D. (1981). Relationship between benzene toxicity and the disposition of 14C-labelled benzene metabolites in the rat. Chem Biol Interact *33*, 285-299.

Grynkiewicz, G., Poenie, M., and Tsien, R. Y. (1985). A new generation of Ca2+ indicators with greatly improved fluorescence properties. J Biol Chem *260*, 3440-3450.

Ha, H. C., and Snyder, S. H. (1999). Poly(ADP-ribose) polymerase is a mediator of necrotic cell death by ATP depletion. Proc Natl Acad Sci U S A *96*, 13978-13982.

Hajnoczky, G., Csordas, G., Das, S., Garcia-Perez, C., Saotome, M., Sinha Roy, S., and Yi, M. (2006). Mitochondrial calcium signalling and cell death: approaches for assessing the role of mitochondrial Ca2+ uptake in apoptosis. Cell Calcium *40*, 553-560.

Hake, S. B., Xiao, A., and Allis, C. D. (2004). Linking the epigenetic 'language' of covalent histone modifications to cancer. Br J Cancer *90*, 761-769.

Halliwell, B. (1995). Antioxidant characterization. Methodology and mechanism. Biochem Pharmacol *49*, 1341-1348.

Hanson, C. J., Bootman, M. D., and Roderick, H. L. (2004). Cell signalling: IP3 receptors channel calcium into cell death. Curr Biol *14*, R933-935.

Hara, Y., Wakamori, M., Ishii, M., Maeno, E., Nishida, M., Yoshida, T., Yamada, H., Shimizu, S., Mori, E., Kudoh, J.*, et al.* (2002). LTRPC2 Ca2+-permeable channel activated by changes in redox status confers susceptibility to cell death. Mol Cell *9*, 163-173.

Harriman, J. F., Liu, X. L., Aleo, M. D., Machaca, K., and Schnellmann, R. G. (2002). Endoplasmic reticulum Ca(2+) signaling and calpains mediate renal cell death. Cell Death Differ *9*, 734-741.

Harteneck, C. (2005). Function and pharmacology of TRPM cation channels. Naunyn Schmiedebergs Arch Pharmacol *371*, 307-314.

Hengartner, M. O. (2000). The biochemistry of apoptosis. Nature *407*, 770-776.

Henriquez, M., Armisen, R., Stutzin, A., and Quest, A. F. (2008). Cell death by necrosis, a regulated way to go. Curr Mol Med *8*, 187-206.

Hill, J. W., Hu, J. J., and Evans, M. K. (2008). OGG1 is degraded by calpain following oxidative stress and cisplatin exposure. DNA Repair (Amst) *7*, 648-654.

Ho, T. C., Yang, Y. C., Cheng, H. C., Wu, A. C., Chen, S. L., Chen, H. K., and Tsao, Y. P. (2006). Activation of mitogen-activated protein kinases is essential for hydrogen peroxide -induced apoptosis in retinal pigment epithelial cells. Apoptosis *11*, 1899-1908.

Hofmann, B., Hecht, H. J., and Flohe, L. (2002). Peroxiredoxins. Biol Chem *383*, 347-364.

Homburg, S., Visochek, L., Moran, N., Dantzer, F., Priel, E., Asculai, E., Schwartz, D., Rotter, V., Dekel, N., and Cohen-Armon, M. (2000). A fast signal-induced activation of Poly(ADP-ribose) polymerase: a novel downstream target of phospholipase c. J Cell Biol *150*, 293-307.

Hong, S. J., Dawson, T. M., and Dawson, V. L. (2004). Nuclear and mitochondrial conversations in cell death: PARP-1 and AIF signaling. Trends Pharmacol Sci *25*, 259-264.

IARC (1999). Hydroquinone. IARC Monogr Eval Carcinog Risks Hum *71 Pt 2*, 691-719.

IPCS, I. P. o. C. S. (1996). Hyroquinone Health and Safety Guide, Health and Safety. World Health Organization, Geneva *Guide No. 101*.

Jacobson, E. L., and Jacobson, M. K. (1997). Tissue NAD as a biochemical measure of niacin status in humans. Methods Enzymol *280*, 221-230.

Jang, H. H., Kim, S. Y., Park, S. K., Jeon, H. S., Lee, Y. M., Jung, J. H., Lee, S. Y., Chae, H. B., Jung, Y. J., Lee, K. O.*, et al.* (2006). Phosphorylation and concomitant structural changes in human 2-Cys peroxiredoxin isotype I differentially regulate its peroxidase and molecular chaperone functions. FEBS Lett *580*, 351-355.

Jang, H. H., Lee, K. O., Chi, Y. H., Jung, B. G., Park, S. K., Park, J. H., Lee, J. R., Lee, S. S., Moon, J. C., Yun, J. W.*, et al.* (2004). Two enzymes in one; two yeast peroxiredoxins display oxidative stress-dependent switching from a peroxidase to a molecular chaperone function. Cell *117*, 625-635.

Jenuwein, T., and Allis, C. D. (2001). Translating the histone code. Science *293*, 1074-1080.

Jeong, J. K., Dybing, E., Soderlund, E., Brunborg, G., Holme, J. A., Lau, S. S., and Monks, T. J. (1997a). DNA damage, gadd153 expression, and cytotoxicity in plateau-phase renal proximal tubular epithelial cells treated with a quinol thioether. Arch Biochem Biophys *341*, 300-308.

Jeong, J. K., Huang, Q., Lau, S. S., and Monks, T. J. (1997b). The response of renal tubular epithelial cells to physiologically and chemically induced growth arrest. J Biol Chem *272*, 7511-7518.

Jeong, J. K., Stevens, J. L., Lau, S. S., and Monks, T. J. (1996). Quinone thioether-mediated DNA damage, growth arrest, and gadd153 expression in renal proximal tubular epithelial cells. Mol Pharmacol *50*, 592-598.

Jia, Z. (2004) Mechanisms of 11-deoxy-16,16-dimethyl prostaglandin E2 meidated cytoprotection, The Univitersity of Texas at Austin.

Jones, D. P. (2008). Radical-free biology of oxidative stress. Am J Physiol Cell Physiol *295*, C849-868.

Juarez-Salinas, H., Sims, J. L., and Jacobson, M. K. (1979). Poly(ADP-ribose) levels in carcinogen-treated cells. Nature *282*, 740-741.

Kanduc, D., Mittelman, A., Serpico, R., Sinigaglia, E., Sinha, A. A., Natale, C., Santacroce, R., Di Corcia, M. G., Lucchese, A., Dini, L.*, et al.* (2002). Cell death: apoptosis versus necrosis (review). Int J Oncol *21*, 165-170.

Kang, S. W., Chae, H. Z., Seo, M. S., Kim, K., Baines, I. C., and Rhee, S. G. (1998). Mammalian peroxiredoxin isoforms can reduce hydrogen peroxide generated in response to growth factors and tumor necrosis factor-alpha. J Biol Chem *273*, 6297-6302.

Kang, S. W., Rhee, S. G., Chang, T. S., Jeong, W., and Choi, M. H. (2005). 2-Cys peroxiredoxin function in intracellular signal transduction: therapeutic implications. Trends Mol Med *11*, 571-578.

Kang, Y. H., Yi, M. J., Kim, M. J., Park, M. T., Bae, S., Kang, C. M., Cho, C. K., Park, I. C., Park, M. J., Rhee, C. H.*, et al.* (2004). Caspase-independent cell death by arsenic trioxide in human cervical cancer cells: reactive oxygen species-mediated poly(ADP-ribose) polymerase-1 activation signals apoptosis-inducing factor release from mitochondria. Cancer Res *64*, 8960-8967.

Kerr, J. F., Wyllie, A. H., and Currie, A. R. (1972). Apoptosis: a basic biological phenomenon with wide-ranging implications in tissue kinetics. Br J Cancer *26*, 239-257.

Key, M. M., Henschel, A.F., Butler, J., Ligo, R.N. and Tabershaw, I.R. (1977). Hydroquinone. Occupational diseases A guide to their recognition, 249-250.

Kim, M. Y., Mauro, S., Gevry, N., Lis, J. T., and Kraus, W. L. (2004). NAD+-dependent modulation of chromatin structure and transcription by nucleosome binding properties of PARP-1. Cell *119*, 803-814.

Kirichok, Y., Krapivinsky, G., and Clapham, D. E. (2004). The mitochondrial calcium uniporter is a highly selective ion channel. Nature *427*, 360-364.

Koh, D. W., Dawson, T. M., and Dawson, V. L. (2005). Mediation of cell death by poly(ADP-ribose) polymerase-1. Pharmacol Res *52*, 5-14.

Kroemer, G., Zamzami, N., and Susin, S. A. (1997). Mitochondrial control of apoptosis. Immunol Today *18*, 44-51.

Krysko, D. V., Vanden Berghe, T., D'Herde, K., and Vandenabeele, P. (2008). Apoptosis and necrosis: detection, discrimination and phagocytosis. Methods *44*, 205-221.

Kukreja, R. C., Kontos, H. A., Hess, M. L., and Ellis, E. F. (1986). PGH synthase and lipoxygenase generate superoxide in the presence of NADH or NADPH. Circ Res *59*, 612-619.

Kun, E., Kirsten, E., Mendeleyev, J., and Ordahl, C. P. (2004). Regulation of the enzymatic catalysis of poly(ADP-ribose) polymerase by dsDNA, polyamines, Mg2+, Ca2+, histones H1 and H3, and ATP. Biochemistry *43*, 210-216.

Kwon, C. H., Yoon, C. S., and Kim, Y. K. (2008). Ciglitazone induces caspase-independent apoptosis via p38-dependent AIF nuclear translocation in renal epithelial cells. Toxicology *244*, 13-24.

Lau, S. S., Hill, B. A., Highet, R. J., and Monks, T. J. (1988a). Sequential oxidation and glutathione addition to 1,4-benzoquinone: correlation of toxicity with increased glutathione substitution. Mol Pharmacol *34*, 829-836.

Lau, S. S., Kleiner, H. E., and Monks, T. J. (1995). Metabolism as a determinant of species susceptibility to 2,3,5-(triglutathion-S-yl)hydroquinone-mediated nephrotoxicity. The role of N-acetylation and N-deacetylation. Drug Metab Dispos *23*, 1136-1142.

Lau, S. S., McMenamin, M. G., and Monks, T. J. (1988b). Differential uptake of isomeric 2-bromohydroquinone-glutathione conjugates into kidney slices. Biochem Biophys Res Commun *152*, 223-230.

Lau, S. S., and Monks, T. J. (1987). Co-oxidation of 2-bromohydroquinone by renal prostaglandin synthase. Modulation of prostaglandin synthesis by 2-bromohydroquinone and glutathione. Drug Metab Dispos *15*, 801-807.

Lau, S. S., Monks, T. J., Everitt, J. I., Kleymenova, E., and Walker, C. L. (2001). Carcinogenicity of a nephrotoxic metabolite of the "nongenotoxic" carcinogen hydroquinone. Chem Res Toxicol *14*, 25-33.

Lee, H. T., Kim, M., Song, J. H., Chen, S. W., Gubitosa, G., and Emala, C. W. (2008). Sevoflurane-mediated TGF-beta1 signaling in renal proximal tubule cells. Am J Physiol Renal Physiol *294*, F371-378.

Leist, M., Single, B., Castoldi, A. F., Kuhnle, S., and Nicotera, P. (1997). Intracellular adenosine triphosphate (ATP) concentration: a switch in the decision between apoptosis and necrosis. J Exp Med *185*, 1481-1486.

Lemasters, J. J., Nieminen, A. L., Qian, T., Trost, L. C., Elmore, S. P., Nishimura, Y., Crowe, R. A., Cascio, W. E., Bradham, C. A., Brenner, D. A., and Herman, B. (1998). The mitochondrial permeability transition in cell death: a common mechanism in necrosis, apoptosis and autophagy. Biochim Biophys Acta *1366*, 177-196.

Lemasters, J. J., Qian, T., He, L., Kim, J. S., Elmore, S. P., Cascio, W. E., and Brenner, D. A. (2002). Role of mitochondrial inner membrane permeabilization in necrotic cell death, apoptosis, and autophagy. Antioxid Redox Signal *4*, 769-781.

Levitt, J. (2007). The safety of hydroquinone: a dermatologist's response to the 2006 Federal Register. J Am Acad Dermatol *57*, 854-872.

Lillig, C. H., Berndt, C., and Holmgren, A. (2008). Glutaredoxin systems. Biochim Biophys Acta *1780*, 1304-1317.

Liu, X., Van Vleet, T., and Schnellmann, R. G. (2004). The role of calpain in oncotic cell death. Annu Rev Pharmacol Toxicol *44*, 349-370.

Lledias, F., Rangel, P., and Hansberg, W. (1998). Oxidation of catalase by singlet oxygen. J Biol Chem *273*, 10630-10637.

Madeo, F., Frohlich, E., Ligr, M., Grey, M., Sigrist, S. J., Wolf, D. H., and Frohlich, K. U. (1999). Oxygen stress: a regulator of apoptosis in yeast. J Cell Biol *145*, 757-767.

Majima, H. J., Oberley, T. D., Furukawa, K., Mattson, M. P., Yen, H. C., Szweda, L. I., and St Clair, D. K. (1998). Prevention of mitochondrial injury by manganese superoxide dismutase reveals a primary mechanism for alkaline-induced cell death. J Biol Chem *273*, 8217-8224.

Majno, G., and Joris, I. (1995). Apoptosis, oncosis, and necrosis. An overview of cell death. Am J Pathol *146*, 3-15.

Marks, A. R. (1997). Intracellular calcium-release channels: regulators of cell life and death. Am J Physiol *272*, H597-605.

Marnett, L. J. (1999). Lipid peroxidation-DNA damage by malondialdehyde. Mutat Res *424*, 83-95.

Martin, D. R., Lewington, A. J., Hammerman, M. R., and Padanilam, B. J. (2000). Inhibition of poly(ADP-ribose) polymerase attenuates ischemic renal injury in rats. Am J Physiol Regul Integr Comp Physiol *279*, R1834-1840.

Martindale, J. L., and Holbrook, N. J. (2002). Cellular response to oxidative stress: signaling for suicide and survival. J Cell Physiol *192*, 1-15.

Martinez, G. R., Loureiro, A. P., Marques, S. A., Miyamoto, S., Yamaguchi, L. F., Onuki, J., Almeida, E. A., Garcia, C. C., Barbosa, L. F., Medeiros, M. H., and Di Mascio, P. (2003). Oxidative and alkylating damage in DNA. Mutat Res *544*, 115-127.

Masutani, M., Suzuki, H., Kamada, N., Watanabe, M., Ueda, O., Nozaki, T., Jishage, K., Watanabe, T., Sugimoto, T., Nakagama, H.*, et al.* (1999). Poly(ADP-ribose) polymerase gene disruption conferred mice resistant to streptozotocin-induced diabetes. Proc Natl Acad Sci U S A *96*, 2301-2304.

Mates, J. M., Perez-Gomez, C., and Nunez de Castro, I. (1999). Antioxidant enzymes and human diseases. Clin Biochem *32*, 595-603.

Mates, J. M., and Sanchez-Jimenez, F. (1999). Antioxidant enzymes and their implications in pathophysiologic processes. Front Biosci *4*, D339-345.

Mattson, M. P. (2000). Apoptosis in neurodegenerative disorders. Nat Rev Mol Cell Biol *1*, 120-129.

Mertens, J. J., Gibson, N. W., Lau, S. S., and Monks, T. J. (1995). Reactive oxygen species and DNA damage in 2-bromo-(glutathion-S-yl) hydroquinone-mediated cytotoxicity. Arch Biochem Biophys *320*, 51-58.

Michiels, C., Raes, M., Toussaint, O., and Remacle, J. (1994). Importance of Se-glutathione peroxidase, catalase, and Cu/Zn-SOD for cell survival against oxidative stress. Free Radic Biol Med *17*, 235-248.

Miesel, R., Kurpisz, M., and Kroger, H. (1995). Modulation of inflammatory arthritis by inhibition of poly(ADP ribose) polymerase. Inflammation *19*, 379-387.

Mitsuoka, K., Shirasaka, Y., Fukushi, A., Sato, M., Nakamura, T., Nakanishi, T., and Tamai, I. (2009). Transport characteristics of L-citrulline in renal apical membrane of proximal tubular cells. Biopharm Drug Dispos *30*, 126-137.

Monks, T. J. (1995). Modulation of quinol/quinone-thioether toxicity by intramolecular detoxication. Drug Metab Rev *27*, 93-106.

Monks, T. J., Hanzlik, R. P., Cohen, G. M., Ross, D., and Graham, D. G. (1992). Quinone chemistry and toxicity. Toxicol Appl Pharmacol *112*, 2-16.

Monks, T. J., Highet, R. J., and Lau, S. S. (1988). 2-Bromo-(diglutathion-S-yl)hydroquinone nephrotoxicity: physiological, biochemical, and electrochemical determinants. Mol Pharmacol *34*, 492-500.

Monks, T. J., Jones, T. W., Hill, B. A., and Lau, S. S. (1991). Nephrotoxicity of 2-bromo-(cystein-S-yl) hydroquinone and 2-bromo-(N-acetyl-L-cystein-S-yl) hydroquinone thioethers. Toxicol Appl Pharmacol *111*, 279-298.

Monks, T. J., and Lau, S. S. (1994). Glutathione conjugation as a mechanism for the transport of reactive metabolites. Adv Pharmacol *27*, 183-210.

Monks, T. J., and Lau, S. S. (1997). Biological reactivity of polyphenolic-glutathione conjugates. Chem Res Toxicol *10*, 1296-1313.

Monks, T. J., and Lau, S. S. (1998). The pharmacology and toxicology of polyphenolic-glutathione conjugates. Annu Rev Pharmacol Toxicol *38*, 229-255.

Monks, T. J., Lau, S. S., Highet, R. J., and Gillette, J. R. (1985). Glutathione conjugates of 2-bromohydroquinone are nephrotoxic. Drug Metab Dispos *13*, 553-559.

Monks, T. J., Xie, R., Tikoo, K., and Lau, S. S. (2006). Ros-induced histone modifications and their role in cell survival and cell death. Drug Metab Rev *38*, 755-767.

Moon, J. C., Hah, Y. S., Kim, W. Y., Jung, B. G., Jang, H. H., Lee, J. R., Kim, S. Y., Lee, Y. M., Jeon, M. G., Kim, C. W.*, et al.* (2005). Oxidative stress-dependent structural and functional switching of a human 2-Cys peroxiredoxin isotype II that enhances HeLa cell resistance to H2O2-induced cell death. J Biol Chem *280*, 28775-28784.

Morais, C., Westhuyzen, J., Pat, B., Gobe, G., and Healy, H. (2005). High ambient glucose is effect neutral on cell death and proliferation in human proximal tubular epithelial cells. Am J Physiol Renal Physiol *289*, F401-409.

Moubarak, R. S., Yuste, V. J., Artus, C., Bouharrour, A., Greer, P. A., Menissier-de Murcia, J., and Susin, S. A. (2007). Sequential activation of poly(ADP-ribose) polymerase 1, calpains, and Bax is essential in apoptosis-inducing factor-mediated programmed necrosis. Mol Cell Biol *27*, 4844-4862.

Murphy, M. P. (2009). How mitochondria produce reactive oxygen species. Biochem J *417*, 1-13.

Nicholls, D. G. (2005). Mitochondria and calcium signaling. Cell Calcium *38*, 311-317.

Nicotera, P., Ankarcrona, M., Bonfoco, E., Orrenius, S., and Lipton, S. A. (1997). Neuronal necrosis and apoptosis: two distinct events induced by exposure to glutamate or oxidative stress. Adv Neurol *72*, 95-101.

Nicotera, P., Leist, M., and Manzo, L. (1999). Neuronal cell death: a demise with different shapes. Trends Pharmacol Sci *20*, 46-51.

Niculescu, R., Renz, J. F., and Kalf, G. F. (1996). Benzene-induced bone marrow cell depression caused by inhibition of the conversion of pre-interleukins-1alpha and -1beta to active cytokines by hydroquinone, a biological reactive metabolite of benzene. Adv Exp Med Biol *387*, 329-337.

NIOSH, E. (1978). Criteria for a recommended standard. Occupational exposure to hydroquinone. Cincinnati, Ohio, US National Institute for Occupational Safety and Health.

Nonn, L., Berggren, M., and Powis, G. (2003). Increased expression of mitochondrial peroxiredoxin-3 (thioredoxin peroxidase-2) protects cancer cells against hypoxia and drug-induced hydrogen peroxide-dependent apoptosis. Mol Cancer Res *1*, 682-689.

Nordberg, J., and Arner, E. S. (2001). Reactive oxygen species, antioxidants, and the mammalian thioredoxin system. Free Radic Biol Med *31*, 1287-1312.

O'Brien, P. J. (1991). Molecular mechanisms of quinone cytotoxicity. Chem Biol Interact *80*, 1-41.

Oliver, F. J., Menissier-de Murcia, J., Nacci, C., Decker, P., Andriantsitohaina, R., Muller, S., de la Rubia, G., Stoclet, J. C., and de Murcia, G. (1999). Resistance to endotoxic shock as a consequence of defective NF-kappaB activation in poly (ADP-ribose) polymerase-1 deficient mice. Embo J *18*, 4446-4454.

Orrenius, S. (2007). Reactive oxygen species in mitochondria-mediated cell death. Drug Metab Rev *39*, 443-455.

Palmer, A. D. H. (2004) Histone H3 Phosphorylation During Reactive Oxygen Species-induced Oncosis is Distinct from Mitotic Phosphorylation in Renal Proximal Tubular Epithelial Cells, The University of Texas at Austin.

Patterson, R. L., Boehning, D., and Snyder, S. H. (2004). Inositol 1,4,5-trisphosphate receptors as signal integrators. Annu Rev Biochem *73*, 437-465.

Pattingre, S., Espert, L., Biard-Piechaczyk, M., and Codogno, P. (2008). Regulation of macroautophagy by mTOR and Beclin 1 complexes. Biochimie *90*, 313-323.

Peraldi, M. N., Berrou, J., Dulphy, N., Seidowsky, A., Haas, P., Boissel, N., Metivier, F., Randoux, C., Kossari, N., Guerin, A.*, et al.* (2009). Oxidative stress mediates a reduced expression of the activating receptor NKG2D in NK cells from end-stage renal disease patients. J Immunol *182*, 1696-1705.

Perraud, A. L., Takanishi, C. L., Shen, B., Kang, S., Smith, M. K., Schmitz, C., Knowles, H. M., Ferraris, D., Li, W., Zhang, J.*, et al.* (2005). Accumulation of free ADP-ribose from mitochondria mediates oxidative stress-induced gating of TRPM2 cation channels. J Biol Chem *280*, 6138-6148.

Peters, M. M., Jones, T. W., Monks, T. J., and Lau, S. S. (1997). Cytotoxicity and cell-proliferation induced by the nephrocarcinogen hydroquinone and its nephrotoxic metabolite 2,3,5-(tris-glutathion-S-yl)hydroquinone. Carcinogenesis *18*, 2393-2401.

Pieper, A. A., Brat, D. J., Krug, D. K., Watkins, C. C., Gupta, A., Blackshaw, S., Verma, A., Wang, Z. Q., and Snyder, S. H. (1999a). Poly(ADP-ribose) polymerase-deficient mice are protected from streptozotocin-induced diabetes. Proc Natl Acad Sci U S A *96*, 3059-3064.

Pieper, A. A., Verma, A., Zhang, J., and Snyder, S. H. (1999b). Poly (ADP-ribose) polymerase, nitric oxide and cell death. Trends Pharmacol Sci *20*, 171-181.

Pieper, A. A., Walles, T., Wei, G., Clements, E. E., Verma, A., Snyder, S. H., and Zweier, J. L. (2000). Myocardial postischemic injury is reduced by polyADPripose polymerase-1 gene disruption. Mol Med *6*, 271-282.

Proskuryakov, S. Y., Konoplyannikov, A. G., and Gabai, V. L. (2003). Necrosis: a specific form of programmed cell death? Exp Cell Res *283*, 1-16.

Pryor, W. A. (1997). Cigarette smoke radicals and the role of free radicals in chemical carcinogenicity. Environ Health Perspect *105 Suppl 4*, 875-882.

Pryor, W. A., Houk, K. N., Foote, C. S., Fukuto, J. M., Ignarro, L. J., Squadrito, G. L., and Davies, K. J. (2006). Free radical biology and medicine: it's a gas, man! Am J Physiol Regul Integr Comp Physiol *291*, R491-511.

Przedborski, S. (2007). Peroxiredoxin-2 links Cdk5 to neurodegeneration. Nat Med *13*, 907-909.

Rabilloud, T., Heller, M., Gasnier, F., Luche, S., Rey, C., Aebersold, R., Benahmed, M., Louisot, P., and Lunardi, J. (2002). Proteomics analysis of cellular response to oxidative stress. Evidence for in vivo overoxidation of peroxiredoxins at their active site. J Biol Chem *277*, 19396-19401.

Racusen, L. C., Monteil, C., Sgrignoli, A., Lucskay, M., Marouillat, S., Rhim, J. G., and Morin, J. P. (1997). Cell lines with extended in vitro growth potential from human renal proximal tubule: characterization, response to inducers, and comparison with established cell lines. J Lab Clin Med *129*, 318-329.

Ramachandiran, S., Huang, Q., Dong, J., Lau, S. S., and Monks, T. J. (2002). Mitogen-activated protein kinases contribute to reactive oxygen species-induced cell death in renal proximal tubule epithelial cells. Chem Res Toxicol *15*, 1635-1642.

Rapizzi, E., Pinton, P., Szabadkai, G., Wieckowski, M. R., Vandecasteele, G., Baird, G., Tuft, R. A., Fogarty, K. E., and Rizzuto, R. (2002). Recombinant expression of the voltage-dependent anion channel enhances the transfer of Ca2+ microdomains to mitochondria. J Cell Biol *159*, 613-624.

Rhee, S. G., Kang, S. W., Chang, T. S., Jeong, W., and Kim, K. (2001). Peroxiredoxin, a novel family of peroxidases. IUBMB Life *52*, 35-41.

Richter, C., and Kass, G. E. (1991). Oxidative stress in mitochondria: its relationship to cellular Ca2+ homeostasis, cell death, proliferation, and differentiation. Chem Biol Interact *77*, 1-23.

Rogakou, E. P., Pilch, D. R., Orr, A. H., Ivanova, V. S., and Bonner, W. M. (1998). DNA double-stranded breaks induce histone H2AX phosphorylation on serine 139. J Biol Chem *273*, 5858-5868.

Ryan, M. J., Johnson, G., Kirk, J., Fuerstenberg, S. M., Zager, R. A., and Torok-Storb, B. (1994). HK-2: an immortalized proximal tubule epithelial cell line from normal adult human kidney. Kidney Int *45*, 48-57.

Ryter, S. W., Kim, H. P., Hoetzel, A., Park, J. W., Nakahira, K., Wang, X., and Choi, A. M. (2007). Mechanisms of cell death in oxidative stress. Antioxid Redox Signal *9*, 49-89.

Sautin, Y. Y., Lu, M., Gaugler, A., Zhang, L., and Gluck, S. L. (2005). Phosphatidylinositol 3-kinase-mediated effects of glucose on vacuolar H+-ATPase assembly, translocation, and acidification of intracellular compartments in renal epithelial cells. Mol Cell Biol *25*, 575-589.

Schanne, F. A., Kane, A. B., Young, E. E., and Farber, J. L. (1979). Calcium dependence of toxic cell death: a final common pathway. Science *206*, 700-702.

Schreiber, V., Dantzer, F., Ame, J. C., and de Murcia, G. (2006). Poly(ADP-ribose): novel functions for an old molecule. Nat Rev Mol Cell Biol *7*, 517-528.

Seo, M. S., Kang, S. W., Kim, K., Baines, I. C., Lee, T. H., and Rhee, S. G. (2000). Identification of a new type of mammalian peroxiredoxin that forms an intramolecular disulfide as a reaction intermediate. J Biol Chem *275*, 20346-20354.

Shan, X. Q., Aw, T. Y., and Jones, D. P. (1990). Glutathione-dependent protection against oxidative injury. Pharmacol Ther *47*, 61-71.

Silva, M. T., do Vale, A., and dos Santos, N. M. (2008). Secondary necrosis in multicellular animals: an outcome of apoptosis with pathogenic implications. Apoptosis *13*, 463-482.

Slemmer, J. E., Zhu, C., Landshamer, S., Trabold, R., Grohm, J., Ardeshiri, A., Wagner, E., Sweeney, M. I., Blomgren, K., Culmsee, C*., et al.* (2008). Causal role of apoptosis-inducing factor for neuronal cell death following traumatic brain injury. Am J Pathol *173*, 1795-1805.

Smith, C. C., Davidson, S. M., Lim, S. Y., Simpkin, J. C., Hothersall, J. S., and Yellon, D. M. (2007). Necrostatin: a potentially novel cardioprotective agent? Cardiovasc Drugs Ther *21*, 227-233.

Smith, M. T., Robertson, M. L., Yager, J. W., and Eastmond, D. A. (1990). Role of metabolism in benzene-induced myelotoxicity and leukemogenesis. Prog Clin Biol Res *340B*, 125-136.

Snyder, R., Chepiga, T., Yang, C. S., Thomas, H., Platt, K., and Oesch, F. (1993a). Benzene metabolism by reconstituted cytochromes P450 2B1 and 2E1 and its modulation by cytochrome b5, microsomal epoxide hydrolase, and glutathione transferases: evidence for an important role of microsomal epoxide hydrolase in the formation of hydroquinone. Toxicol Appl Pharmacol *122*, 172-181.

Snyder, R., Witz, G., and Goldstein, B. D. (1993b). The toxicology of benzene. Environ Health Perspect *100*, 293-306.

Song, Z. F., Ji, X. P., Li, X. X., Wang, S. J., and Wang, S. H. (2007). Inhibition of the activity of Poly(ADP-Ribose) Polymerase reduces heart ischemia/reperfusion injury via suppressing JNK mediated AIF translocation. J Cell Mol Med.

Song, Z. F., Ji, X. P., Li, X. X., Wang, S. J., Wang, S. H., and Zhang, Y. (2008). Inhibition of the activity of poly (ADP-ribose) polymerase reduces heart ischaemia/reperfusion injury via suppressing JNK-mediated AIF translocation. J Cell Mol Med *12*, 1220-1228.

Starkov, A. A. (2008). The role of mitochondria in reactive oxygen species metabolism and signaling. Ann N Y Acad Sci *1147*, 37-52.

Strasser, A., O'Connor, L., and Dixit, V. M. (2000). Apoptosis signaling. Annu Rev Biochem *69*, 217-245.

Stubberfield, C. R., and Cohen, G. M. (1988). NAD+ depletion and cytotoxicity in isolated hepatocytes. Biochem Pharmacol *37*, 3967-3974.

Subrahmanyam, V. V., Doane-Setzer, P., Steinmetz, K. L., Ross, D., and Smith, M. T. (1990). Phenol-induced stimulation of hydroquinone bioactivation in mouse bone marrow in vivo: possible implications in benzene myelotoxicity. Toxicology *62*, 107-116.

Sun, S., Ning, X., Zhang, Y., Lu, Y., Nie, Y., Han, S., Liu, L., Du, R., Xia, L., He, L., and Fan, D. (2009). Hypoxia-inducible factor-1alpha induces Twist expression in tubular epithelial cells subjected to hypoxia, leading to epithelial-to-mesenchymal transition. Kidney Int.

Sung, M. J., Kim, D. H., Jung, Y. J., Kang, K. P., Lee, A. S., Lee, S., Kim, W., Davaatseren, M., Hwang, J. T., Kim, H. J.*, et al.* (2008). Genistein protects the kidney from cisplatin-induced injury. Kidney Int *74*, 1538-1547.

Susin, S. A., Lorenzo, H. K., Zamzami, N., Marzo, I., Snow, B. E., Brothers, G. M., Mangion, J., Jacotot, E., Costantini, P., Loeffler, M.*, et al.* (1999). Molecular characterization of mitochondrial apoptosis-inducing factor. Nature *397*, 441-446.

Szabo, C., and Dawson, V. L. (1998). Role of poly(ADP-ribose) synthetase in inflammation and ischaemia-reperfusion. Trends Pharmacol Sci *19*, 287-298.

Szabo, C., Lim, L. H., Cuzzocrea, S., Getting, S. J., Zingarelli, B., Flower, R. J., Salzman, A. L., and Perretti, M. (1997). Inhibition of poly (ADP-ribose) synthetase attenuates neutrophil recruitment and exerts antiinflammatory effects. J Exp Med *186*, 1041-1049.

Taatjes, D. J., Sobel, B. E., and Budd, R. C. (2008). Morphological and cytochemical determination of cell death by apoptosis. Histochem Cell Biol *129*, 33-43.

Takada, E., Hata, K., and Mizuguchi, J. (2008). c-Jun NH2-terminal kinase (JNK)-dependent nuclear translocation of apoptosis-inducing factor (AIF) following engagement of membrane immunoglobulin on WEHI-231 B lymphoma cells. J Cell Biochem *104*, 1927-1936.

Tanaka, T., Hosoi, F., Yamaguchi-Iwai, Y., Nakamura, H., Masutani, H., Ueda, S., Nishiyama, A., Takeda, S., Wada, H., Spyrou, G., and Yodoi, J. (2002). Thioredoxin-2 (TRX-2) is an essential gene regulating mitochondria-dependent apoptosis. Embo J *21*, 1695-1703.

Tanuma, S., Kawashima, K., and Endo, H. (1986). Purification and properties of an (ADP-ribose)n glycohydrolase from guinea pig liver nuclei. J Biol Chem *261*, 965-969.

Thannickal, V. J., and Fanburg, B. L. (2000). Reactive oxygen species in cell signaling. Am J Physiol Lung Cell Mol Physiol *279*, L1005-1028.

Thiemermann, C., Bowes, J., Myint, F. P., and Vane, J. R. (1997). Inhibition of the activity of poly(ADP ribose) synthetase reduces ischemia-reperfusion injury in the heart and skeletal muscle. Proc Natl Acad Sci U S A *94*, 679-683.

Tikoo, K., Lau, S. S., and Monks, T. J. (2001). Histone H3 phosphorylation is coupled to poly-(ADP-ribosylation) during reactive oxygen species-induced cell death in renal proximal tubular epithelial cells. Mol Pharmacol *60*, 394-402.

Torres, M., and Forman, H. J. (2003). Redox signaling and the MAP kinase pathways. Biofactors *17*, 287-296.

Trump, B. F., Berezesky, I. K., Chang, S. H., and Phelps, P. C. (1997). The pathways of cell death: oncosis, apoptosis, and necrosis. Toxicol Pathol *25*, 82-88.

Ueda, S., Masutani, H., Nakamura, H., Tanaka, T., Ueno, M., and Yodoi, J. (2002). Redox control of cell death. Antioxid Redox Signal *4*, 405-414.

van Wijk, S. J., and Hageman, G. J. (2005). Poly(ADP-ribose) polymerase-1 mediated caspase-independent cell death after ischemia/reperfusion. Free Radic Biol Med *39*, 81-90.

Vanlangenakker, N., Berghe, T. V., Krysko, D. V., Festjens, N., and Vandenabeele, P. (2008). Molecular mechanisms and pathophysiology of necrotic cell death. Curr Mol Med *8*, 207-220.

Varagant, J. (1981). Hydroquinone, resorcinol, and catechol. Grayson Med Kirk-Othmer encyclopedia of chemical technology, 39-69.

Vaughan, A. T., Betti, C. J., Villalobos, M. J., Premkumar, K., Cline, E., Jiang, Q., and Diaz, M. O. (2005). Surviving apoptosis: a possible mechanism of benzene-induced leukemia. Chem Biol Interact *153-154*, 179-185.

Verkhratsky, A. (2007). Calcium and cell death. Subcell Biochem *45*, 465-480.

Verzola, D., Gandolfo, M. T., Salvatore, F., Villaggio, B., Gianiorio, F., Traverso, P., Deferrari, G., and Garibotto, G. (2004). Testosterone promotes apoptotic damage in human renal tubular cells. Kidney Int *65*, 1252-1261.

Wagner, E., Luche, S., Penna, L., Chevallet, M., Van Dorsselaer, A., Leize-Wagner, E., and Rabilloud, T. (2002). A method for detection of overoxidation of cysteines:

peroxiredoxins are oxidized in vivo at the active-site cysteine during oxidative stress. Biochem J *366*, 777-785.

Waldmeier, P. C., Zimmermann, K., Qian, T., Tintelnot-Blomley, M., and Lemasters, J. J. (2003). Cyclophilin D as a drug target. Curr Med Chem *10*, 1485-1506.

Walisser, J. A., and Thies, R. L. (1999). Poly(ADP-ribose) polymerase inhibition in oxidant-stressed endothelial cells prevents oncosis and permits caspase activation and apoptosis. Exp Cell Res *251*, 401-413.

Wang, H., Yu, S. W., Koh, D. W., Lew, J., Coombs, C., Bowers, W., Federoff, H. J., Poirier, G. G., Dawson, T. M., and Dawson, V. L. (2004a). Apoptosis-inducing factor substitutes for caspase executioners in NMDA-triggered excitotoxic neuronal death. J Neurosci *24*, 10963-10973.

Wang, Y., Wysocka, J., Perlin, J. R., Leonelli, L., Allis, C. D., and Coonrod, S. A. (2004b). Linking covalent histone modifications to epigenetics: the rigidity and plasticity of the marks. Cold Spring Harb Symp Quant Biol *69*, 161-169.

Waring, P. (2005). Redox active calcium ion channels and cell death. Arch Biochem Biophys *434*, 33-42.

Watabe, S., Hiroi, T., Yamamoto, Y., Fujioka, Y., Hasegawa, H., Yago, N., and Takahashi, S. Y. (1997). SP-22 is a thioredoxin-dependent peroxide reductase in mitochondria. Eur J Biochem *249*, 52-60.

Wehage, E., Eisfeld, J., Heiner, I., Jungling, E., Zitt, C., and Luckhoff, A. (2002). Activation of the cation channel long transient receptor potential channel 2 (LTRPC2) by hydrogen peroxide. A splice variant reveals a mode of activation independent of ADP-ribose. J Biol Chem *277*, 23150-23156.

Wei, Y., Yu, L., Bowen, J., Gorovsky, M. A., and Allis, C. D. (1999). Phosphorylation of histone H3 is required for proper chromosome condensation and segregation. Cell *97*, 99-109.

Whysner, J., Verna, L., English, J. C., and Williams, G. M. (1995). Analysis of studies related to tumorigenicity induced by hydroquinone. Regul Toxicol Pharmacol *21*, 158-176.

Winterbourn, C. C., and Hampton, M. B. (2008). Thiol chemistry and specificity in redox signaling. Free Radic Biol Med *45*, 549-561.

Witz, G., Zhang, Z., and Goldstein, B. D. (1996). Reactive ring-opened aldehyde metabolites in benzene hematotoxicity. Environ Health Perspect *104 Suppl 6*, 1195-1199.

Wonsey, D. R., Zeller, K. I., and Dang, C. V. (2002). The c-Myc target gene PRDX3 is required for mitochondrial homeostasis and neoplastic transformation. Proc Natl Acad Sci U S A *99*, 6649-6654.

Wood, Z. A., Poole, L. B., and Karplus, P. A. (2003a). Peroxiredoxin evolution and the regulation of hydrogen peroxide signaling. Science *300*, 650-653.

Wood, Z. A., Schroder, E., Robin Harris, J., and Poole, L. B. (2003b). Structure, mechanism and regulation of peroxiredoxins. Trends Biochem Sci *28*, 32-40.

Wyllie, A. H., Kerr, J. F., and Currie, A. R. (1980). Cell death: the significance of apoptosis. Int Rev Cytol *68*, 251-306.

Xie, J., and Guo, Q. (2007). Par-4 is a novel mediator of renal tubule cell death in models of ischemia-reperfusion injury. Am J Physiol Renal Physiol *292*, F107-115.

Xu, Y., Huang, S., Liu, Z. G., and Han, J. (2006). Poly(ADP-ribose) polymerase-1 signaling to mitochondria in necrotic cell death requires RIP1/TRAF2-mediated JNK1 activation. J Biol Chem *281*, 8788-8795.

Yan, J., Yang, S., Zhang, J., Zhai, C., and Zhu, T. (2009). BMP6 attenuates oxidant injury in HK-2 cells via Smad-dependent HO-1 induction. Free Radic Biol Med *46*, 1275-1282.

Yang, M. Y., Lau, S. S., and Monks, T. J. (2005). 2,3,5-tris(Glutathion-S-yl)hydroquinone (TGHQ)-mediated apoptosis of human promyelocytic leukemia cells is preceded by mitochondrial cytochrome c release in the absence of a decrease in the mitochondrial membrane potential. Toxicol Sci *86*, 92-100.

Yu, S. W., Andrabi, S. A., Wang, H., Kim, N. S., Poirier, G. G., Dawson, T. M., and Dawson, V. L. (2006). Apoptosis-inducing factor mediates poly(ADP-ribose) (PAR) polymer-induced cell death. Proc Natl Acad Sci U S A *103*, 18314-18319.

Yu, S. W., Wang, H., Poitras, M. F., Coombs, C., Bowers, W. J., Federoff, H. J., Poirier, G. G., Dawson, T. M., and Dawson, V. L. (2002). Mediation of poly(ADP-ribose) polymerase-1-dependent cell death by apoptosis-inducing factor. Science *297*, 259-263.

Yuan, J. (2008). Inducing autophagy harmlessly. Autophagy *4*, 249-250.

Zhang, H., Go, Y. M., and Jones, D. P. (2007a). Mitochondrial thioredoxin-2/peroxiredoxin-3 system functions in parallel with mitochondrial GSH system in protection against oxidative stress. Arch Biochem Biophys *465*, 119-126.

Zhang, S., Lin, Y., Kim, Y. S., Hande, M. P., Liu, Z. G., and Shen, H. M. (2007b). c-Jun N-terminal kinase mediates hydrogen peroxide-induced cell death via sustained poly(ADP-ribose) polymerase-1 activation. Cell Death Differ *14*, 1001-1010.

Zingarelli, B., Salzman, A. L., and Szabo, C. (1998). Genetic disruption of poly (ADP-ribose) synthetase inhibits the expression of P-selectin and intercellular adhesion molecule-1 in myocardial ischemia/reperfusion injury. Circ Res *83*, 85-94.

Zingarelli, B., Szabo, C., and Salzman, A. L. (1999). Blockade of Poly(ADP-ribose) synthetase inhibits neutrophil recruitment, oxidant generation, and mucosal injury in murine colitis. Gastroenterology *116*, 335-345.